COMENIUS UNIVERSITY IN BRATISLAVA
FACULTY OF MATHEMATICS, PHYSICS AND INFORMATICS

Simulations of cosmogenic radionuclide production rates in meteorites and Earth's atmosphere

PhD thesis

Bratislava 2014 Mgr. Juraj Beňo

COMENIUS UNIVERSITY IN BRATISLAVA
FACULTY OF MATHEMATICS, PHYSICS AND INFORMATICS

Simulations of cosmogenic radionuclide production rates in meteorites and Earth's atmosphere

PhD thesis

STUDY PROGRAMME:	Nuclear and Subnuclear Physics
BRANCH OF STUDY:	4.1.5 Nuclear and Subnuclear Physics
DEPARTMENT:	Department of Nuclear Physics and Biophysics
SUPERVISOR:	Prof. RNDr. Jozef Masarik, DrSc

Bratislava, 2014 **Mgr. Juraj Beňo**

Acknowledgements

I am very thankful to all people who contributed to the completion of this work. Firstly, I would like to thank to my supervisor professor Jozef Masarik for introducing me to the applied nuclear physics, study of cosmogenic nuclide production and his valuable time dedicated to enlightening scientific discussions. I also thank to my colleagues at the department for support and help with everyday problems.

Declaration

I hereby declare, that submitted PhD thesis is my own work elaborated with the use of listed references.

Bratislava, April 2014 Juraj Beňo

Abstract

In this work, purely physical models describing the depth-dependence of the production of cosmogenic nuclides in Earth's atmosphere and meteoroids with different geometries and chemical composition are presented. Models are based on Monte Carlo simulation of intra- and inter-nuclear cascades, by which depth-dependent spectra of primary and secondary protons and secondary neutrons are derived. The Work discusses multiple topics related to current problems in applied nuclear physics, which are connected to production of cosmogenic nuclides in extra-terrestrial matter and Earth's atmosphere.

The production of cosmogenic nuclides in meteoroids is dependent on many factors such as incident particle flux, pre-atmospheric size, bulk chemical composition. Those factors have been studied in detail in past decades; therefore we focused our attention on effects of parent body shape. The Chapter 2.1 presents results of calculations for modelled objects with different geometries and show influence of the meteoroid's shape on chosen cosmogenic radionuclides produced by low-energy neutron capture (^{60}Co), by high-energy spallation reactions (^{10}Be) and also discusses changes in fluxes within modelled objects.

The influence of variations in solar activity on production of many different short-lived cosmogenic radionuclides in meteoroids is discussed in Chapter 2.2. Here we present calculation model for short-lived cosmogenic nuclides which uses derived semi-empiric equations for the spectrum of galactic cosmic rays and measured variations in solar activity in the past decades. The model was applied on real meteorite falls and evaluates variations in production of cosmogenic radionuclides during solar cycles.

The meteorite falls provide useful information for the study of the interaction of cosmic rays with matter, evolution of the solar system and meteorites itself. This information is obtained from analysis of meteorite fragments. Many fragments from falls of the Chelyabinsk and the Košice meteorite were analysed. In chapters 2.3 and 2.4 we use experimental data from both meteorites and calculated production rates and activities of measured cosmogenic radionuclides. The pre-atmospheric size of the Košice meteorite and position of fragments within both meteorites have been estimated.

^{81}Kr (half-life = 229 +/- 11 kyr) produced in the atmosphere is cosmogenic in origin and records the GCR flux on the timescale of 10^5 years, yet it provides a complementary perspective to and is quite different from that of ^{10}Be or ^{36}Cl. The most important difference resides in their transport and residence in the atmosphere ^{81}Kr is a noble-gas nuclide and due its properties is held in the atmosphere throughout its lifetime. The ^{81}Kr/Kr ratio in the atmosphere is the perfect whole-earth integrator of the GCR flux in the time scale of 10^5 years. The measured ^{81}Kr/Kr ratio, due to its simplicity, can help verify models simulating cosmic-ray fluxes and calculating production rates of cosmogenic nuclides.

Keywords: meteorite, meteoroid, cosmogenic radionuclide, production rate, activity, depth profile, particle flux, simulations

Abstrakt

V tejto práci sú prezentované fyzikálne simulačné modely popisujúce hĺbkovú závislosť produkcie kozmogénnych rádionuklidov v meteoritoch s rôznymi geometriami a chemickým zložením a v atmosfére Zeme. Modely sú založené na Monte Carlo simuláciách interakcií častíc, z ktorých boli získané hĺbkové profily primárnych a sekundárnych protónov a sekundárnych neutrónov. Táto práca sa venuje viacerým témam súvisiacim s produkciou kozmogénnych rádionuklidov v mimozemskej hmote ako aj zemskej atmosfére.

Produkcia kozmogénnych rádionuklidov v meteoritoch je závislá od rôznych faktorov ako napríklad: veľkosť meteoroidu, jeho chemické zloženie a tok kozmického žiarenia. Tieto faktory boli už detailne študované v minulosti a preto sme upriamili pozornosť na štúdium vplyvu tvaru meteoroidu na tok častíc a produkciu nuklidov. V prvej výsledkovej kapitole sú prezentované výsledky zo simulácií meteoroidov s rôznymi geometrickými tvarmi. Výpočty boli zamerané na poukázanie na zmeny v tokoch častíc vo vnútri meteoroidu v závislosti od tvaru objektu a taktiež na zmeny produkcie vybraných rádionuklidov produkovaných rozdielnymi procesmi. ^{60}Co ako produkt nízkoenergetických záchytových reakcií neutrónov a ^{10}Be ako produkt vysokoenergetických trieštivých reakcií.

Vplyv variácií slnečnej aktivity na produkciu rôznych krátkožijúcich kozmogénnych rádionuklidov je diskutovaná v druhej výsledkovej kapitole. V nej sa prezentuje výpočtový model pre krátkožijúce kozmogénne radionuklidy, ktorý bol odvodený zo semiempirických rovníc popisujúcich zmenu galaktického kozmického žiarenia pod vplyvom slnečnej aktivity a z nameraných variácii v slnečnej aktivite za posledné dekády. Model bol aplikovaný na reálne prípady nájdených meteoritov. Takýmto spôsobom boli odhadnuté variácie v produkcii kozmogénnych rádionuklidov v rámci slnečného cyklu.

Analýzy fragmentov meteoritov nájdených po ich dopade na Zem prinášajú užitočné informácie pre štúdium interakcie kozmického žiarenia s hmotou, vývoji slnečnej sústavy ako aj meteoritov samotných. Prípadmi tohto druhu boli aj úlomky nájdené po páde meteoritov Čeljabinsk a Košice. Tretia a štvrtá výsledková kapitola je venovaná výsledkom simulácií produkčných rýchlostí a aktivít rádionuklidov pre oba meteority, ktoré boli vypočítané na základe

dostupných experimentálnych dát. V práci je taktiež prezentovaný odhad hĺbok jednotlivých vzoriek pre oba meteority a odhad veľkosti pre meteoroid Košice.

^{81}Kr vyprodukovaný v atmosfére ma kozmogénny pôvod a z hľadiska procesov skúmaných v časovej škále na úrovni 10^5 rokov prináša doplnkový náhľad oproti bežne používaným rádionuklidom ^{10}Be a ^{36}Cl. Najpodstatnejší rozdiel spočíva v transporte a záchyte v atmosfére, ktorý je daný jeho charakterom vzácneho plynu. Týmto sa stáva veľmi vhodným nástrojom, ktorý umožňuje verifikovať modely simulujúce toky kozmických častí ako aj produkčné rýchlosti kozmogénnych nuklidov.

Kľúčové slová: meteorit, meteoroid, produkčná rýchlosť, aktivita, kozmogénny rádionuklid, hĺbkový profil, tok častíc, simulácia

Table of contents

1. Introduction

Long time before mankind learned to understand world around them the cosmic rays were leaving records in ambient environment. Those records tell us about past and evolution of our Earth, Sun and galaxy. The cosmic rays have complex characteristic and varies from day to day, year to year and over a timescale of many thousand years. It is only in the past few decades, that we have had the means to determine, in a quantitative manner, the relationship between cosmic radiation and the production of the cosmogenic nuclides. Few major technological advances made that possible. Satellites orbiting earth, deep space probes as well as instrumentation on earth provide necessary knowledge of composition, energy dependence and time variations of cosmic radiation. Large networks of computers with highly complex mathematical codes that simulate propagation and interaction of cosmic rays with terrestrial and extraterrestrial matter provide the knowledge important for interpretation of cosmogenic data from the past. The development of accelerator mass spectrometers at about the same time provided another major stimulus to the use of cosmogenic radionuclides in wide range of applications.

A large variety of stable and radioactive cosmogenic nuclides is produced by interaction of cosmic ray particles with matter. The investigation of these cosmogenic nuclides allows us to study the history of the irradiated bodies in the solar system as well as that of the cosmic radiation itself. For interpretation of measured abundances of cosmogenic nuclides a precise and accurate modelling of the depth and size dependence of cosmic ray interactions in target body is necessary. At the present time stochastic models using Monte Carlo simulation of particle transport in matter are used. Physical models calculate production rates by using basic physical principles and nuclear quantities. In such models complex occurrences of the intranuclear cascades are described, in particular transport of secondary particles.

This work is divided into two main parts. The first one Introduction consists of selected parts of theory which describes general knowledge and findings necessary for understanding of obtained results. The second part named Results provide additional information to particular topic with in detail description of used techniques and important discussions.

The subject of this thesis is study of cosmogenic nuclide production in terrestrial and extraterrestrial matter using Monte Carlo simulation techniques.

The specific goals of the thesis are:

- Study of cosmogenic nuclide production rates dependence on the preatmospheric shape of irradiated body.
- Investigation of solar activity on short lived cosmogenic nuclide production by galactic cosmic rays.
- Modelling of production rates for Košice and Chelyabinsk meteorites.
- Simulation of ^{81}Kr production in the Earth's atmosphere.

1.1 Cosmic rays

Cosmic rays (CR) are high energy particles capable to produce cascades of secondary particles and induce various effects in affected matter. At the Earth's orbit CR are primarily composed of protons, α-particles, some heavier nuclei, electrons and photons. The CR intensities vary with geomagnetic latitude and solar phenomena. For purpose of this work we will further consider only particles of primary CR that have enough energy to induce nuclear reactions.

With respect to origin CR can be divided into two main types: galactic cosmic rays (GCR) and solar cosmic rays (SCR). GCR and SCR differ in particle composition, energy distribution, flux intensity and temporal variations (Table 1.1-1). Both GCR and SCR are able to penetrate into solids and interact with them, and both are able to produce recognizable chemical effects, atomic displacement and ionization. Particles with energy higher than ~10 MeV also produce nuclear reaction. Despite their similarities it is easy to study GCR and SCR separately. The SCR particles have lower energies their flux is higher and irregular. The records of both particle types have been studied in terrestrial and extraterrestrial samples, such as meteorites, lunar rocks and soils.

Table 1.1-1: Energies, mean fluxes and interaction depths of various types of CR particles [8].

Radiation	Energy (MeV nucleon^{-1})	Mean flux (particles cm^{-2} s^{-1})	Effective depth (cm)
	Solar cosmic radiation		
Proton and α-particles	5 to 100	~ 100	0 to 2
Iron group and heavier nuclei	1 to 50	~ 1	0 to 0.1
	Galactic cosmic radiation		
Proton and α-particles	100 to 3000	~ 3	0 to 100
Iron group and heavier nuclei	~ 100	~ 0.03	0 to 10

1.1.1 Galactic cosmic rays

The GCR are originating outside of Solar system. The initial sources of GCR particles involve two types of sources: supernovae explosions (discreet sources) and interstellar medium (diffusive sources) [13]. As the particles are transported to the solar system, various interactions including acceleration occur. The nuclear component of GCR consist of ~ 87 % hydrogen, ~ 12 % helium and ~ 1 % of all heavier nuclei in the general energy range where they have the highest intensity [9]. The flux of GCR is isotropic and continuous with time variations caused by Sun's activity.

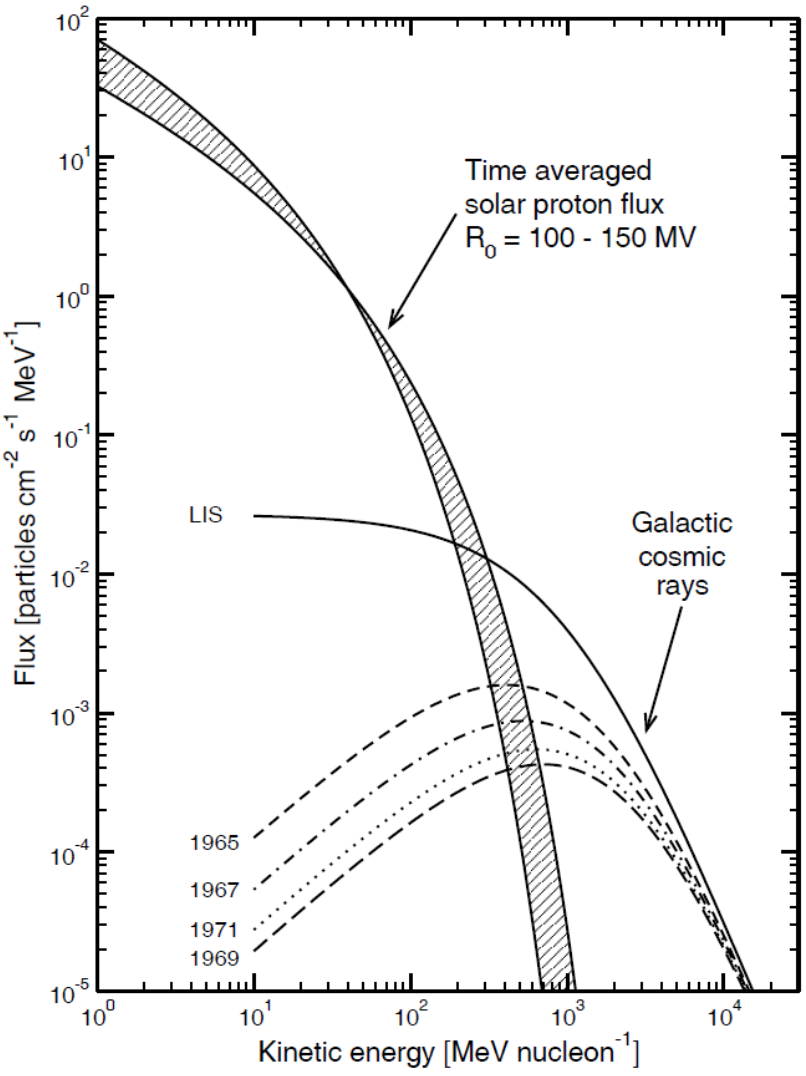

Figure 1.1.1-1: The Long-term average fluxes of solar protons determined from lunar data and GCR-proton fluxes for different modulation levels [8].

The differential flux of GCR protons *J(Φ, T)* (particles $s^{-1}m^{-2}MeV^{-1}$) in vicinity of Earth can be described by [6,54]:

$$J(\Phi,T) = A\frac{T(T+2E_0)(T+m)^{-\gamma}}{(T+\Phi)(T+2E_0+\Phi)} \qquad (1.1.1\text{-}1)$$

where T (MeV) is the proton kinetic energy, E_o its rest energy [MeV], Φ is the modulation parameter (MeV) or the energy lost by particles in traversing the heliosphere while reaching the earth, $A = 9.9 \cdot 10^8$, $m = 780 \exp(-2.5 \cdot 10^{-4}\ T)$ and $\gamma = 2.65$.

Modulation parameter Φ [MeV] represents energy loss of a particle entering to Sun's heliosphere and propagating at certain distance from the Sun. The value of modulation parameter during solar cycles is ranging from 250 to 1500 MeV that cover the whole range of observed modulation in the past. The modulation is due to scattering of particles on irregularities of interplanetary magnetic fields, which are convected outwards by solar wind plasma. Solar modulation is dominant source of the observed GCR variability (Figure 1.1.1-1).

The fluxes of 200-500 MeV particles are modulated by an order of magnitude during solar cycle. At energy above 5 to 10 $GeV.nucleon^{-1}$ particles are not influenced much by solar activity. Most nuclear interactions that produce records are induced by particles with energy higher than 1 $GeV.nucleon^{-1}$ which are affected only slightly by solar modulation [8].

1.1.2 Solar cosmic rays

SCR are produced by the Sun at a distance of 1 AU from Earth. Majority of particles are emitted during large solar flares and constitute important source of medium energy particles (E < 100 MeV nucleon^{-1}). SCR are mostly protons ~ 98 %, rest consist of α-particles and traces of heavier nuclei. Only a few large flares are able to produce most of the SCR particles emitted during 11-year sunspot cycle. The sunspot number is related to current solar activity. When solar activity is low number of sunspot (several tens) is also low and only few energetic particles are emitted.

The energy spectrum of solar particles is composed of many particles with energy > 10 MeV but only few with energy > 100 MeV (Figures 1.1.1-1, 1.1.2-1). Spectrum of SCR can be described well by $E^{-\gamma}$, where E is kinetic energy per nucleon. For proton energies between 20 and 80 MeV γ typically ranges from 2 to 4, with an average of 2.9 [8].

The energy distribution of solar protons can be expressed by rigidity spectra [5]:

$$J(R)dr = k\ \exp\left(-\frac{R}{R_0}\right)dR \qquad (1.1.2\text{-}1)$$

where R_0 is the characteristic rigidity.

Expressing the rigidity R (MV) in terms of the proton energy E (MeV) by:

$$R^2 = E^2 + 1876\,E \qquad (1.1.2\text{-}2)$$

The relatively low-energy SCR are stopped in the first few centimetres of surface of affected matter by energy loss due to ionization processes. The energies of SCR particles are not high enough to produce considerable amounts of nuclear-active secondary particles.

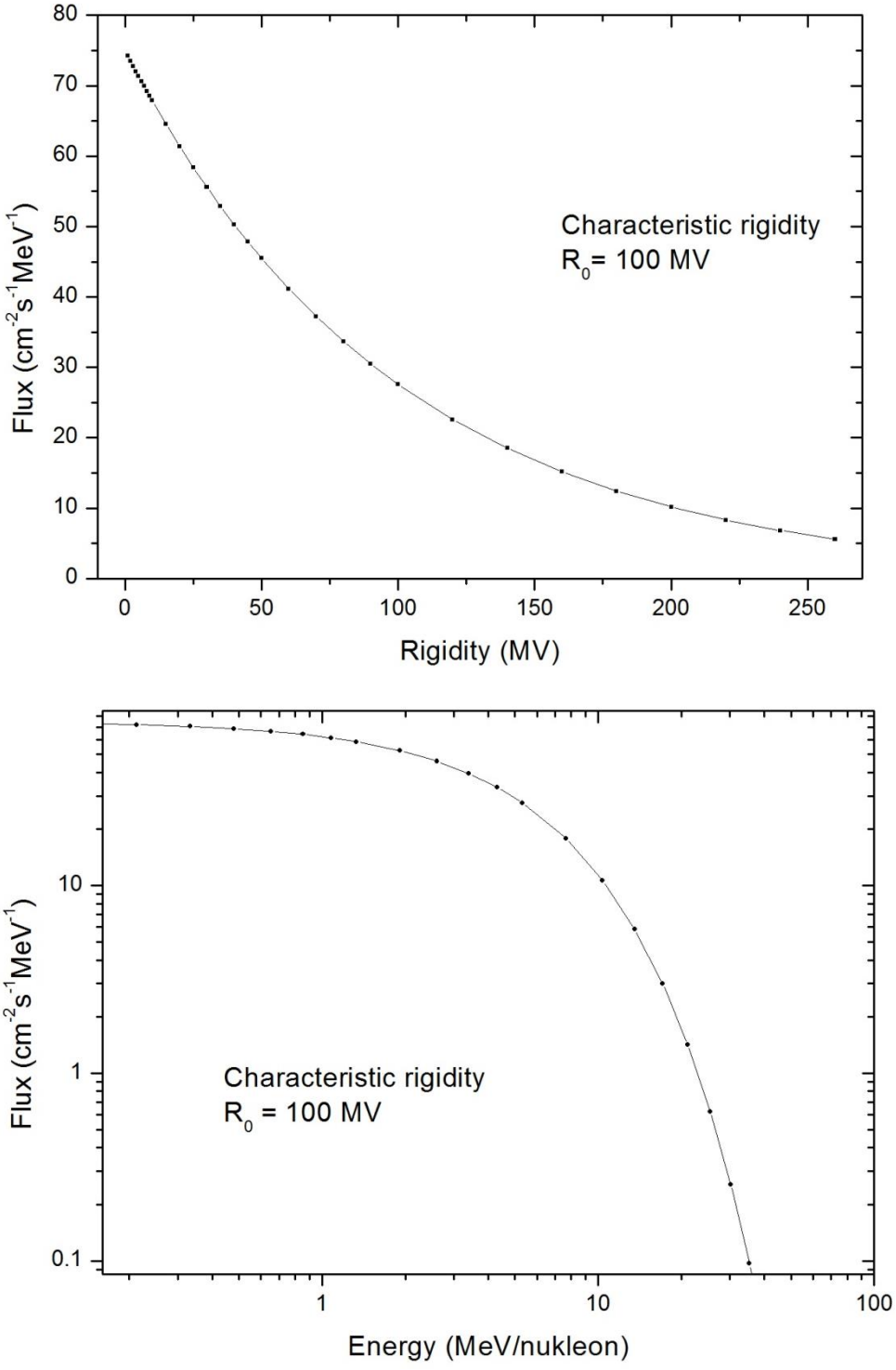

Figures 1.1.2-1: Flux of solar protons (from expression 1.1.2-1 and 1.1.2-2) dependent on Rigidity (up) and Energy (down) for characteristic rigidity R_0 = 100 MeV.

1.1.3 Heliospheric modulation of cosmic rays.

In the section 1.1.1 we have discussed the most commonly used approximation of local interstellar spectrum - LIS (which is also mainly used in this work) and derived basic characteristics of the GCR particles. The differential energy spectrum of galactic cosmic rays in the vicinity of the Earth can be parameterized by so-called force field model which has only one parameter, the modulation potential Φ, for a given LIS. The LIS represent the cosmic ray spectrum that would be observed outside of the heliosphere. Clearly the spectrum observed near Earth will be determined, in a large part, by the intensity and energy (or rigidity) dependence on LIS. Unfortunately there is no direct measurement of the LIS yet, and estimations based on measurement near Earth must be used. Over the past decades many observations has been made in the outer heliosphere where there is less solar modulation and multiple analytical approximation has been established.

The general equation which describes differential cosmic ray flux $J_T(E,\Phi)$ at Earth's orbit can be written as:

$$J_T(E,\Phi) = J_{LIS}(E+\Phi)\frac{E(E+2E_0)}{(E+\Phi)(E+\Phi+2E_0)} \qquad (1.1.3-1)$$

where E is kinetic energy, E_0 is rest mass energy, Φ is the modulation parameter and $J_{LIS}(E+\Phi)$ represents unmodulated differential cosmic ray spectra (LIS). Second term describes modulation of cosmic ray flux.

There are few LIS formulations that are used the most commonly (Figure 1.1.3-1).

1, Garcia - Muonz et al. (1975) based on the early satellite data and adopted by many authors since 1980 [54].

$$J_{LIS}(E+\Phi) = 9.9\cdot 10^8 (E+780\exp(-0.00025\,E))^{-2.65} \qquad (1.1.3-2)$$

where E and J are given in MeV and in [particles/(sr m^2 s MeV)] respectively.

2, Weber and Higbie (2003) [55] which uses recent satellite measurement of cosmic ray intensity in outer helisphere.

$$J_{LIS}(E+\Phi) = \frac{2.11 \cdot 10^4 E^{-2.8}}{1 + 5.85 E^{-1.22} + 1.18 E^{-2.54}} \qquad (1.1.3-3)$$

where E and J are given in GeV and in [particles/(sr m^2 s GeV)] respectively.

3, Usoskin (2005) based on previous approximations by Burger [36].

$$J_{LIS}(E+\Phi) = \frac{1.9 \cdot 10^4 P(E)^{-2.78}}{1 + 0.4866\ P(E)^{-2.51}} \qquad (1.1.3-4)$$

where $P(E) = \sqrt{E(E+2E_0)}$ E and J are expressed in units of [particles/(sr m^2 s GeV/nucleon)] and GeV/nucleon, respectively.

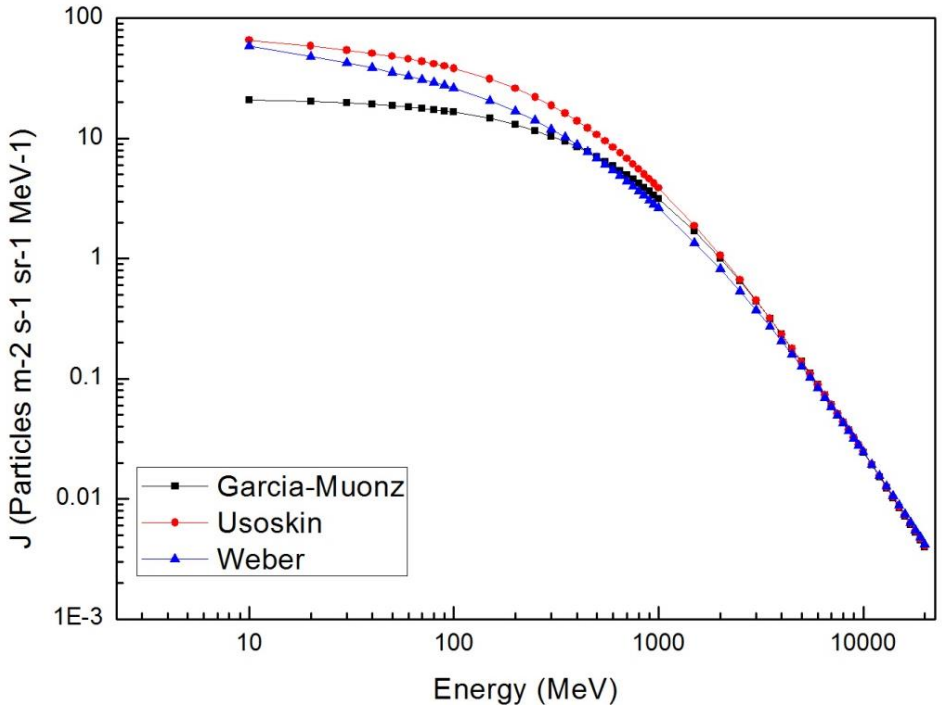

Figure 1.1.3-1: Three estimations of LIS of proton component of the cosmic radiation (Φ = 0 MeV) derived from equations 1.1.3-2,3,4.

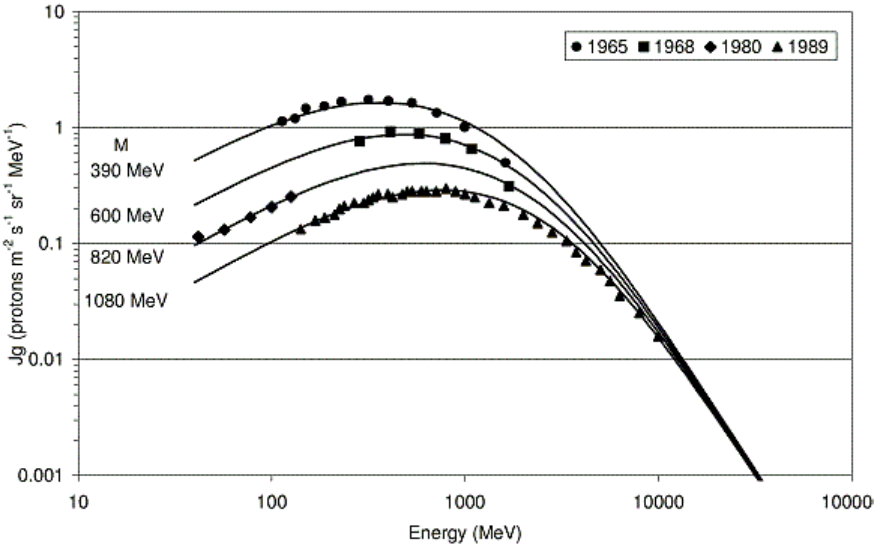

Figure 1.1.3-2: Differential cosmic-ray spectra obtained from equations 1.1.3-1,2 for different values of the modulation parameter Φ = 390, 600, 1080 MeV corresponding to the measurement performed with balloons or spacecrafts during 1965, 1968, 1980 and 1989 respectively [53].

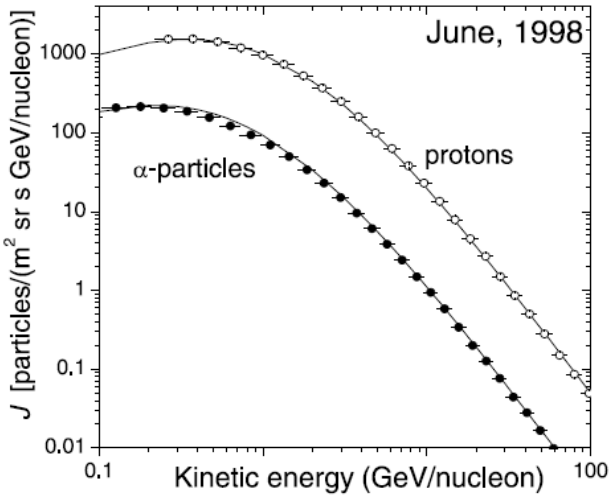

Figure 1.1.3-3: Differential energy spectra of cosmic rays. Open and filled circles depict the results of measurements. Measurements by AMS-01 in June for protons and α-particles fitted with $\Phi = 530 \pm 15$ MV. Curves are the best fit model results derived from equations 1.1.3-1,4.

All shown LIS approximations provide remarkably good fit of measured data (Figures 1.1.3-2,3) use different estimation of LIS and therefore different scaling of modulation parameter Φ. Modulation function of α-particles are related by $\Phi_\alpha = \Phi_p$ and for heavier cosmic rays, $\Phi_h = Z\,\Phi_p$.

1.2 Meteorites

Meteoroid is a small rocky or metallic body revolving in interplanetary space around the Sun. A meteoroid is significantly smaller than an asteroid; its size is ranging from small grains or particles to the size of large boulders. The light phenomenon which results when a meteoroid enters the Earth's atmosphere and vaporizes is called meteor or a shooting star. Solid bodies of extraterrestrial material that penetrate the atmosphere and reach the Earth's surface are called meteorites.

Meteoroids are mostly created by catastrophic collisions of larger extraterrestrial bodies in main asteroid belt (1.8-4.5 AU). There are hundreds of thousands of known objects in the main belt. Roughly two million objects with diameters 1 km and larger are believed to be present in the asteroid belt. The size distribution is heavily weighted toward the small end, however; less than 5,000 of those objects are thought to be larger than 10 km [33]. Meteoroids travel around the Sun in variety of orbits at various velocities. Typical meteoroid enters atmosphere at speed ranging from 1 $km.s^{-1}$ to 72 $km.s^{-1}$. The wide range in meteoroid speeds is caused partly by the fact that the Earth itself is traveling at a speed about 30 $km.s^{-1}$ as it revolves around the Sun. Meteoroids during fall through the atmosphere are heated up and partially melted. Body of meteoroids can be fragmented into pieces of various sizes or completely vaporized depending on their size, composition and angle of the fall.

Meteorite falls are those meteorites that are collected soon after being witnessed to fall, whereas meteorite finds are discovered at a later time. Fall of a meteorite can be observed by people or automated devices (fireball networks, observatories...). Meteorites are given names based on the location where they were recovered (e.g., the Peekskill meteorite fell in Peekskill, New York) [19].

1.2.1 Classification of meteorites

Based on their bulk compositions and textures, meteorites can be divided into two major categories, chondritic and anchondritic meteorites. The scheme (Figure 1.2.1-1) includes the primitive chondrites and igneously differentiated meteorites. They are further classified into groups using a classification scheme based on their oxygen isotopes, chemistry, mineralogy, and petrography. The goals of this classification scheme are to provide descriptive labels for classes of meteorites with similar origins or formation histories that could be derived from the same asteroidal or planetary body, and to reveal possible genetic links between various classes [20].

There are 15 chondrite groups, including 8 carbonaceous (CI, CM, CO, CV, CK, CR, CH, CB), 3 ordinary (H, L, LL), 2 enstatite (EH, EL), and R and K chondrites (Figure 1.2.1-1). Several chondrites cannot be assigned to the existing groups and may represent the first members of new groups. Some groups are subdivided into subgroups, which may have resulted from asteroidal processing of a single group of meteorites. Each chondrite group is considered to have sampled a separate parent body. Some chondrite groups and ungrouped chondrites show chemical and mineralogical similarities and are grouped together into clans.

Chondrites are stony (non-metallic) meteorites that have not been modified due to melting or differentiation of the parent body. They are formed when various types of dust and small grains that were present in the early solar system accreted to form primitive asteroids. They are the most common type of meteorite that falls to Earth (Table 1.2.1-1).

Table 1.2.1-1: Relative abundance of common meteorite types [77,78,79]:

Chondrites	86.2 % =>	Carbonaceous	4.4 %			
		Enstatite	1.6 %			
		Other	0.2 %			
		Ordinary	80 %	=>	H	33.8 %
					H/L	0.1 %
					L	37 %
					LL/L	0.9 %
					LL	8.2 %
Achondrites	8.2 %					
Irons	4.6 %					
Stony irons	1.0 %					

Chondrites are mostly composed from Oxygen, Iron, Silicon and Magnesium. Because they accumulated from material that formed very early in the history of the solar system, and because chondritic asteroids did not melt, they have very primitive compositions (abundances of most chemical elements well-represent entire solar system). CI chondrites seem to be nearly identical in composition to the sun for all but the gas-forming elements (e.g., hydrogen, carbon, nitrogen, and noble gases) and their study provides important clues for understanding the origin and age of the Solar System and the synthesis of organic compounds [12].

Iron meteorites are meteorites that consist overwhelmingly of an iron-nickel alloy known as meteoric iron. The chemical composition is dominated by the elements Fe, Ni and Co, which make up more than 95%. Ni is always present; the concentration is nearly always higher than 5% and may be as high as about 25% [21].

The primitive achondrites represent recrystallization or residues from a low-degree partial melting of chondriticmaterials.

Achondrites resulted from a high degree of melting of chondrites and include asteroidal (angrites, aubrites, howardites-diogenites-eucrites, mesosiderites, 3 groups of pallasites, 15 groups of irons plus many ungrouped irons) and planetary (Martian, lunar) meteorites [7,20].

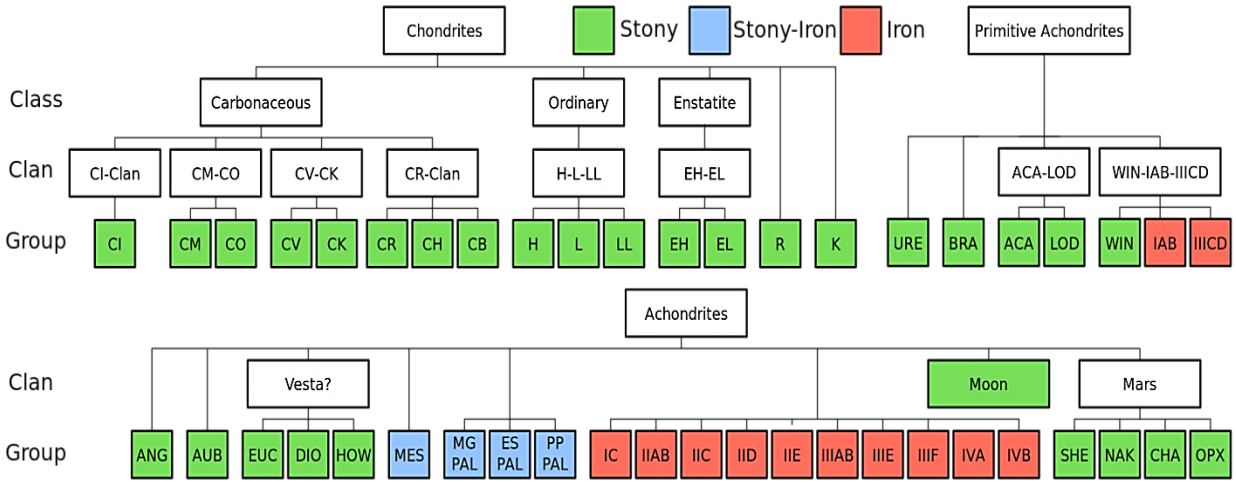

Figure 1.2.1-1: Diagram expressing the systematics of meteorite classification and showing the major meteorite divisions, classes, clans, and groups and relationships among meteorite groups [7].

1.3 Interaction of cosmic rays with matter

Matter which is exposed to cosmic radiation undergoes characteristic changes in its chemical and isotopic composition. Products formed by interaction of cosmic rays with matter are determined by several factors related to incident particles, ambient environment and composition of the target. Type of interaction process is mainly determined by the energy, mass and charge of the incident particle and chemical composition and mineralogy of the target. There are two main ways of interaction of energetic particles with matter. All charged particles continuously lose energy by ionization of atoms as they pass through matter and the damage produced by radiation can accumulate and be detected. Nuclei of low energy and high charge lose energy rapidly by ionization and come to rest. Incident particles can induce nuclear reaction with target nucleus which leads to formation of new secondary particles (proton, neutron, gamma rays…) and residual nucleus which can undergo further changes. Nuclei of high energy and low charge lose energy more slowly and frequently induce nuclear reaction before stopping.

Effective depth of interactions of cosmic rays with matter varies much with type of incident particle and its energy. Relatively low-energy particles of SCR are stopped by ionization losses in distance of several millimetres form surface and the fluxes of SCR particles as a function of depth can be calculated accurately from ionization-energy loss relations [8].

High-energy GCR particles usually produce many secondary particles especially neutrons. The flux of incident GCR particles decrease exponentially with depth and the flux of secondary particles increase with depth near surface, but then decrease exponentially with depth. Particles of GCR leave records of their interaction much deeper than particles of SCR (Table 1.1-1).

1.3.1 Cosmic rays records in solar matter

Cosmic rays continuously irradiate all matter in solar system such as planets, asteroids, meteoroids or cosmic dust and induce measurable records like cosmogenic nuclides and nuclear tracks in their bodies. Study of those records gives significant information about history of irradiated bodies as well as cosmic radiation itself. The important targets in extraterrestrial environment, for cosmic rays are the common elements like oxygen, magnesium; silicon and iron (see Table 1.3.1-1). The mass of product is similar to or less than that of target nucleus. Analysis of cosmogenic noble gases and cosmogenic radionuclides (^{53}Mn, ^{26}Al...) provide evidence that most or all classes of meteorites originate in main asteroid belt. Exposure age of a meteorite is most precisely measured with stable-radioactive pairs of nuclides.

The comparison of abundance of cosmic rays with abundances of elements in the solar system is shown in figure 1.3.1-1. The light nuclei Li, Be an B are several order of magnitude more abundant in cosmic ray radiation than in solar system and local galaxy; likewise nuclei Sc, Ti, V, Cr and Mn are few orders of magnitude more abundant in cosmic rays.

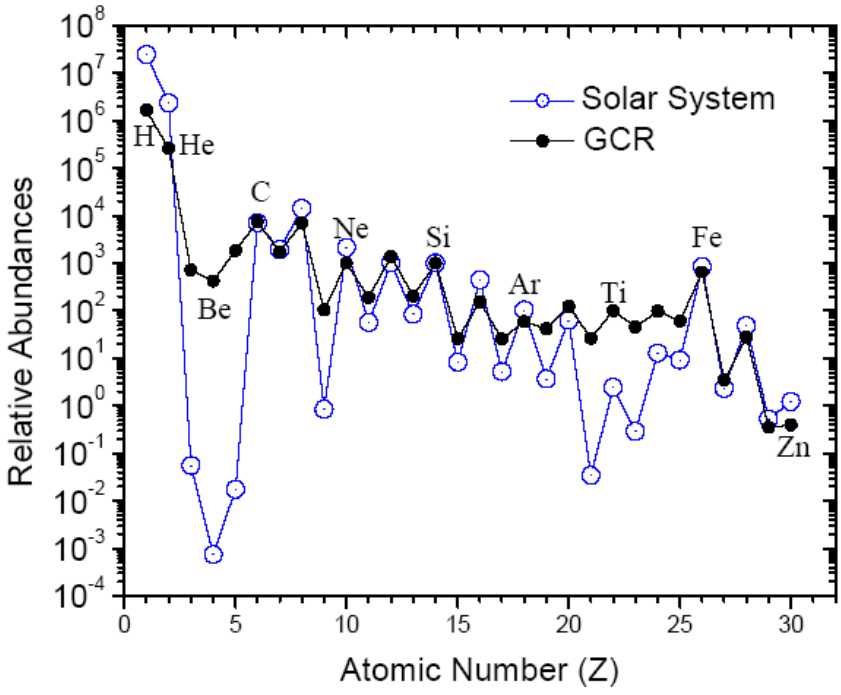

Figure 1.3.1-1: The elemental abundances of cosmogenic radiation near Earth compared to solar system abundances [45][2].

This phenomenon is well understood and is related to propagation and confinement of cosmic rays in galaxy. These elements are essentially absent as end product of stellar nucleosynthesis. They are nevertheless present in the cosmic radiation as spallation product of the abundant nuclei of carbon and oxygen (part with light nuclei) and of iron (part with heavier elements). From this knowledge one can learn something about amount of matter traversed by cosmic rays between production and observation.

Table 1.3.1-1: Cosmogenic nuclides frequently measured in extraterrestrial matter

Isotope	Half-life		Main production mechanisms
^{3}H	12.323	y	spallation on O, Mg, Si
^{3}He	stable		spallation on O, Mg, Si
^{10}Be	$1.36x10^{6}$	y	spallation on O, Mg, Si
^{14}C	5730	y	spallation on O, Mg, Si
^{21}Ne	stable		spallation on Al, Mg, Si
^{22}Ne	stable		spallation on Al, Mg, Si
^{22}Na	2.602	y	spallation on Al, Mg, Si
^{26}Al	$7.17x10^{5}$	y	spallation on Al, Si
^{36}Cl	$3.01x10^{5}$	y	spallation on Ca, Fe; $^{35}Cl(n,\gamma)^{36}Cl$
^{37}Ar	35	d	spallation on Ca, Fe
^{39}Ar	269	y	spallation on Ca, Fe, K
^{40}K	$1.28x10^{9}$	y	spallation on Fe
^{41}Ca	$1.03x10^{5}$	y	spallation on Fe, Ni; $^{40}Ca(n, \gamma)^{41}Ca$
^{46}Sc	83.79	d	spallation on Fe, Ti
^{48}V	15.97	d	spallation on Fe, Ti
^{53}Mn	$3.74x10^{6}$	y	spallation on Fe
^{54}Mn	312.3	d	spallation on Fe
^{59}Ni	$7.6x10^{4}$	y	$^{58}Ni(n, \gamma)^{59}Ni$
^{60}Co	5.27	y	spallation on Ni; $^{59}Co(n, \gamma)^{60}Co$
^{80}Kr	stable		$^{79}Br(n, \gamma)^{80}Br(\beta^{-})^{80}Kr$
^{82}Kr	stable		$^{81}Br(n, \gamma)^{82}Br(\beta^{-})^{82}Kr$
^{129}I	$1.57x10^{7}$	y	$^{129}Te(n, \gamma)^{129}Te(\beta^{-})^{129}I$
^{131}Xe	stable		$^{130}Ba(n, \gamma)^{131}Ba(2\beta^{-})^{131}Xe$
^{150}Sm	stable		$^{149}Sm(n, \gamma)^{150}Sm$
^{152}Sm	stable		$^{151}Eu(n, \gamma)^{152}Eu(EC)^{152}Sm$
^{152}Gd	$1.08x10^{14}$	y	$^{151}Eu(n, \gamma)^{152}Eu(\beta^{-})^{152}Gd$
^{156}Gd	stable		$^{155}Gd(n, \gamma)^{156}Gd$
^{158}Gd	stable		$^{157}Gd(n, \gamma)^{158}Gd$

1.3.2 Cosmic rays records in terrestrial matter

The largest number of nuclear transformations induced by cosmic rays takes place within the atmosphere, since most of the cosmic ray energy is dissipated there. Almost all transformation are produced by nucleons, contribution from mesons, muons, electrons and γ-rays is small by comparison. Air in the atmosphere is mainly composed of nitrogen ~78 %, oxygen ~21%, argon ~1% (percentage by volume) and small amount of other gases [42]. The Earth's atmosphere contains several different layers that can be defined according to air temperature (troposphere, stratosphere, mesosphere, thermosphere, and exosphere) ranging from Earth's surface to about 10 00 km altitude. Air density and pressure decreases with increasing altitude. At sea level at 15 °C air has a density of an approximately 1.225 $kg.m^{-3}$. Interaction depth of cosmic rays in whole atmosphere is approximately equal to 10 meters of water or 2 meters of rock. About 75 % of mass of the atmosphere is within 11 km from Earth's surface.

The outermost layer of the Earth's crust constitutes a second region where nuclear transformation occurs. The rate at which nuclear transformation occurs in this region is several hundred times smaller than in atmosphere, but the Earth's surface contains many elements which are not present in atmosphere contribution for particular isotope production is important [41]. At greater depths beneath the Earth's surface only muon and neutrino components of cosmic ray survive [3].

The magnetic field of the Earth (the geomagnetic field) is approximately 10^4 times stronger than the interplanetary magnetic field, however its strength has varied significantly over time in past. The geomagnetic field of the earth approximates a classical magnetic dipole and it is caused by electrical currents in the core of the Earth. The 1-100 GeV cosmic rays that produce the cosmogenic radionuclides are strongly deflected by the geomagnetic field (deflection is charge, angle and energy dependent).

For the same energy per nucleon a ^4He cosmic ray has four times the momentum of a proton of the same energy. It only has twice the electrical charge of the proton. Therefore, ^4He is less deflected from its path by magnetic field than the proton, and it may penetrate the geomagnetic field more easily, and again access to parts of the Earth that proton of the same

energy per nucleon cannot reach. To simplify the problem, it is usual convention to use the geomagnetic cut-off rigidity [2].

The geomagnetic cut-off rigidity is given by:

$$P_c = \frac{M}{R^2} \frac{Cos^4\lambda}{[(1+cos\theta.cos^3\lambda+1]^2} \qquad (1.3.2\text{-}1)$$

where M and R are the magnetic dipole moment and radius of the Earth, respectively, λ presents geomagnetic latitude, θ is angle between the trajectory of the arriving particle and the vector to magnetic West in the horizontal plane. The angle $\theta = 0°$ for cosmic ray arriving from western horizon, $\theta = 90°$ for any direction in the magnetic North-South vertical plane, and $\theta = 180°$ for cosmic rays arriving from eastern horizon.

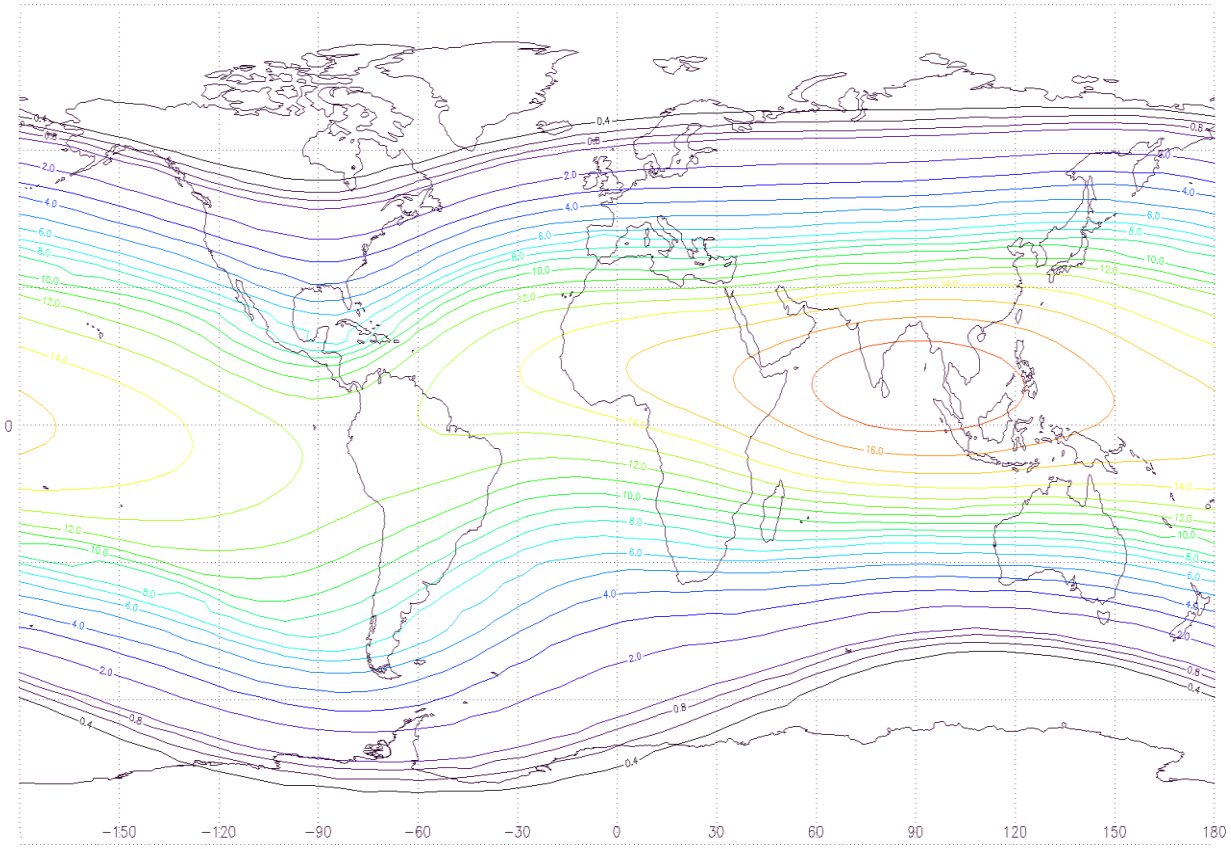

Figure 1.3.2-1: Vertical cut-off rigidities on the Earth surface evaluated for 20. march 2004 12:00 UTC in model with Tsyganenko 96 external geomagnetic field. Horizontal axis - East Longitude, vertical axis - Latitude [14].

Effects of cosmic radiation in comparison with extraterrestrial samples are weak and not preserved because outer layers of earth are in continuous motion; atoms participate in various cycles between atmosphere, biosphere, geosphere. During these cycles irradiated matter become mixed with non-irradiated matter and effects caused by cosmic rays become less observable.

In the atmosphere interaction of neutron and protons with nitrogen, oxygen, argon dominates the production rate of cosmogenic radionuclides nuclides. Many isotopes produced by cosmic rays in the atmosphere have been detected (Table 1.3.2-1). Each nuclide is characterized by specific number of protons and neutrons. To produce cosmogenic nuclide it is necessary to change the number of nucleons in the atmospheric atom. ^{14}C are almost completely produced from atmospheric nitrogen ^{14}N and oxygen ^{16}O atoms. Since the binding energy for nucleons is large > 8 MeV, this never occurs as a result of thermal atmospheric collisions processes. The majority of cosmogenic nuclides produced in atmosphere have masses below 16. Masses up to 40 are rare because of low argon weight fraction (1.3 %). Heavier cosmogenic radionuclides are very rare because of very small amounts of krypton and xenon in atmosphere. Production rate depends on: intensity of the primary cosmic rays their modulation by solar activity, and the intensity of geomagnetic field. Production rate varies also with location in the atmosphere, atmospheric depth and geomagnetic latitude, where the production take places [2].

Table 1.3.2-1: Frequently measured atmospheric cosmogenic nuclides [3].

Isotope(s)	Half-life		Main targets in atmosphere
^{3}H	12.323	y	N,O
^{3}He, ^{4}He	stable		N,O
^{10}Be	$1.36x10^{6}$	y	N,O
^{14}C	5730	y	N
^{22}Na	2.602	y	Ar
^{26}Al	$7.17x10^{5}$	y	Ar
^{32}Si	153	y	Ar
^{36}Cl	$3.01x10^{5}$	y	Ar
^{39}Ar	269	y	Ar
^{81}Kr	$2.1x10^{5}$	y	Kr
^{129}I	$1.57x10^{7}$	y	Xe

Most of the cosmogenic nuclides are produced high up in the atmosphere, and consequently atoms must travel long distance before they are stored in archives that are accessible to our investigations (ice, sediments etc.). The global atmospheric circulation varies with season, and from year to year. So even if the production rate of cosmogenic nuclide is constant, the flux of cosmogenic radionuclides reaching the archive will vary due to circulations and scavenging processes. About 1/3 of cosmogenic nuclides are deposited on the continent and are stored in ice sheets and soils. About 2/3 are removed from atmosphere into the ocean and continue their travel according to their chemical properties. Chemically reactive nuclides such as ^{10}Be and ^{26}Al attach themselves to particles and are scavenged within 500-100 years into the sea-floor sediment [2, 4].

1.4 Cosmogenic nuclides production

The production rate of cosmogenic nuclides is dependent on composition and shielding conditions (size and shape of the object, sample location within the object). For production of cosmogenic nuclides in matter, two types of reactions are the most important, spallation reactions and neutron capture reactions (Table 1.3.1-1).

The production rate P_j [atoms s^{-1} g^{-1}] of cosmogenic nuclide *j* at the depth *d* in an irradiated body with radius *R* is given by

$$P_j(R,d,M) = \sum_i N_i \sum_k \int_0^\infty \sigma_{jik}(E_k) J_k(E_k,R,d,\Phi) dE_k \qquad (1.4\text{-}1)$$

where M is modulation parameter [MeV] of primary GCR spectrum,

N_i represent number of atoms of element i per gram of material,

k is type of reacting particle (p, n, ^{4}He, pions,…),

$\sigma_{jik}(E_k)$ is energy-dependent cross section (excitation function) [cm^2] for the production of nuclides *j* from target element *i* by particle of type *k*,

$J_k(E_k,R,d,M)$ represents total flux density [cm^{-2} s^{-1} MeV^{-1}] sum of primary and/or secondary particles of type k at depth d inside body with radius *R*, when irradiated with a primary GCR spectrum of particle k characterized by a modulation parameter Φ. Note that these spectra are also dependent on the chemical composition of target body.

Starting from primary GCR spectra, the size- and depth- dependent spectra of secondary particles are calculated by Monte Carlo codes. Using experimental and theoretical cross sections it is possible to calculate production rate of particular nuclide. Further detail can be found in following sections.

Production rate is given in various units. For stable noble gases production rate is given in units $cm^3STPg^{-1}Ma^{-1}$ (STP means stable particles). $dpm.kg^{-1}$ which is mostly used in this work represents disintegration of particular nuclide per minute in kilogram of matter or pure element.

1.5 Exposure time calculation

The classic idea of a cosmic-ray exposure (CRE) age for a meteorite is based on a simple but useful picture of meteorite evolution, the one-stage irradiation model. The precursor rock starts out on a parent body, buried under a mantle of material many meters thick that screens out cosmic rays. At a time t_i, a collision excavates a precursor rock. The newly liberated meteoroid, now fully exposed to cosmic rays, orbits the Sun until a time t_f, when it strikes the Earth, where the overlying blanket of air (and possibly of water or ice) again shuts out almost all cosmic rays. The quantity $t_f - t_i$ is called the CRE age, t. To obtain the CRE age of a meteorite, we measure the concentrations of one or more cosmogenic radionuclides nuclides (^{14}C, ^{59}Ni, ^{81}Kr, ^{10}Be, ^{53}Mn, ^{41}Ca, ^{36}Cl, ^{129}I, ^{26}Al) or stable cosmogenic nuclides (^{3}He, ^{21}Ne, ^{38}Ar, ^{83}Kr, ^{126}Xe) in it. Many shorter-lived radionuclides such as ^{22}Na and ^{60}Co can also provide valuable information, but can be measured only in meteorites that fell within the last few half-lives of those nuclides (for half-life see Table 1.3.1-1, 1.3.2-2) [12].

The standard calculations for a one-stage irradiation require knowledge of cosmogenic nuclides production rates, P.

Concentration of stable cosmogenic nuclide increases with time as:

$$s = P_s t \tag{1.5-1}$$

And in the case of radioactive cosmogenic nuclide r, with decay constant λ:

$$r = \frac{P_r(1-e^{-\lambda t})}{\lambda} \tag{1.5-2}$$

By combination of equations 1.5-1 and 1.5-2 we have:

$$\frac{s}{r} = \frac{P_s}{P_r}\frac{\lambda t}{(1-e^{-\lambda t})} \tag{1.5-3}$$

Given either s and P_s, or r and P_r, or the ratios s/r and P_s/P_r , one may calculate a CRE age. The question is how to get the production rates or the ratio P_s/P_r. The CRE ages of stony meteoroids rarely exceed 100 Myr. The average ages of stony irons are typically between 50 Myr and 200 Myr; the CRE ages of irons vary with group but they rarely exceed 200 Myr [12].

1.6 Nuclear reaction and transport simulation

Productions rates of cosmogenic nuclides are calculated by using equation 1.4-1. From this equation all variable are known except flux density of nuclearly active particles $J_k(E_k, R, d, M)$. In this work transport and interaction of particles are calculated by using LAHET, HMCNP and GEANT. The accurate modelling of the production processes is prerequisite for the physical interpretation of measured depth profiles of cosmogenic nuclides and particle fluxes within the body of particular objects.

All codes used in this work are based on the Monte Carlo simulation methods. The Monte Carlo is designed for numerical processing of statistical problem (interaction of particles with matter), which can't be calculated by codes using deterministic methods. The individual events of particular process are simulated in precise order. Every event is sampled form statistical distribution to describe whole investigated phenomenon. The sampling is based on generation of random number. The method describes every simulated particle from its origin to its termination (absorption, escape form designed volume).

LCS

The LAHET (Los Alamos High Energy Transport) Code System => (LCS) has been developed at Los Alamos National Laboratory as general-purpose Monte Carlo code for particle production and transport [15]. Figure 1.6-1 shows schematic code linkage and data flow in LAHET. A common physical processes and problems can be treated by using a combination of particular codes. Codes are linked via data files, where result from one code is subsequently processed by another code.

Actual particle transport is provided by the LAHET an HMCNP codes, the PHT and MRGNTP codes are used for data merging and conversion. HMCNP and HTAPE extract data from files and provide outputs in readable form.

The LAHET is able to treat all interactions by protons, pions, muons and light nuclei, but treat neutron interactions only above a cutoff energy 20 MeV. The kinematic parameters of neutrons with energy below cutoff energy are recorded on a neutron file NEUTP (these can be processed by HMCNP). The LAHET as an internuclear cascade model uses ISABEL code, which

allows hydrogen, helium and antiprotons as projectiles. The Fermi breakup model treats breakup of light nuclei.

Since the LCS is based on coupling LAHET to HMCNP via neutron file, LAHET uses the MCNP geometry system. HMCNP is a modification of MCNP code [16,17] which accepts NEUTP, GAMTP, or COMPT file as input source.

The MCNP is a general Monte Carlo N-Particle transport code that can be used for neutron, photon, electron, or coupled neutron/photon/electron transport. Pointwise cross-section data are used. For neutrons, all reactions given in a particular cross-section evaluation (such as ENDF/B-VI) are accounted for. Thermal neutrons are described by both the free gas and S(α,β) models. For photons, the code accounts for incoherent and coherent scattering, the possibility of fluorescent emission after photoelectric absorption, and absorption in electron-positron pair production. Electron-positron transport processes account for angular deflection through multiple Coulomb scattering, collisional energy loss with optional straggling, and the production of secondary particles including K x-rays, knock-on and Auger electrons, bremsstrahlung, and annihilation gamma rays from positron annihilation at rest. Electron transport does not include the effects of external or self-induced electromagnetic fields. Photonuclear physics is available for a limited number of isotopes [16].

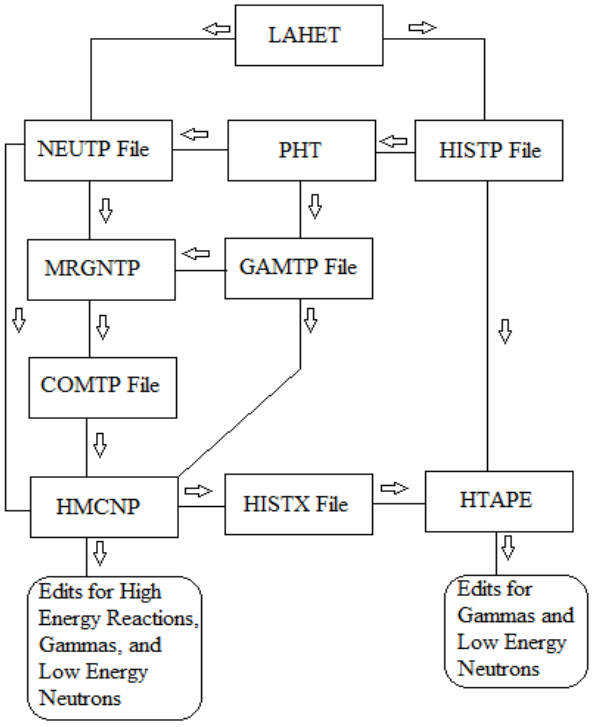

Figure 1.6-1: Code Linkage and data flow for the LCS

The GEANT is a toolkit for the simulation of the passage of particles through matter. In this work the GEANT is used for the simulation of transport and interactions of all charged particles (protons, alpha particles, electrons, pions, muons, etc.) and neutrons with energies above 20 MeV. The complete information about neutrons below 20 MeV (coordinates and kinematical parameters) is stored in a special file, which serves as an input file for the MCNP code. This code was designed to simulate transport and interactions of such neutrons.

The transition from LCS to GEANT in terrestrial cosmogenic nuclide production rate calculations was dictated by the built-in physics of these codes. The LCS model is applicable only for particles with energies of a few GeV, and with some approximations to 10 GeV. Because of the deflection of low-energy cosmic ray particles by the geomagnetic field, only particles with energies above 10 GeV are allowed to penetrate into the atmosphere at low latitudes. GEANT was written for particle physics and is well suited to study the cosmic ray interactions in the atmosphere [22].

1.7 Cross sections

A cross section is the effective area that governs the probability of some scattering or absorption event. In other words, the concept of a cross section is used to express the likelihood of interaction between particles. Values of cross sections depend on the energy of the bombarding particle and the kind of reaction. The dependence of cross section on energy is usually referred as an excitation function. The main cross section used in this work can be found in appendices.

The proton induced cross sections are fairly well known as they have been extensively studied by using accelerator techniques which can provide monoenergetic source of particles. All published proton cross sections can be found in standard nuclear reaction data libraries EXFOR, JENDL, ENDF [23,23,25]. The only important kind of reaction for production of cosmogenic nuclides via proton interaction is a spallation reaction. The threshold for proton spallation reactions is ranging from few MeV to dozen tens MeV. Measurements of proton cross sections are mostly performed by accelerators which irradiate pure target materials (usually thin foils). The particular final cross section is determined according to concentration of measured residual nuclei.

The neutron induced cross sections can be divided into three regions according to their energy. The low energy region (up to ~20 MeV), middle energy region (~20 to ~100 MeV) and high energy region.

Monoenergetic neutrons below energies of 20 MeV are most conveniently produced by reactions between the hydrogen isotopes or between protons and ^{7}Li. By proper choice of reaction type monoenergetic neutrons can be produced with negligible secondary background radiation. The bombarding energies needed to initiate the reactions are modest and can be provided by electrostatic generators. The typical reactions to be considered are ^{7}Li(p,n), T(p,n), D(d,n) and T(d,n) [26]. A neutron source can be considered to be monoenergetic if the energy spectrum consists of a single peak which has an energy spread which is much less than the energy of the peak.

For neutron of intermediate and high energies almost no experimental data exists for most reactions due to difficulties connected to design of monoenergetic neutron source. Neutron is a

particle with no electric charge, and it can't be directly accelerated by electric field to certain energy level nor can its trajectory be curved by magnetic field.

The most practical way of producing neutrons of intermediate energies are quasi-monoenergetic neutrons beams created by the bombardment of light elements with protons. For the energies under consideration here it is not possible to produce strictly monoenergetic neutron beams because the proton energy always exceeds the thresholds for particle breakup and the formation of excited states in the product nucleus. The neutron spectrum will always therefore contain a continuum of lower energy neutrons which can be filtered electronically. The most favourable targets for neutron production with proton beams in the 20–100 MeV range are generally considered to be ^{2}H, ^{6}Li, ^{7}Li and ^{9}Be [27].

For applications which require use of neutron spallation cross section of high energies proton cross sections are used instead (i.e. (n,2n) reaction is swapped with (p,pn) reaction). This is reasonable for high energies, where interaction of proton and neutron with targets is not so dissimilar due their comparable properties. This is only used in case when theoretical cross sections are unavailable or rather unrealistic [28],[29]. There are several codes which apply theoretical model of nuclear reactions in different energy regions [30],[31].

Some experimental group (Robert C.Reedy (Planetary Science Institute, USA) and Rolf Michel (Leibniz-University, Germany) have done evaluation of less consistent neutron excitation functions. Those cross sections are based on measured experimental data and using of corresponding proton reactions and theoretical estimations [32].

2. Results

This work covers five main topics: effect of pre-atmospheric shape on cosmogenic nuclide production rates, calculational model for short-lived cosmogenic radionuclides, the Chelyabinsk meteorite, the Košice meteorite and Atmospheric ^{81}Kr as an integrator of cosmic-ray flux over the past 800 kyr. Every chapter begins with introduction to the topic and description of experimental methods utilized by many scientific groups that obtained experimental data used for comparison with our model calculations. The own work of the author are calculated nucleon fluxes, depth profiles, production rates and activities of cosmogenic radionuclides presented in all investigated topics, theoretical results were obtained by model presented in chapter 2.2. The concluding section in every topic discuss primarily own results of the author.

Codes used in this work are Lahet, HMCNP4, HTAPE [15] (for examples of used inputs see appendices). Newer version of MCNP code has been released (MCNPX, MCNP6), but comparison of codes [59] shows no remarkable changes in results.

The model calculation used in this work takes into account only GCR protons as primary particles. This limitation comes from design of used codes. GCR alpha particles need to be considered in every realistic Monte Carlo simulation. The primary spectra of GCR protons and alpha particles are very similar and difference in cross section for an emission of secondary protons and neutrons by reactions of GCR protons and alpha-particles are also small. Thus, the contribution of alpha particles can be simply included by applying proper normalization factor, which was found on basis of particle flux study [34].

Cross section used in this work comes mostly from standard databases EXFOR [23], ENDEF [24], JENDL [25] in some cases when experimental cross sections are not available gaps in excitation function are filled with theoretical cross sections tallys [30]. Statistical uncertainties from simulation of particle interaction are low (usually less than ~ 2%). Results are also influenced by not known systematic errors related to a use of theoretical and experimental cross sections from various models and experimental groups

2.1 Effect of pre-atmospheric shape on cosmogenic nuclide production

Productions rates of cosmogenic nuclides are dependent on few major factors such as: incident particle fluxes, the meteoroid's preatmospheric shape and size, and its bulk chemical composition. Size effects [80] and bulk chemical composition effects [81] have been studied in details in the past years. Effects related to changes in production rate of cosmogenic radionuclides caused by incident GCR particles are discussed in chapter 2.2; therefore we concentrate our attention in this chapter on effects of the parent body shape.

Extraterrestrial objects revolving in space may have many different shapes from symmetrical to very irregular. One can say that shape irregularity of an extraterrestrial object is related to its size; whereas larger bodies (planets, moons) tend to have more symmetrical shape, smaller solar system bodies like asteroids and meteoroids are usually fragments from collisions and tend to have very irregular shapes.

Our calculations were carried out for a meteorite with composition of an average L chondrite, which belong to the most frequent meteorite types (Table 1.2.1-1). Sizes of investigated spherical meteoroids were 90 and 180 cm in diameter. Such range of diameters covers the most typical sizes of meteoroids and allowed us to investigate potential changes in shape effects related to the various sizes of meteoroids. Volumes and masses of modelled object with different geometries were equal. This allowed us to distinguish size and shape effects in final data.

The Peekskill meteorite used for comparison of experimental data with simulation has fallen on 9th October 1992 in Peekskill, New York [61]. The fall of the meteorite was observed and recorded by many observers. Object was fragmented into over 70 pieces. Analysis of meteorite fragments classified the Peekskill meteorite as H6 chondrite [61]. Based on dynamic data of the observed fireball a flattened geometry for the Peekskill meteoroid has been suggested [62]. Also measured activities of cosmogenic radionuclides, especially ^{60}Co, suggest either multistage exposure of the meteorite or flattened geometry [61].

2.1.1 Simulations

The nucleon spectra were calculated by using the LCS and MCNP. Both codes are capable to calculate particles transport in particular material. Having calculated particle fluxes the production rates of cosmogenic nuclides are calculated by folding these spectra with experimental and theoretical cross sections of nuclear reactions leading to the production rate of a particular nuclide.

The geometries investigated in this work were sphere with radius 45 cm, ellipsoids with various ratios between semiaxes (a:b:c = 3:2:1 , a:b:c = 3:1:1) and cylinders with length : radius ratios (l : r = 4 : 1, 2 : 1). All investigated spheres, ellipsoids and cylinders had equal volumes. Model objects were divided into concentric shells with specific thickness dependent on distance from the surface of the meteoroid. In all shells proton and neutron fluxes were calculated. Particle fluxes for sphere were averaged through the whole surface of the every shell. In the cases of ellipsoids and cylinders fluxes were calculated for the small areas created by interception of particular surface and small cylinder with radius 2.5 cm crossing the modelled body (see figure 2.1.1-1). This approach allowed to calculate particle fluxes and production rate of radionuclides in vicinity of major axis of a particular geometry (figures 2.1.2-1,2,4).

We have also investigated larger geometries; spherical meteoroid with radius 90 cm and ellipsoidal meteoroid with the same ratios between semiaxes as in the previous cases (labelled as Ellipsoid_321b). Volumes of both geometries were equal. In this case radius of cylinder used in elliptical geometry was 4 cm (for results see figure 2.1.2-3).

All simulated geometries were irradiated by averaged GCR flux with Φ = 550 MeV and energy integrated primary cosmic ray particle flux 4.8 part. cm^{-2} s^{-1}(Garcia-Muonz approach see chapter 1.1.3).

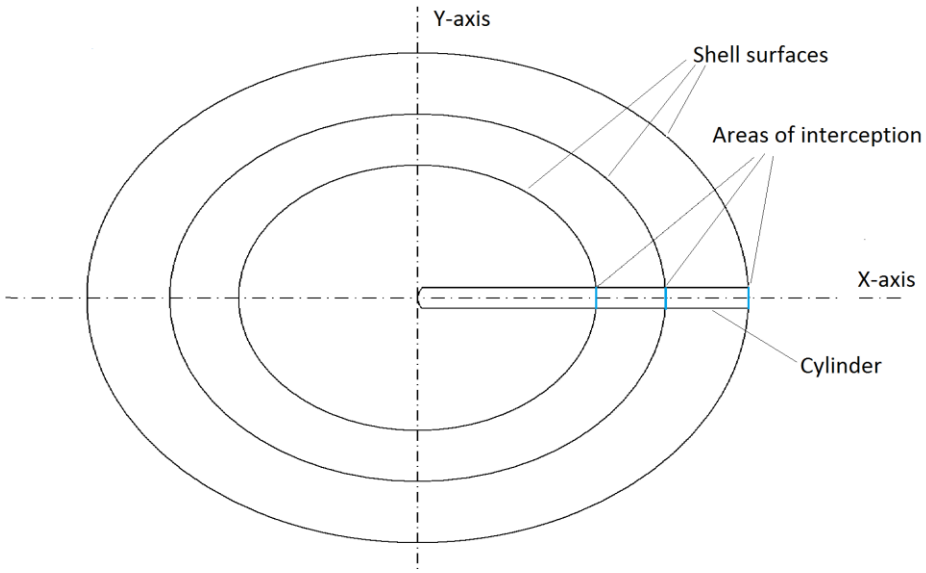

Figure 2.1.1-1: Cross section through the ellipsoidal geometry. Particle fluxes were calculated in small interception areas.

Characteristic parameters of modeled bodies:

Smaller geometries:

Sphere : R = 45 cm

Ellipsoid_321 : a : b : c = 3 : 2 : 1 → a = 74.29 cm b = 49.53 cm c = 24.76 cm

Ellipsoid_311 : a : b : c = 3 : 1 : 1 → a = 93.6 cm b = 31.20 cm c = 31.20 cm

Cylinder_21 : l : r = 4 : 1 → l = 124.8 cm r = 31.2 cm

Cylinder_11 : l : r = 2 : 1 → l = 78.6 cm r = 39.3 cm

Larger geometries:

Sphere : R = 90 cm

Ellipsoid : a : b : c = 3 : 2 : 1 → a = 148.59 cm b = 99.06 cm c = 49.53 cm

R – radius of sphere, a,b,c – semiaxes of ellipsoids, l – length of cylinders, r – radius of cylinders

2.1.2 Results and discussion

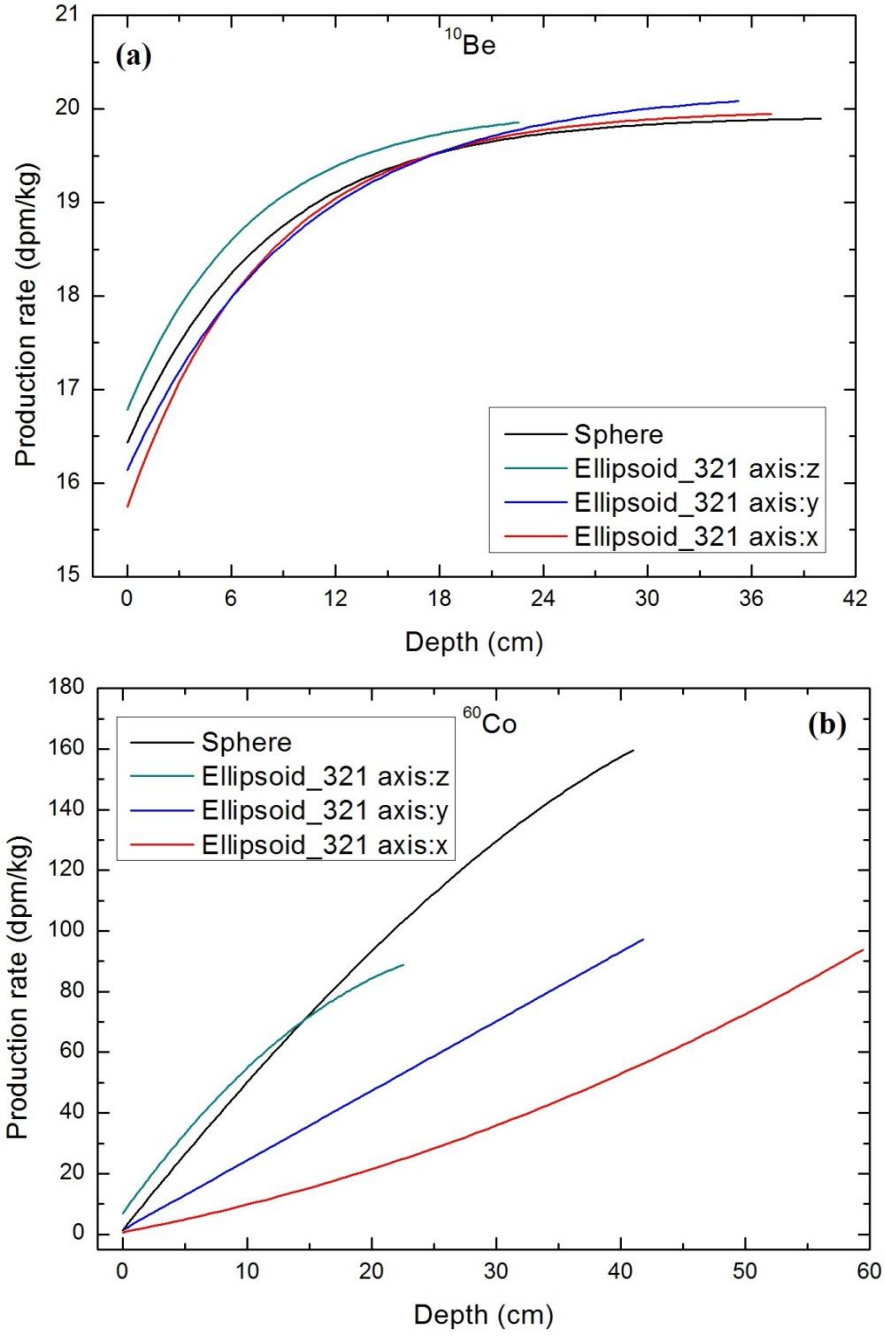

Figure 2.1.2-2: Depth profile for ellipsoidal geometry with semi-axes ratio 3:2:1 (x:y:z) in comparison with spherical geometry (R = 45 cm)

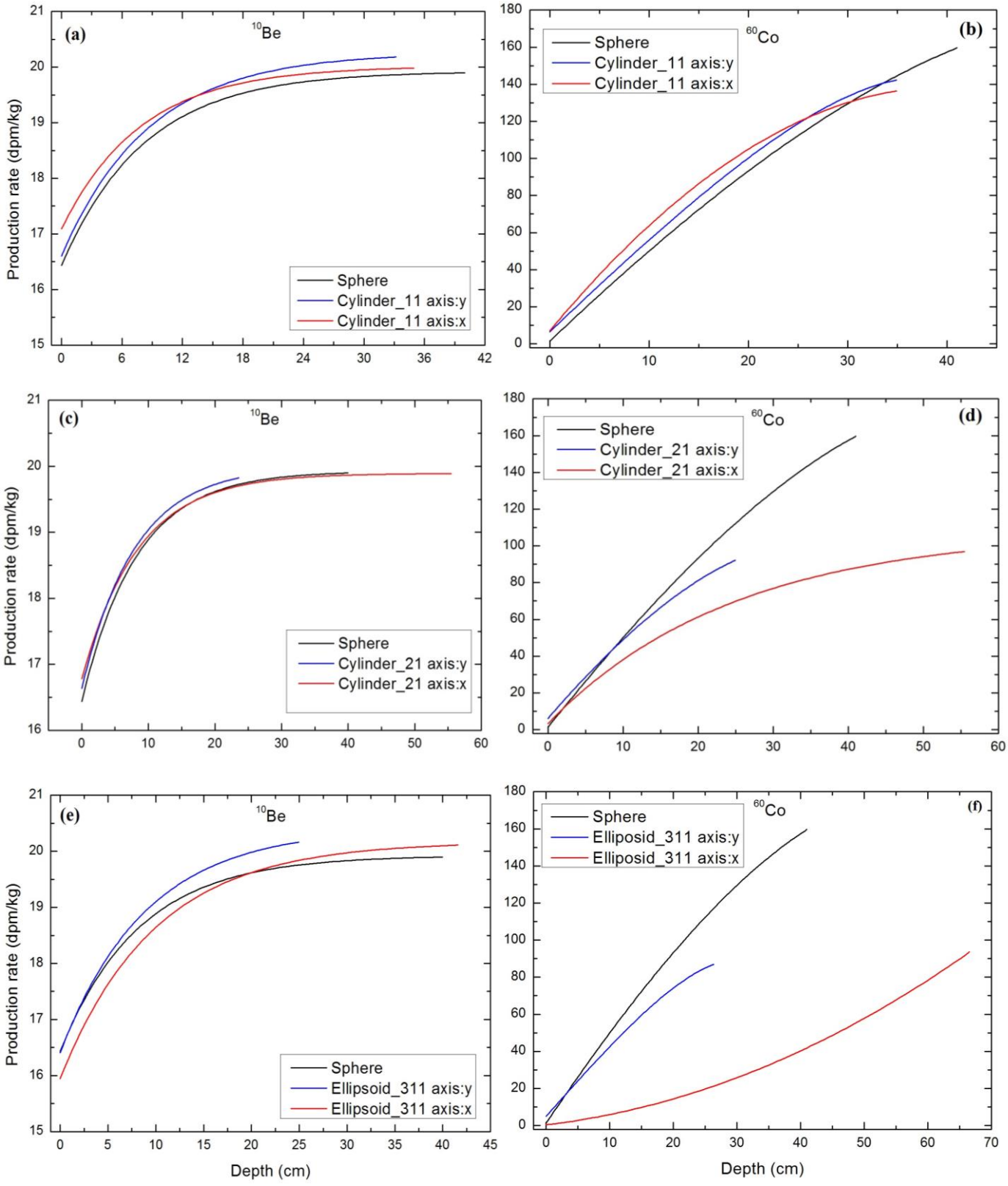

Figure 2.1.2-3: Depth profile for cylinders and ellipsoid with various parameters in comparison with spherical geometry (R = 45 cm)

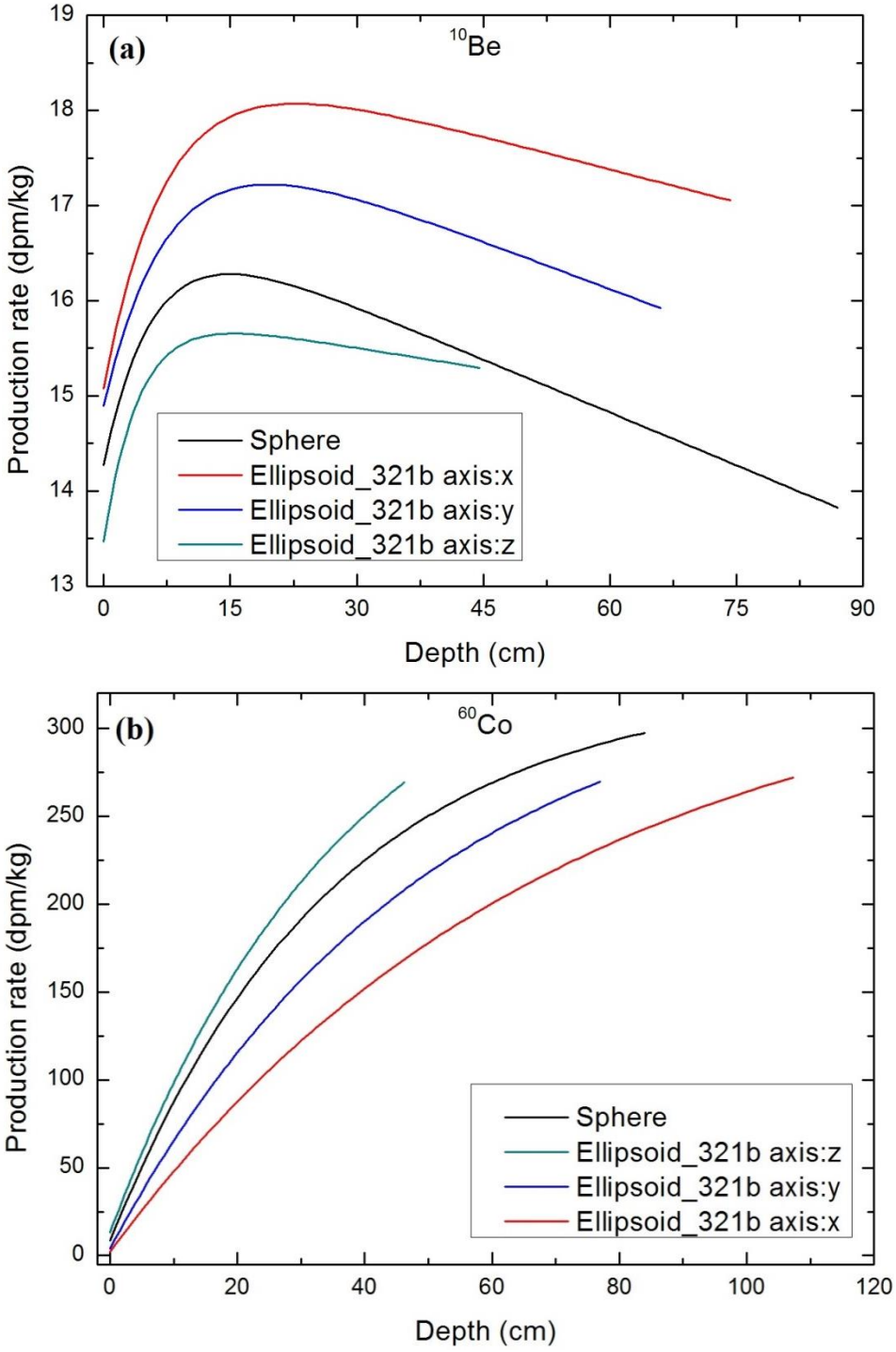

Figure 2.1.2-4: Depth profile for ellipsoidal geometry with semi-axes ratio 3:2:1 (x:y:z) in comparison with spherical geometry (R = 90 cm)

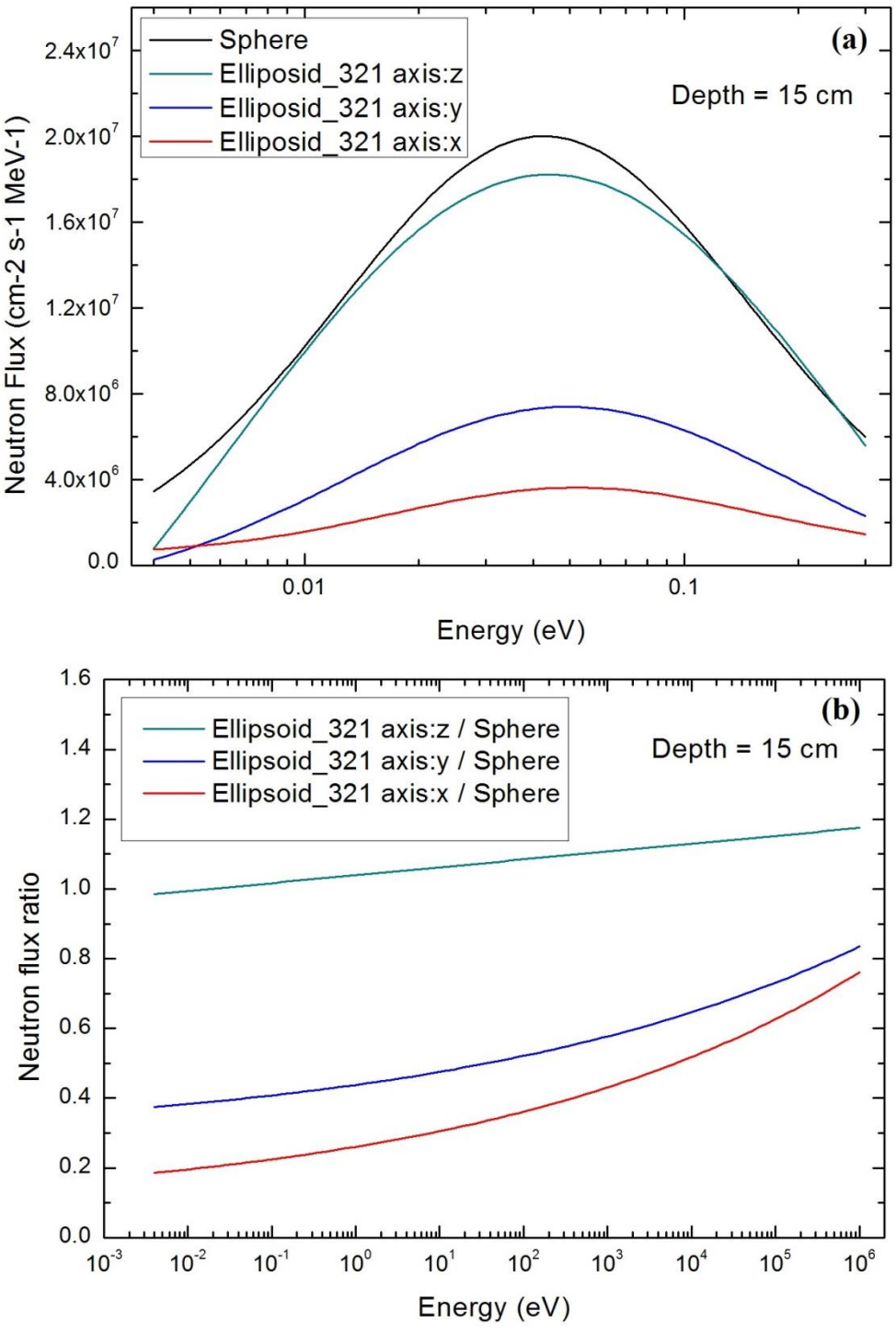

Figure 2.1.2-5: a, Comparison of the low-energy neutron fluxes in vicinity of semi axes of ellipsoid and sphere at depth of 15 cm.

b, Ratio of neutron fluxes in ellipsoid to neutron flux in sphere at depth of 15 cm

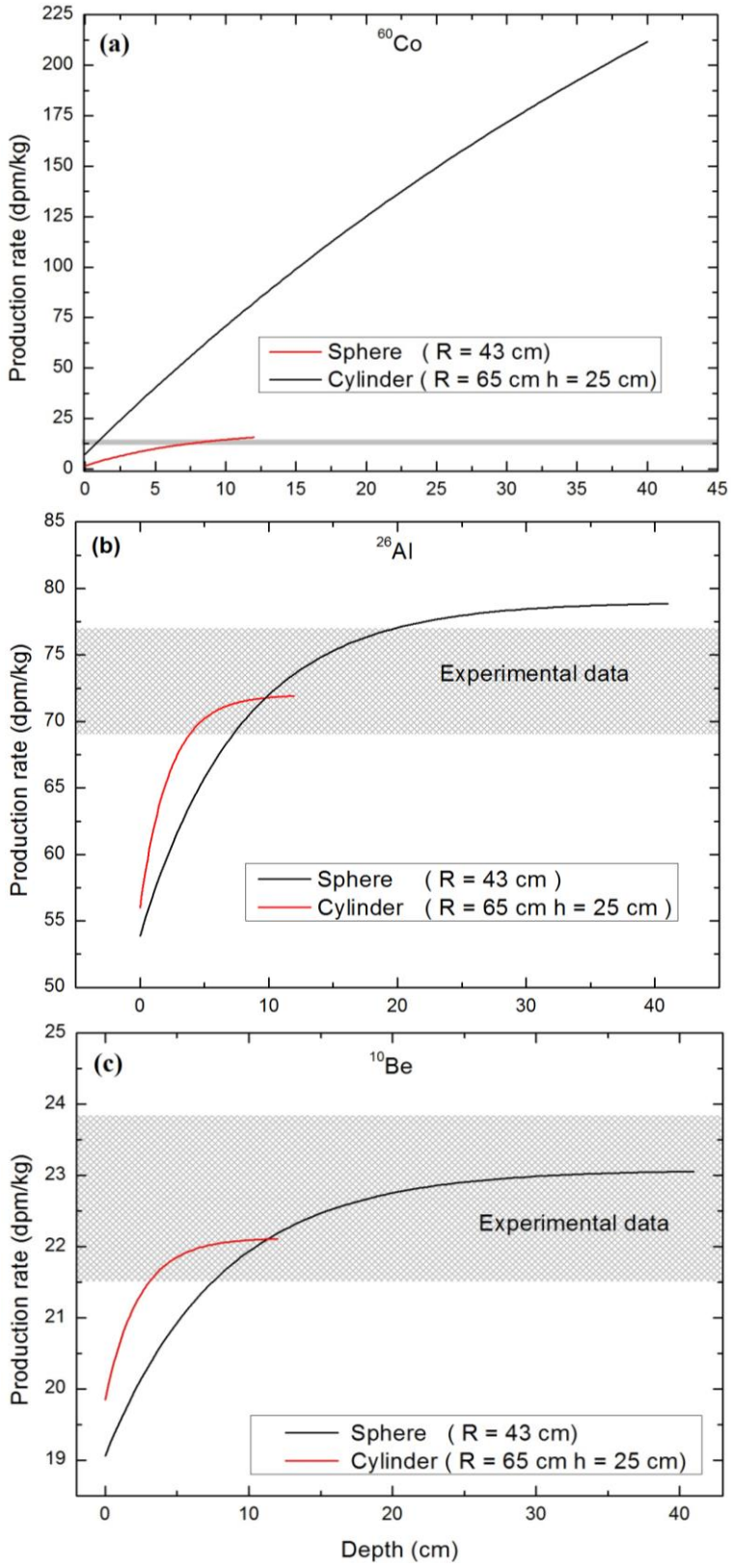

Figure 2.1.2-6: Depth profiles of ^{60}Co, ^{26}Al, ^{10}Be in the Peekskill meteorite for cylindrical and spherical geometry in comparison with range of measured experimental data (grey).

The LCS/HMCP code has been used for an investigation of effect of preatmospheric shape on production rates of cosmogenic radionuclides. The geometries investigated in this work were a sphere with radius R = 45 cm (which represent medium sized meteoroid). Further an ellipsoidal geometry with various ratios between semiaxes (3:2:1, 3:1:1), and cylindrical geometries with various length to radius ratios (4:1, 2:1). The objects were divided into concentric shells. Volume of modelled geometries was equal and average bulk chemical composition corresponds to L chondrite. For the sphere particle fluxes were calculated over the whole surface of the shell and in the case of ellipsoids and cylinders fluxes were calculated in the small area in the vicinity of major axes for the particular geometry. The cosmogenic radionuclides calculated are ^{10}Be (as a product of high-energy spallation reactions) and ^{60}Co (as a product of low-energy neutron capture). Results from these simulations are showed on figures 2.1.2-2,3,5. As one can see from figures 2.1.2-2a 2.1.2-3a,c,e, for the meter-sized meteoroid production rates for ^{10}Be are insensitive to shape of the preatmospheric body as the simulated depth profile for all axes of all geometries are almost identical and small differences in calculated depth profiles are rather issue related to statistic. The production rates of ^{60}Co are significantly different from those of ^{10}Be. Figures 2.1.2-2b and 2.1.2-3d,f show that production rate of ^{60}Co vary significantly and this variation is related to the deformation of an object. One can see that for the same depth within the meteoroid's body but for the different axis very different production rate is obtained. Further, all depth profiles converge to the same value (in the centre of meteoroid) but this value is lowered in comparison with maximal value obtained in the case spherical geometry. This is not the case for the geometry displayed on figure 2.1.2-3b. This geometry is cylindrical with length to radius ratio 2:1, which means that bulk of this object is similar to sphere with rather deformed surface (the length of the main object's axes are the same). Calculated depth profiles of ^{10}Be and ^{60}Co lead to the conclusion that the shape of the preatmospheric body rather influences particles of lower energies than those of higher energies. This effect is demonstrated on figure 2.1.2-5 a,b, where figure a, shows differences in the fluxes for simulated ellipsoidal geometry in a short energy interval and figure b, shows ratios of fluxes on semiaxes of ellipsoid to fluxes in sphere which are obviously differ for lower energies and tend to converge with increasing energy. This investigation clarifies calculated depth profiles and theirs features. Explanation for observed effects is based on number of particles which escape from investigated body. Particle entering the body of meteoroid is involved in series of reactions and create many secondary particles. During

this process particles either lose their energy or are absorbed. Considering shown examples we can say that the more is axis of an object elongated (and other shortened in comparison with spherical equivalent) in one direction the more is particle flux lowered due to reduced length for cascade development. This effect explain difference between particle fluxes and production rates in vicinity of axes of modelled bodies and also reduced maximal value reached in centre of the objects in comparison to value reached in sphere.

Considering ~2 meter-sized geometries (Figures 2.1.2-4a,b) one can see different depth profiles form those for ~1 meter-sized geometries. This is due to the additional effect related to the size of modelled bodies. In the case of ^{60}Co (Figure 2.1.2-4b) similar results are reached (as in previous case) but differences among production rates on axes are lowered and also maximal value in comparison to sphere is similar. This is due to the additional space for cascade development added by enlarging the size of meteoroid resulting into slight compensation of differences in depth profiles. The depth profiles of ^{10}Be (Figure 2.1.2-4a) show not only remarkable differences in production rate for the same depth but also inverted effect, where production rate is reduced on shortest axis (and sphere) and increased on longer axes at the same depth. The shape of depth profile curves is rising to about 15-20 cm of depth then follows slow decrease. This behaviour is related to size of modelled object and flux intensity of high-energy secondary particles. Flux is rising due to very high energy of primary particles, which induce cascades of particles of lower energy until they reach energy at which corresponding excitation function for ^{10}Be production reaches its maximum, but decrease of energy continues after that and naturally also production rate of ^{10}Be starts decreasing with depth. In conclusion flattening renders the interior of the meteoroid to more accessible by high-energy particles, while increasing leakage of particles with lower energies.

The Peekskill meteorite was modelled as H chondrite with specific composition and with the proposed flattened geometry [61]. The modelled geometry was cylindrical with radius 65 cm and height of 25 cm and spherical geometry was modelled with radius 43 cm. The results of simulations shown on figures 2.1.1-6a,b,c show sufficient agreement for both proposed geometries in the case of ^{10}Be and possibly also for ^{26}Al (figures 2.1.2-6b,c). The comparison of depth profiles of ^{60}Co for spherical and cylindrical geometry yet shows large differences and measured experimental data are in better agreement with cylindrical geometry. This is caused by

number of particles escaping form particular geometry (as it was already described in previous section). In the case of the cylindrical geometry, the contribution to the production rate is low due to small base to centre distance and low effective cascade development from lateral side of the cylinder. The precise determination of the pre-atmospheric shape of a meteorite is not really possible due to very deformed shapes of real meteoroids; however approximation used in our work suggest possible explanation of measured data.

2.2 Calculation model for short-lived cosmogenic radionuclides

As we discussed in chapter 1.1.1 processes in the Sun and solar activity notably affects processes in heliosphere through generation of a perturbing heliospheric magnetic field. Those changes influence intensity of GCR flux in solar system mainly during eleven-year Schwabe cycle and the 22-year solar magnetic polarity cycle (other cycles are less pronounced). Variation in solar activity can induce only negligible effects on production of long-lived cosmogenic radionuclides as ^{26}Al ($T_{1/2}$ = 7.17x10^5 y), ^{53}Mn (3.74x10^6 y), ^{10}Be (1.36x10^6 y). This is due to the fact that activities measured in meteorites are produced by average GCR flux represented with modulation parameter Φ = 550 MeV [36]. Mentioned nuclide require millions years to reach their saturation and therefore mentioned cycles average out. If we consider short-lived radionuclides with half-lives ranging from days to few years one can expect much more noticeable effects caused by primary flux intensity variation during solar cycles

Equation, which describes production of unstable isotope during irradiation by invariable source can by written as:

$$\frac{dN}{dt} = -\lambda N(t) + P_r \qquad (2.2\text{-}1)$$

where N(t) - number of radionuclides, λ - decay constant, P_r - constant production rate. (P_r is given by composition, size, shape, depth within a meteoroid and invariable source)

with solution in the form:

$$N(t) = \frac{P_r}{\lambda}(1 - e^{-\lambda t}) \qquad (2.2\text{-}2)$$

If we consider long-enough time (according to half-life of particular radionuclide) equation 2.2-1 can be simplified to the form:

$$A \cong P_r \qquad (2.2\text{-}3)$$

The equation 2.2-3 describes activity of radionuclides in equilibrium, where activity in time reaches its saturated state and it's equal to production rate. This condition is valid if the half-life of particular radionuclide much longer than length of solar cycle.

In the case of short-lived cosmogenic radionuclides situation can't be described and solved as simple as in the case of long-lived cosmogenic radionuclides due to large variation in GCR particle fluxes over the solar cycle (Figure 2.2-1). In this case we can't use averaged GCR particle flux due to current activity of radionuclide is produced in short period of time during the solar cycle.

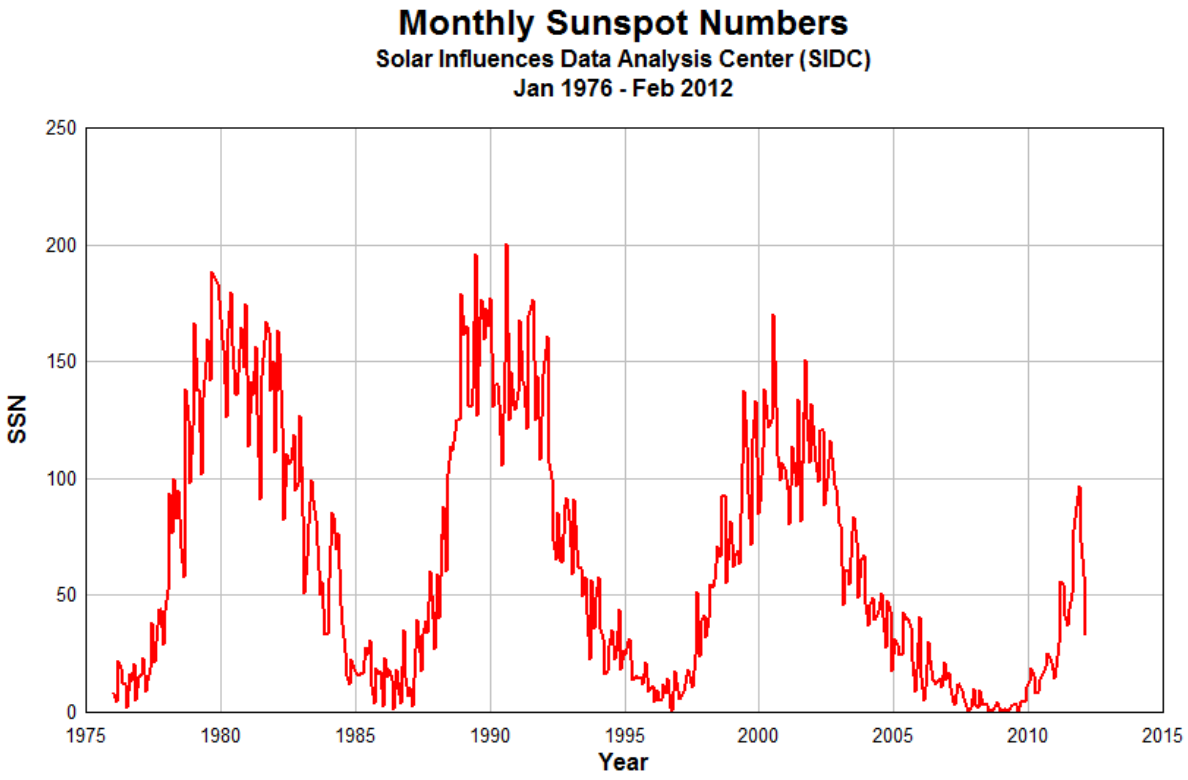

Figure 2.2-1: Solar activity in past decades represented through the number of sunspots [37]

2.2.1 Calculation model

Our effort here is to find the way to calculate production of a radionuclide with short half-life with consideration of temporal variation in source of radiation.

For this purpose we have modified equation 2.2-1 to a form:

$$\frac{dN}{dt} = -\lambda N(t) + P_r(t) \qquad (2.2.1\text{-}1)$$

And we were looking for exact formula for production rate $P_r(t)$.

Using equation (1.1.3-1,4) we were able to obtain GCR spectrum and effective coefficients for various modulation parameters Φ (Table 2.2.1-1).

We applied calculated effective coefficients and GCR source spectrum to a chosen meteoroids (Chelyabinsk, Košice) and obtained production rates per every depth and every chosen radionuclide for a spectrum of chosen modulation parameters (Φ = 250 - 1400) which are covering variation in solar cycles in past decades.

Table 2.2.1-1: Table of effective fluxes derived from equations 1.1.3-1,4 (Usoskin)

Φ –Modulation parameter (MeV)	**Effective flux** (particles cm^{-2} s^{-1})
250	9.202
550	6.156
800	4.823
1000	4.096
1200	3.546
1400	3.116

*Uncertainties of calculated values are negligible as they come only from numerical integration.

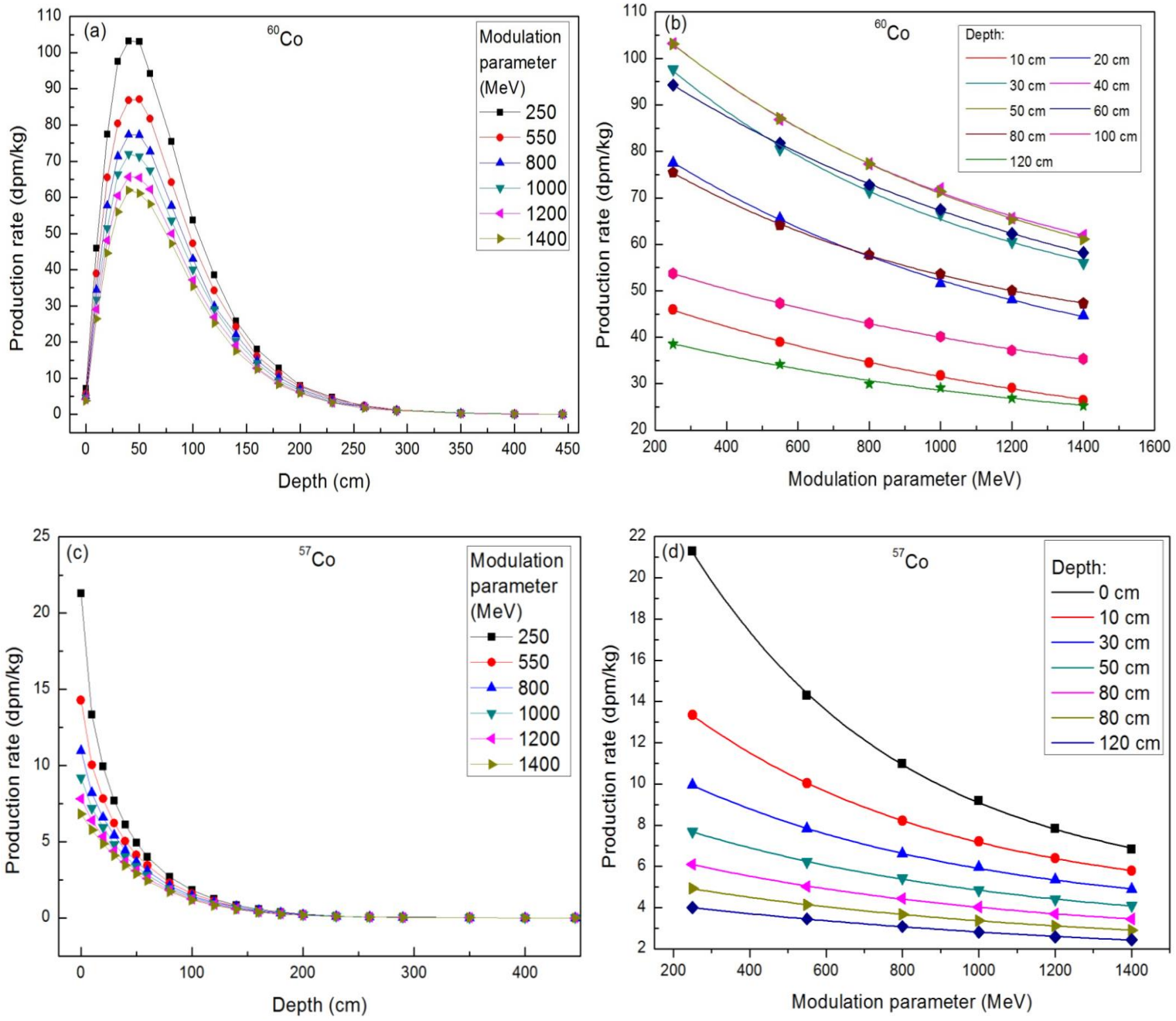

Figures 2.2.1-1: (a),(c) - depth profile of ^{60}Co, ^{57}Co in Chelyabinsk meteorite for various values of modulation parameter.

(b),(d) - production rate in the specific depth in the Chelyabinsk meteorite as a function of modulation parameter fitted by exponential function: $ae^{b\emptyset(t)} + e$.

As we can see from shown example (Figures 2.2.1-2b,d) all calculated dependences of production rate for particular radionuclide in specific depth on modulation parameter can be fitted well by simple exponential function $f = a\, e^{b\Phi(t)} + e$. This dependence follows directly from the shape of GCR spectrum given by equations 1.1.3-1,4. Fit of experimental data with this function is sufficient for every simulated meteorite of various sizes, composition and for every particular depth and radionuclide (despite decreasing tendency with depth). With this consideration equation to 2.2.1-1 can be adjusted to:

$$\frac{dN}{dt} = -\lambda N(t) + ae^{b\Phi(t)} + e \qquad (2.2.1\text{-}2)$$

Further use of equation 2.2.1-2 requires knowledge of changes of modulation parameter Φ over the periods of solar cycle. The Data required for this purpose are measured by neutron monitors and are consequently evaluated in order to obtain dependence on modulation parameter Φ (figure: 2.2.1-2) [36,38].

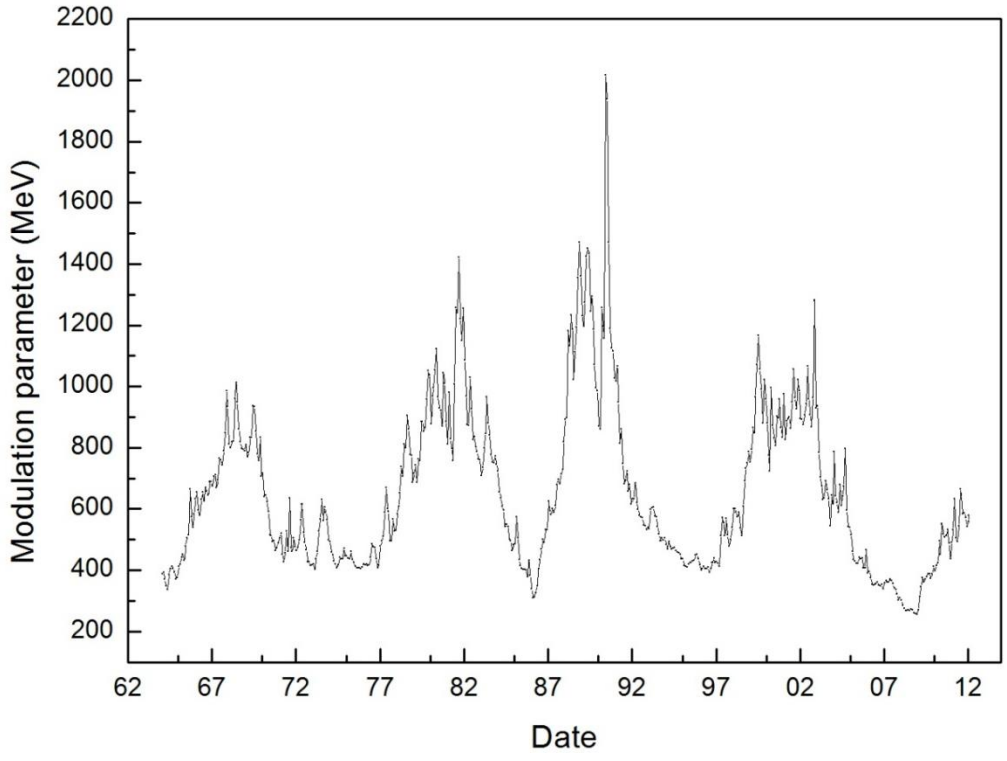

Figure 2.2.1-2: Time profile of reconstructed modulation parameter ø. Mean 68% uncertainties are 140 MeV for July 1936 to January 1951; 44 MeV for February 1951 to March 1964; 26 MeV since April 1964. [36][38].

The activity of a particular radionuclide in given time t_s within a specific depth of a meteoroid can be obtained by solving differential equation 2.2.1-1. Solution can be found with use of a numerical methods and proper fit of the modulation function (2.2.1-2). In this we have to consider the changes in GCR flux in the period of the last ~7 half-lives for particular radionuclide. The most important contribution to the production rates comes from period 2-3 half-lives before t_s (If started with $N_0 = 0$, => 0 concentration of calculated radionuclide).

Based on fact that Φ function data are measured on daily basis ø function can be split into small parts (days or months) which provide 3960 or 132 points per 11-years long cycle and one can use linear approximation among measured data and adjust equation 2.2-5 to the form:

$$\frac{dN}{dt} = -\lambda N(t) + ae^{b(ct+d)} + e \qquad (2.2.1\text{-}3)$$

where N(t) - number of particular radionuclides, λ - decay constant of particular radionuclide, coefficients a,b,e come from fit of exponential function across the chosen Φ parameters and coefficients c and d come from linear approximation of Φ function between chosen time intervals (days, months).

In the next few steps analytical solution for equation 2.2.1-3 will be shown:

By adding $\lambda N(t)$ to equation 2.2.1-3

$$\frac{dN(t)}{dt} + \lambda N(t) = ae^{b(ct+d)} + e$$

Multiplied by $e^{\lambda t}$

$$e^{\lambda t}\frac{dN(t)}{dt} + N(t)\lambda e^{\lambda t} = e^{\lambda t}(ae^{b(ct+d)} + e)$$

With consideration to $\frac{de^{\lambda t}}{dt} = \lambda e^{\lambda t}$

$$e^{\lambda t}\frac{dN(t)}{dt} + N(t)\frac{de^{\lambda t}}{dt} = e^{\lambda t}(ae^{b(ct+d)} + e)$$

Using rule $g\frac{df}{dt} + f\frac{dg}{dt} = \frac{d(f.g)}{dt}, where\ g = e^{\lambda t} and\ f = N(t)$

$$\frac{d(N(t)e^{\lambda t})}{dt} = e^{\lambda t}(\ ae^{b(ct+d)} + e)$$

Integrated

$$N(t)e^{\lambda t} = e\int e^{\lambda t} + \ ae^{bd}\int e^{t(bc+\lambda)}$$

$$N(t)e^{\lambda t} = \frac{e}{\lambda}e^{\lambda t} + \ e^{\lambda t}\frac{a}{bc+\lambda}e^{b(ct+d)} + K$$

Multiplied by $e^{-\lambda t}$

$$N(t) = \frac{e}{\lambda} + \ \frac{a}{bc+\lambda}e^{b(ct+d)} + Ke^{-\lambda t}$$

If we consider $t_0=0$ *and* $N(t_0)=N_0$

$$N_0 = \frac{e}{\lambda} + \frac{ae^{bd}}{bc+\lambda} + K$$

Number of radionuclides in particular time t can be written as:

$$N(t) = \frac{e}{\lambda} + \ \frac{a}{bc+\lambda}e^{b(ct+d)} + e^{-\lambda t}(N_0 - \frac{ae^{bd}}{bc+\lambda} - \frac{e}{\lambda})$$

$$N(t) = \frac{e}{\lambda}(1-e^{-\lambda t}) + \ \frac{ae^{bd}}{bc+\lambda}(e^{bct} - e^{-\lambda t}) \ + N_0e^{-\lambda t} \qquad (2.2.1\text{-}4)$$

Multiplication by λ leads to final form for the activity

$$A(t) = e(1-e^{-\lambda t}) + \ \frac{\lambda ae^{bd}}{bc+\lambda}(e^{bct} - e^{-\lambda t}) \ + A_0e^{-\lambda t} \qquad (2.2.1\text{-}5)$$

The equation 2.2.1-5 describes activity of a radionuclide at specific depth within a meteorite in a small time interval (day, month). The Equation takes into account production influenced by variable source of radiation (using linear change in a very small time interval) and natural decay of certain radionuclide. Term A_0 represent activity at the beginning of the time interval and equation is recursive, so it should be applied multiple times in the way that *A(t)* from previous time period is used as A_0 in subsequent time period. This approach allows us to precisely calculate activity of particular radionuclide over a long time period (limited by the experimental data). Thus provides a way to reconstruct changes of activity of a particular radionuclide influenced by solar activity in long time before the fall of the meteorite.

2.2.2 Results

We have applied approach described in previous section on known meteorites falls Chelyabinsk and Košice and we have reconstructed production of short-lived radionuclides in those meteorites many years back from a moment of the fall (figures 2.2.2-1,2). Composition, size, density, measured experimental data of cosmogenic radionuclides and further details used in the simulation of the Chelyabinsk and the Košice meteorite are discussed in chapter 2.3 and 2.4 respectively. The function of modulation parameter used in this calculation is evaluated for distance of 1 AU from the Sun and therefore activities of cosmogenic radionuclides are calculated for meteorites orbiting at 1 AU.

For the approximate evaluation of relative changes in production of cosmogenic radionuclide simple formula has been used:

$$A_{\Delta} = \frac{A_{(\max)} - A_{(\min)}}{A_{(\min)})} * 100\% \qquad (2.2.2\text{-}1)$$

Where $A_{(max)}$ *and* $A_{(min)}$- represents maximal and minimal calculated activity of specific radionuclide in a meteorite during solar cycle.

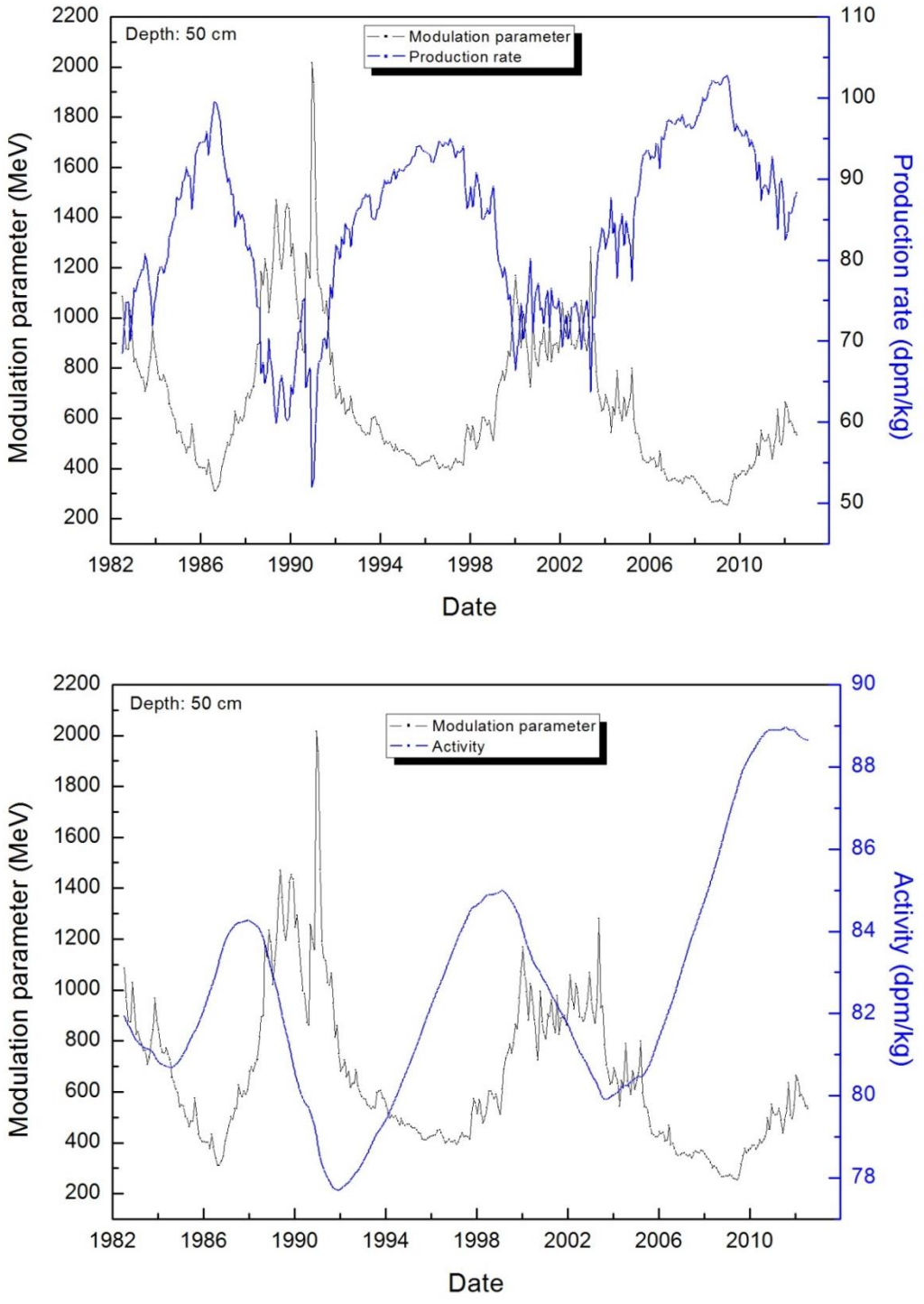

Figure 2.2.2-1: Reconstructed production rate (Up) and activity (Down) of ^{60}Co (5.27 y) in the Chelyabinsk meteorite for a chosen depth. Calculated data are shown together with function of modulation parameter.

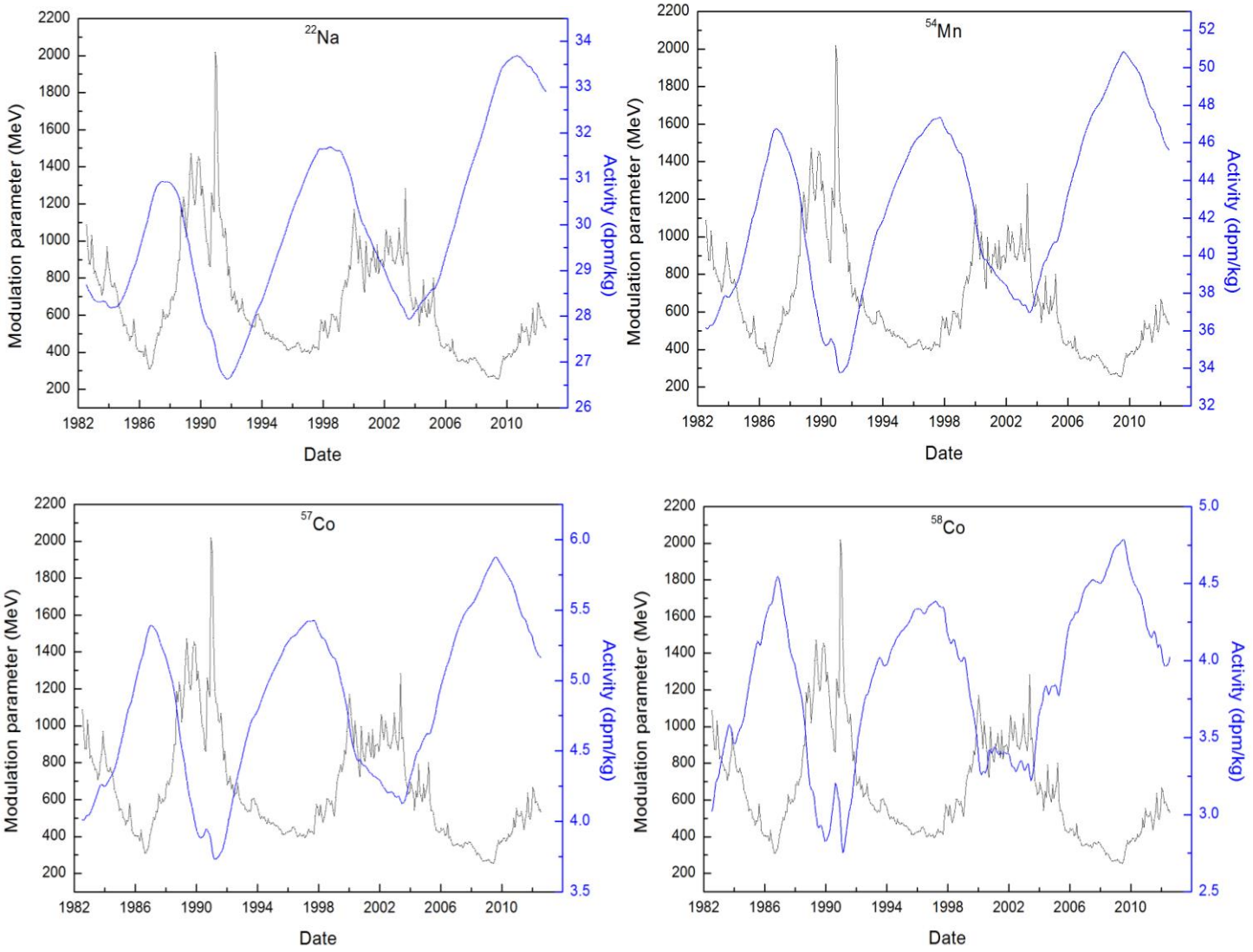

Figure 2.2.2-2: Reconstructed activities of ^{22}Na (2.6 y), ^{54}Mn (312.3 d) , ^{57}Co (271.8 d) , ^{58}Co (70.86 d) in the Chelyabinsk meteorite for a depth of 40 cm. Calculated data are shown together with function of modulation parameter.

2.2.3 Discussion

The calculation model for short-lived radionuclides described in this chapter allowed us to reconstruct production rates and activities of cosmogenic radionuclides for known meteorite falls. Production rate of cosmogenic radionuclide is immediate response to changes in GCR as it is directly dependent on the source of irradiation, while activity rather integrates those changes over time (figure 2.2.2-1). As one can see form figures 2.2.2-1,2 variations in activity of particular radionuclide (in this case between solar maximum and minimum) are dependent on its half-life, radionuclides with longer half-lives ~ few years undergo much lower variation (from equation 2.2.2-1); ~ 14 % for ^{60}Co (5.27 y), ~ 26 % for ^{22}Na (2.6 y) and radionuclide with shorter half-lives ~ tens or few hundred days are influenced much more by current solar activity and therefore we can see very strong variation in their activity; ~ 50 % for ^{54}Mn (312.3 d), ~ 55 % for ^{57}Co (271.8 d), ~ 70 % for ^{58}Co (70.86 d) (figures 2.2.2-1,2). The shape of simulated curves is somehow smoother and the position of local extreme is slightly shifted with increasing half-life. Those effects are due to aggregation and decay of radionuclides through the longer period of time, because radionuclides with longer half-lives are less sensitive on changes in GCR flux and their response to change is weaker and slightly delayed. Radionuclides with half-life much longer than 11y solar cycle period average out changes in solar activity and they are rather influenced by averaged GCR spectrum. As it was described in previous chapter, solar modulation strongly influence particles with lower energies and this influence lose strength with increasing energy, therefore variation in activity of a radionuclide is also naturally higher near surface, where many lower energetic particles contribute to production (but they are not able to penetrate deeply into body of meteoroid), and decreases with depth (figure 2.2.1-1).

Described results clarify behaviour of short-lived nuclides through the solar cycle and have direct impact on their application e.g. the preatmospheric size of a meteoroid that is commonly estimated from activity of ^{60}Co (^{60}Co is the one of the most sensitive depth indicators [52]). Its activity is usually calculated either form averaged GCR flux or using a very rough approximation of the solar activity influence on production rates. Precisely calculated activities of short-lived radionuclides can become useful tool for accurate estimation of depth of a particular sample in meteorite body and it can provide very helpful information about characteristics of investigated meteorite as well (chapters 2.3,2.4).

2.3 The Chelyabinsk meteorite

The Chelyabinsk meteor was asteroid whose orbit brought it into proximity with Earth. On February 15, 2013, a spectacular fireball was observed over Russia near city of Chelyabinsk at 9:22 local time. The observed flash was followed by a powerful explosion resulting into a shock wave that caused damage on building and also resulted in injuries to more than thousand people in the City of Chelyabinsk despite the fact that atmosphere absorbed most of the object's energy. The estimated size of the bolide was about 19 m in diameter [43], with mass of ~ 12,000 tons [44]. The shock wave covered an area in excess of 24,000 km^2 [46].

The Chelyabinsk event was the biggest impact over land since the poorly observed Thunguska impact (probably a comet or an asteroid) in 1908 which occurred over a sparsely-populated region of Siberia, producing a deposited energy with estimated range from 10 to 15 megatons [47]. The Chelyabinsk entered at a pre-atmospheric velocity of ~ 18 $km.s^{-1}$ at a low angle of 20° with respect to the horizon [46]. Size and speed suggest that a shockwave first developed at altitude of 90 km. Observations show that fragmentation and dust formation started around 83 km. The energy of explosion has been estimated to be approximately 400-600 kilotons of TNT equivalent [43].

Shock radiation contributed to surface heating and ablation, but did not completely evaporate all fragments of Chelyabinsk, unlike in the case of Thunguska. In the next few days after the Chelyabinsk event first fragments were recovered by various scientist and collectors. Thousands stones with various sizes (average 1-4 cm) and weights (from mg to few kg) fell as a shower around the villages 40 km south of the City if Chelyabinsk. The largest fragment weighing ~ 650 kg, was recovered months later from Lake Chebarkul. The Fragments are mainly isometric or short in prismatic shape [46].

The chemical composition of the meteorite was examined using several techniques (for detail description see [50]). The texture, mineral chemistry and major elements contents indicated that the Chelyabinsk meteorite is a group LL5 ordinary chondrite (see table 2.3-1 for major element composition). The Chelyabinsk meteorite contains a significant amount (about one-third in volume) of shock-melted material. The impact melt is similar in composition to the major part of the meteorite [50].

Table 2.3-1: Contents of major elements in the Chelyabinsk meteorite [50]

Element	**Weight** [%]
Si	18.3
Ti	0.054
Al	1.18
Fe	20.3
Mn	0.27
Mg	15.5
Ca	1.35
Na	0.76
K	0.10
P	0.10
S	2.38
O	37.4

2.3.1 Cosmogenic radionuclides measurement

Meteorites represent rich natural archives of cosmogenic radionuclides produced by different processes of GCR or SCR particles with meteoroids bodies, that can be measured either by decay counting techniques (gamma-ray spectrometry), or with accelerator mass spectrometry (AMS).

The most frequently-measured cosmogenic radionuclides are positron emitters, such as ^{26}Al and ^{22}Na. For each decaying nuclei, there are characteristic gamma-rays of 1275 keV (^{22}Na), and of 1130 and 1809 keV (^{26}Al) and two annihilation photons of 511 keV each. Other cosmogenic radionuclides are represented by cascade gamma-emitters (^{60}Co), or by single photon emitters (^{54}Mn). Long-lived cosmogenic radionuclides, such as ^{10}Be, ^{14}C, ^{36}Cl, ^{41}Ca, ^{53}Mn, and others, but also long-lived positron emitters, such as ^{26}Al, are mainly analysed by destructive AMS technique [76].

For this interdisciplinary study, 12 meteorite fragments of the Chelyabinsk meteorite were selected for analysis. The weights of selected samples (1-10) range from 2.38 to 10.3 g. The two largest investigated fragments, labelled NHMW N9584 and N9583, have 47.38 and 387.13 g, respectively (table 2.3.2-1).

The whole meteorite fragment was placed in a coincidence-anticoincidence spectrometer with strong shielding operated in gamma spectrometric laboratory at the Comenius University in

Bratislava. The spectrometer consists of sodium iodide (NaI) and High-purity Germanium (HPGe) detectors, which are placed in a shielded container. The shielding consists of successive layers of iron (12 cm), lead (10 cm), electrolytic copper (10 cm), polyethylene with boric acid (10 cm), electrolytic copper (0.1 cm), cadmium (0.1 cm), and polymethylacrylate (1 cm). The GEANT code was used for calibration of efficiency of the HPGe detector used for analysis of irregularly shaped fragments of the Chelyabinsk meteorite [76].

Samples with mass below <4 g were measured at the low-background counting facility at the Gran Sasso Underground Laboratory. To improve precision of the measurement, the gamma-ray spectrometers are located deep underground, where the background is reduced by more than a factor of ten compared to a surface laboratory. [76]

Table 2.3.2-1: Results of analyses of cosmogenic radionuclides in Chelyabinsk samples [76].

Sample number	Mass (g)	Massic activity (mBq/g)					
		^{22}Na	^{26}Al	^{54}Mn	^{57}Co	^{58}Co	^{60}Co
1	10.28	0.51±0.13	0.24±0.12	0.87±0.12			1.27±0.15
2	4.776	1.20±0.21	0.52±0.09	1.01±0.13	0.16±0.04	0.17±0.07	0.95±0.10
3	4.518	0.06±0.01	< 0.06	0.10±0.02	< 0.03	< 0.03	0.15±0.03
4	4.133	< 0.2	< 0.1	< 0.1			< 0.1
5	4.112	< 0.10	< 0.04	< 0.04	< 0.06	< 0.05	< 0.04
6	4.055	0.70±0.13	0.27±0.08	0.93±0.10	0.10±0.02	0.13±0.07	1.52±0.11
7	2.804	1.45±0.17	0.59±0.11	1.38±0.18	0.20±0.06	0.20±0.10	1.36±0.13
8	2.721	1.38±0.19	0.54±0.11	1.10±0.15	0.11±0.05	0.15±0.08	< 0.08
9	2.629	0.70±0.11	0.25±0.05	0.89±0.15	0.11±0.05	0.10±0.06	1.23±0.14
10	2.383	< 0.04	< 0.06	< 0.07	< 0.05	< 0.05	< 0.10
11	47.38	0.17±0.02	0.11±0.03	0.36±0.04			0.69±0.08
12	387.13	1.03±0.04	0.42±0.01	1.34±0.05			1.29±0.05

2.3.2 Simulations

The Calculations of activities in the Chelyabinsk meteorite were carried out by LCS [15]. Interaction of high energy particles (>20 MeV) were calculated by lahet, low energy interactions (<20MeV) were calculated with hmcnp4. For calculations of activities in the Chelyabinsk meteorite two approaches were used. First approach uses standard calculation model for long-lived cosmogenic nuclides (in our case ^{26}Al), where body of the meteorite is irradiated by averaged GCR flux Φ = 550 and integral flux 4.8 nucleons cm^{-2} s^{-1} [49]. For the case of short-lived cosmogenic nuclides (^{22}Na, ^{57}Co, ^{58}Co, ^{60}Co and ^{54}Mn), for which activity in particular time is strongly dependent on dynamical changes of GCR flux due to solar activity variations we have used approach described in chapter 2.2.

The Chelyabinsk-like object modelled in our calculation is LL5 ordinary chondrite with composition of major elements given by table 2.3-1 (and some additional important trace elements [50]) and known average density 3.2 g.cm^{-3} [50]. Modelled object with radius of 9 m was divided into concentric shells with defined thickness, in which fluxes of protons and neutrons were calculated. Having calculated those fluxes and concentrations of target nuclei we used database of available cross sections to obtain final production rates and activities. Our calculations are compared with experimental data (table 2.3.2-1). Results of comparison are shown on figure 2.3.3-1.

Depth profiles for all measured cosmogenic radionuclides were calculated, but only two of them (2.3.3-1) were used for depth estimation of samples due to high uncertainties of measured activities and sensitivity of calculations.

2.3.3 Results and discussion

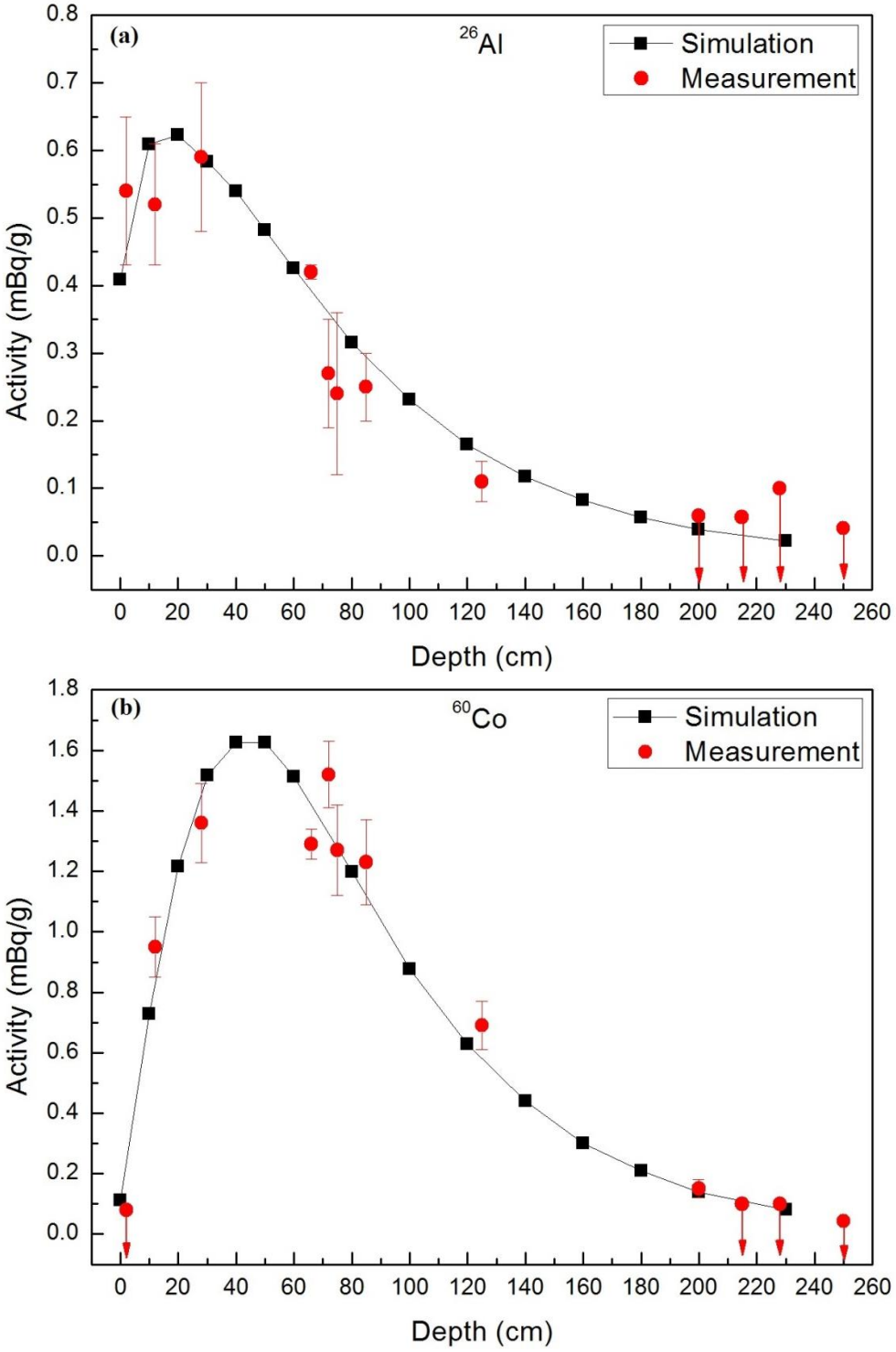

Figure 2.3.3-1: Comparison of the simulated depth profiles (black) with experimental data assigned to depths (red).

The Chelyabinsk meteorite and its fall were analysed by many modern techniques which provided useful source of information about composition, density, trajectory and size of the meteorite for purpose of our simulations. By using available experimental data we were able to model The Chelyabinsk-like object with radius of 9 m, composition given by table 2.3-1 and with measured density. By Monte-Carlo simulation codes and techniques described in previous sections we have calculated activities and production rates within the modelled object. These results were compared with experimental data (table 2.3.2-1 and figure 2.3.3-1). Exact depths of samples showed in table 2.3.3-1 are unknown. According to our calculation we were able to estimate approximate positions for all measured samples inside of the Chelyabinsk meteorite. The estimation of depths was based on calculated depth profiles, where we assigned position for every sample which was in the best agreement with all simulated depth profiles. As we can see from figure 2.3.3-1 simulated curves and experimental data fit well. The obtained results show relatively small activities. This effect is related to the interaction depth of GCR particles and size of meteorite, where large objects (R > 4m) such as the Chelyabinsk meteorite have exclusively 2π-irradiation, which means that incoming GCR particles are not able to induce nuclear reaction in the whole volume of a meteorite.

2.4 The Košice meteorite

On February 28th, 2010 a bright bolide with corresponding sonic booms enlightened night sky over the Central and Eastern Slovakia followed by a meteorite fall near the city of the Košice. Due to the unfavourable weather in the Central Europe no direct optical observation of the flight by the Central European Fireball network has been performed. Fortunately, three surveillance video cameras in Hungary, at least partly recorded the event. These observations allowed reconstruction of the bolide trajectory and impact area of the meteorite [58]. First fragments of the meteorite were found within 3 weeks after the fall. More than 70 fragments of the meteorite have been found by August 2010 of total recovered mass 2.16 kg. Mineralogical analysis of the meteorite fragments classifying it as H5 chondrite [57]. Further analysis of fragments classified the Košice meteorite as a homogeneous fall derived from homogenous parent meteoroid. The bulk density of individual fragment ranges from 3.15 to 3.64 $g.cm^{-3}$ with mean value of 3.43 $g.cm^{-3}$ [56]. The estimated initial mass of a preatmospheric body of the Košice meteorite is about 3500 kg with diameter 1.25 m and the kinetic energy at the entry into the atmosphere was almost 0.1 kt TNT ($4.185 \cdot 10^{11}$ J) [58].

The measurement of cosmogenic radionuclides was performed by non-destructive low-level gamma-spectrometry at Department of Nuclear Physics and Biophysics of the Comenius University in Bratislava. Detail description of experimental set-up can be found in chapter 2.3.2 or [60]. Eighteen fragments of the Košice meteorite have been analysed. The volume and mass of measured samples varied from 2.3 g to 2370 g (table 2.4-2). Special methodology based on monte-carlo simulation (GEANT) and construction of mock-ups must have been used [60] for their determination.

Table 2.4-1: Contents of major elements in the Košice meteorite [82]

Element	**Weight** [%]
Si	16.5
Ti	0.06
Al	1.07
Fe	28.85
Mn	0.23
Mg	13.8
Ca	1.14
Na	0.6
K	0.09
P	0.1
O	37.4

2.4.1 Simulations

Production rates and activities of cosmogenic radionuclides in the Košice meteorite were calculated in LCS (Lahet and HMCP4) with use of the approach described in chapter 2.2.

The modelled object was a H5 ordinary chondrite with composition of major elements given by table 2.4-1 (and some important trace elements [82]) and known average density of 3.4 $g.cm^{-3}$. Unlike in the case of the Chelyabinsk meteorite calculated activities of cosmogenic radionuclides can be used to estimate preatmospheric size of the meteorite. The modelled objects had radii of 40, 45, 55 and 62.5 cm and were divided into concentric shells with defined thickness, for which fluxes of protons and neutrons were calculated. Having calculated fluxes and concentrations of target nuclei we used database of available cross sections to obtain final production rates and activities. Results of our calculation are compared with experimental data from table 2.4.2-1 and shown on figure 2.4.2-1,2.

Table 2.4.1-1 : Results of analyses of cosmogenic radionuclides in Košice samples [82].

frag.	n°	**M1**	**M2**	**M3**	**M4**	**M5**	**M6**	**M7**	**M8**	**M9**
mass	g	27.3	315.5	246.7	193.6	2162.8	210.5	81.4	60.9	106
^{26}Al	($mBq \cdot g^{-1}$)	1.21	1.04	1.14	1.21	1.04	1.03	0.98	1.07	1.05
σ	($mBq \cdot g^{-1}$)	0.15	0.06	0.06	0.07	0.04	0.05	0.09	0.08	0.06
^{60}Co	($mBq \cdot g^{-1}$)	3.15	0.58	2.85	0.77	2.85	1	1.62	0.95	1.82
σ	($mBq \cdot g^{-1}$)	0.54	0.09	0.34	0.11	0.6	0.13	0.23	0.16	0.25

frag.	n°	**M10**	**M11**	**M12**	**M13**	**M14**	**M15**	**M16**	**M17**	**M18**
mass	g	99.9	45.4	51.9	97.2	2370.2	238.6	176.2	127.6	103.2
^{26}Al	($mBq \cdot g^{-1}$)	0.95	1.02	0.87	0.95	1.18	1.09	1.2	1.01	1.1
σ	($mBq \cdot g^{-1}$)	0.07	0.09	0.09	0.06	0.04	0.06	0.04	0.03	0.03
^{60}Co	($mBq \cdot g^{-1}$)	0.36	0.94	0.59	0.32	0.81	2.24	1.4	0.85	2.76
σ	($mBq \cdot g^{-1}$)	0.08	0.13	0.12	0.06	0.06	0.23	0.12	0.07	0.21

2.4.2 Results and discussion

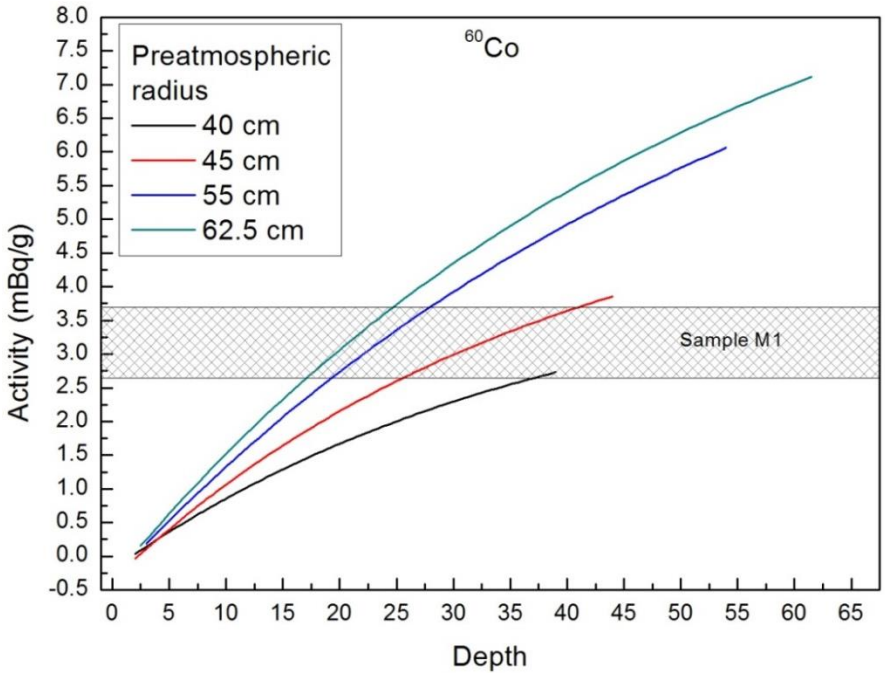

Figure 2.4.2-1: Depth profiles of ^{60}Co for spherical meteoroids with various preatmospheric sizes in comparison with the sample with highest measured activity of ^{60}Co.

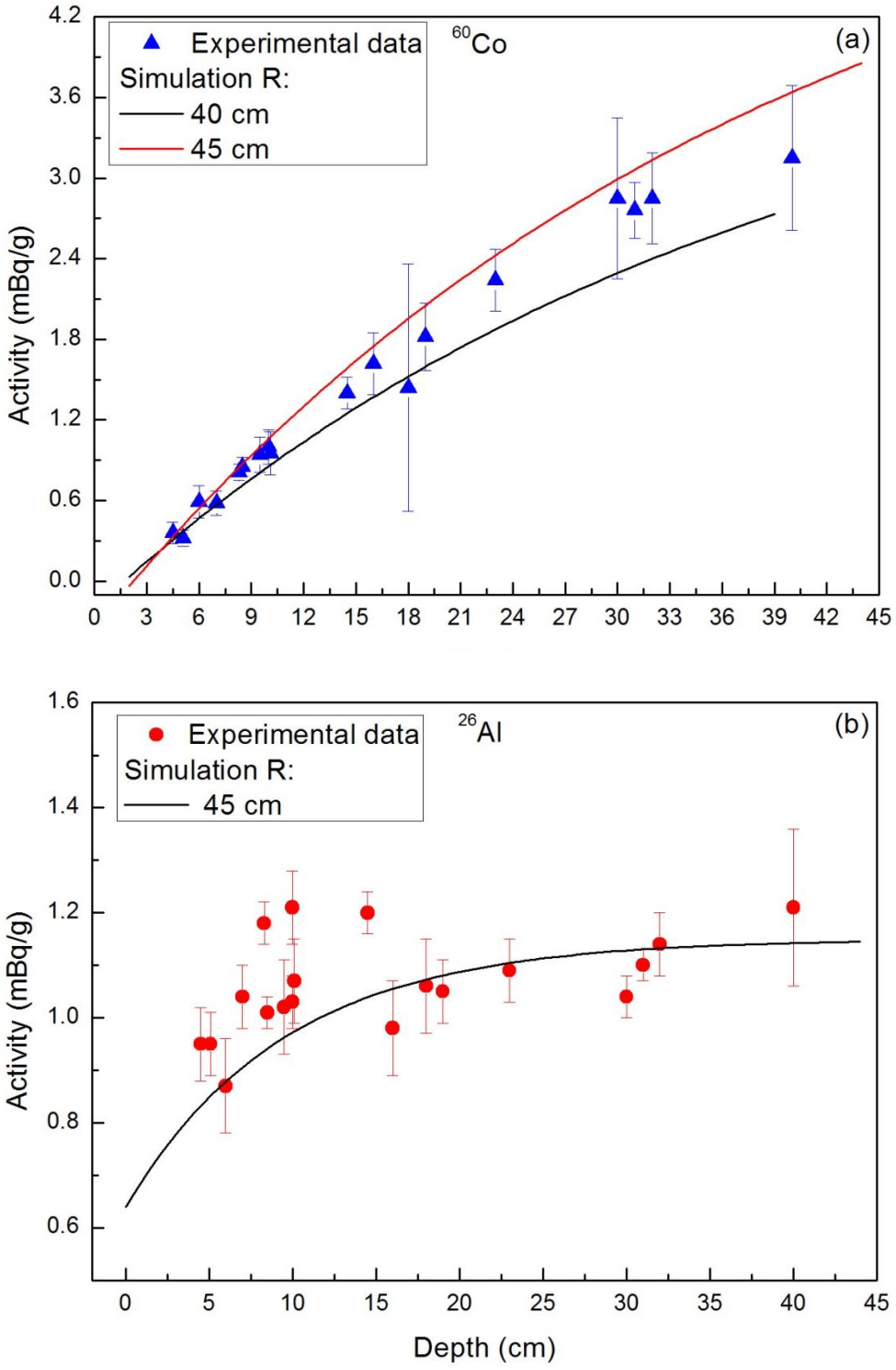

Figure 2.4.2 -2: Comparison of the simulated depth profiles (black, red lines) with experimental data assigned to depths (red, blue points).

Using the composition given by table 2.4-1 The Košice-like spherical meteoroids with radii (40, 45, 55, 62.5 cm) were modelled. By using Monte-Carlo simulation codes and techniques described in previous sections we have calculated activities and production rates within the modelled object. The original size estimate of the Košice meteorite was R ~ 125 cm [58] which was based on calculations related to trajectory of the meteoroid body its estimated mass suppose spherical shape of a meteoroid. This kind of estimation can be performed also by using of the calculated activities of cosmogenic radionuclides. ^{60}Co is the one of the most sensitive depth indicators [52] and therefore was applied also in this study. The comparison of simulations for investigated sizes with sample with highest measured activity (M1) is shown on figure 4.2.2-1. The most probable preatmospheric size of the meteorite is between 40 - 45 cm. Meteorites with smaller sizes would be too small for particle cascade development. This leads to lower activity of ^{60}Co in the centre of the meteorite and consequently sizes with radii < 40 cm can be excluded from estimation. Meteoroids with radii > 45 cm can't be excluded from our size estimation but from comparison of measurement with simulation (figure 4.2.2-1), no fragment form centre would have been found, which is highly unlikely. This estimation (40-45 cm) is in contradiction with estimation based on optical observations (R = 62.5 cm), but still can be reconciled if we consider results from chapter 2.1 (shape effect) that can strongly lower ^{60}Co activity due to non-spherical shape of the meteoroid (both mentioned size estimates use spherical geometry). The shape effect analysis requires further study of the meteorite fragments for noble gasses (^{21}Ne, ^{22}Ne), which provide clues about shielding and locations of the samples within meteoroid body.

We have also estimated approximate position of measured fragments within the meteorite. Results are shown on figure 4.2.2-2. The estimation of depths was based on calculated depth profiles. Determination of position for every sample was based on the requirement of the best agreement of experimental data with all simulated depth profiles. The simulated curves and experimental data fit well. Calculations for remaining radionuclides and measured uncertainties didn't provide sufficient sensitivity for further use.

2.5 Atmospheric 81Kr as an integrator of cosmic-ray flux over the past 800 kyr

Long-lived cosmogenic radionuclides carry important information about the past of the terrestrial and space environments. For example, concentrations of ^{10}Be (half-life = 1.5 Myr) in polar ice and sea sediments reveal the spatial and time variations of the GCR over the past 10^5 years [63]. Variation was found in correlation with changing magnetic field during solar cycles. Considering longer time scale (10^5 yr), the flux is affected by the change of the Earth's magnetic field; this effect has been discovered by comparing concentrations of ^{10}Be concentration and effect caused by magnetic field recorded in sediments [64].

The origin of atmospheric ^{81}Kr (half-life 229 +/- 11 ky) is also cosmogenic and provide somehow complementary and different perspective from that of ^{10}Be and ^{36}Cl on the timescale of 10^5 years. The most important difference resides in their transport and residence in the atmosphere. ^{10}Be is kept in the atmosphere for about a few years and its deposition rate to the archives, affected by GCR distribution and atmospheric transport factors, varies in time and space over the globe by as much as factor of 10 [63]. Understanding of its transport and deposition processes requires robust, sophisticated climate models. In contrast, ^{81}Kr is a noble-gas nuclide and due its inertness and low solubility in water almost all Kr resides in the atmosphere throughout its lifetime. Only about 2% of the total terrestrial Kr content is absorbed into the oceans. Also the tracer is extensively mixed in the atmosphere, and thus free of effects related to the geophysical variations, which means no complicated atmospheric transport model is required for understanding its uniform distribution. The ^{81}Kr/Kr ratio in the atmosphere is the perfect whole-earth integrator of the GCR flux in the time scale of 10^5 years. The measured ^{81}Kr/Kr ratio, due to its simplicity, can help verifying models simulating cosmic-ray fluxes and calculating production rates of cosmogenic nuclides.

2.5.1 A model for the production rate of ^{81}Kr

The interaction of CR particles with gases in the Earth's atmosphere produce cascades of secondary particles. Various models for calculation of the production rates in atmosphere have been developed in recent years. In this chapter we present production rate calculation of ^{81}Kr in the Earth's atmosphere. Additionally, we have investigated the sensitivity of the production rates to various parameters and inputs that undergone changes in the past.

The production rate P_j [atoms s^{-1} g^{-1}] of cosmogenic nuclide j at the atmospheric position d in an irradiated body with radius R is given by equation described in chapter 1.4 with few adjustments.

$$P_j(\Phi, d, M) = \sum_i N_i \sum_k \int_0^\infty \sigma_{jik}(E_k) J_k(E_k, R, d, M) dE_k \qquad 2.5.1\text{-}1$$

where Ni is the number of atoms for target element i per kg material in the sample, $\sigma ijk(E_k)$ represents the cross section for the production of the nuclide j from the target element i by particles of type k with kinetic energy E_k, and $J_k(E_k,d,M,\Phi)$ is the total flux of particles of type k with energy E_k at position d inside the atmosphere for the geomagnetic field M and the solar modulation parameter Φ. This model uses the particle fluxes Jk(Ek,D,M,Φ) calculated using the GEANT and MCNP codes. Merging of these two codes was previously described in Masarik and Beer [65].

The Earth's atmosphere is modelled as a sphere with inner radius of 6378 km and thickness of 100 km. The spherical model is divided into 34 concentric shells of equal thickness (30 g cm^{-2}) and the average chemical composition, further each shell is divided into 9 latitudinal sections matching to steps of 10 degrees in magnetic latitude. The density and temperature of the modelled atmosphere is approximated by the U.S. Standard Atmosphere [66]. The realistic variation in the density, chemical composition and temperature profile of the atmosphere make negligible effects on the production rate of ^{81}Kr and other nuclides [67].

The primary CR flux at the Earth's orbit has two components SCR and GCR. The SCR particles consist mainly from protons with energies up to 100 MeV (see section 1.1.2). Due to their relatively low energies the nuclide production from SCR is restricted to the very top of the atmosphere and is limited to geomagnetic latitudes above 60°. The long-term average production of cosmogenic radionuclides by SCR is expected to be negligible. Earlier calculations showed

that contribution from SCR is below 1% and percentage can increase by a factor of few during solar events and at high latitudes. The main contribution to cosmogenic nuclide production is done by GCR particles. Fits to lunar experimental data showed that the effective flux of protons and alpha particles with energies above 10 MeV per nucleon at distance of 1 A.U. is 4.56 nucleons cm^{-2} s^{-1} [68]. This value corresponds to long-term average value of the modulation parameter Φ = 550 MeV [69].

The geomagnetic field effectively deflects incoming CR particles depending on their angle of incidence and magnetic rigidity, defined as a momentum per charge. For each angle of incidence, there is a critical rigidity below which incoming particles are deflected the way that they cannot reach Earth's atmosphere and induce nuclear reactions. Applied model uses global grid of vertical cut-off [70] to determine nonvertical cut-offs. Simply using the relativistic energy-momentum relationship, the cut-off energies for all nuclides can be determined and nuclei with lower energies are excluded from further calculation. This approach leads to a latitudinal dependence of the primary and secondary particles, and consequently also of the production rates of cosmogenic radionuclides. The particle flux is higher around the magnetic poles and lower in the equatorial regions [70]. From paleomagnetic records, it is known that the geomagnetic field varied in the past in its intensity, direction and polarity [71]. In order to investigate the influence of geomagnetic field variations on particle fluxes and cosmogenic nuclide production rates, the relative intensity of the geomagnetic field is varied from 0 to 2 "relative to the reference field", in steps of 0.25, while the shape of the field remains the same. The dependence of the ^{81}Kr production rate on the geomagnetic field intensity is calculated and is found to fit well with a polynomial of 5th degree, a result is in agreement with dependences previously obtained for other nuclides [72]. The polynomial is then used to investigate the relationship between the variability of the ^{81}Kr production rate and past changes in the geomagnetic field.

Records of past magnetic field intensity, dating back to 800 kyr BP, have been obtained from paleomagnetic studies on marine sediments [73]. This most reliable continuous record is used in this calculation, and yields relative paleointensity variations. Guyodo and Valet (1996) calibrated their record with absolute paleointensities obtained from a discontinuous record of lava flows for the past 40 kyr. The mean virtual axis dipole moment (VADM) of the calibrated data of the past 10 kyr, except the one at 2 kyr BP, is very close to the present day VADM of 8.0 x

1022 A m^{-2}. By normalizing the 800 kyr VADM data set to its present day value, the record agrees with independent reconstructions of field intensity obtained from other approaches. For this recent period, we adopt the dendrochronologically derived ^{14}C record [73] to reconstruct the relative field intensity. This can be done more reliably because major ocean circulation changes can be excluded for the Holocene period.

2.5.2 Results and discussion

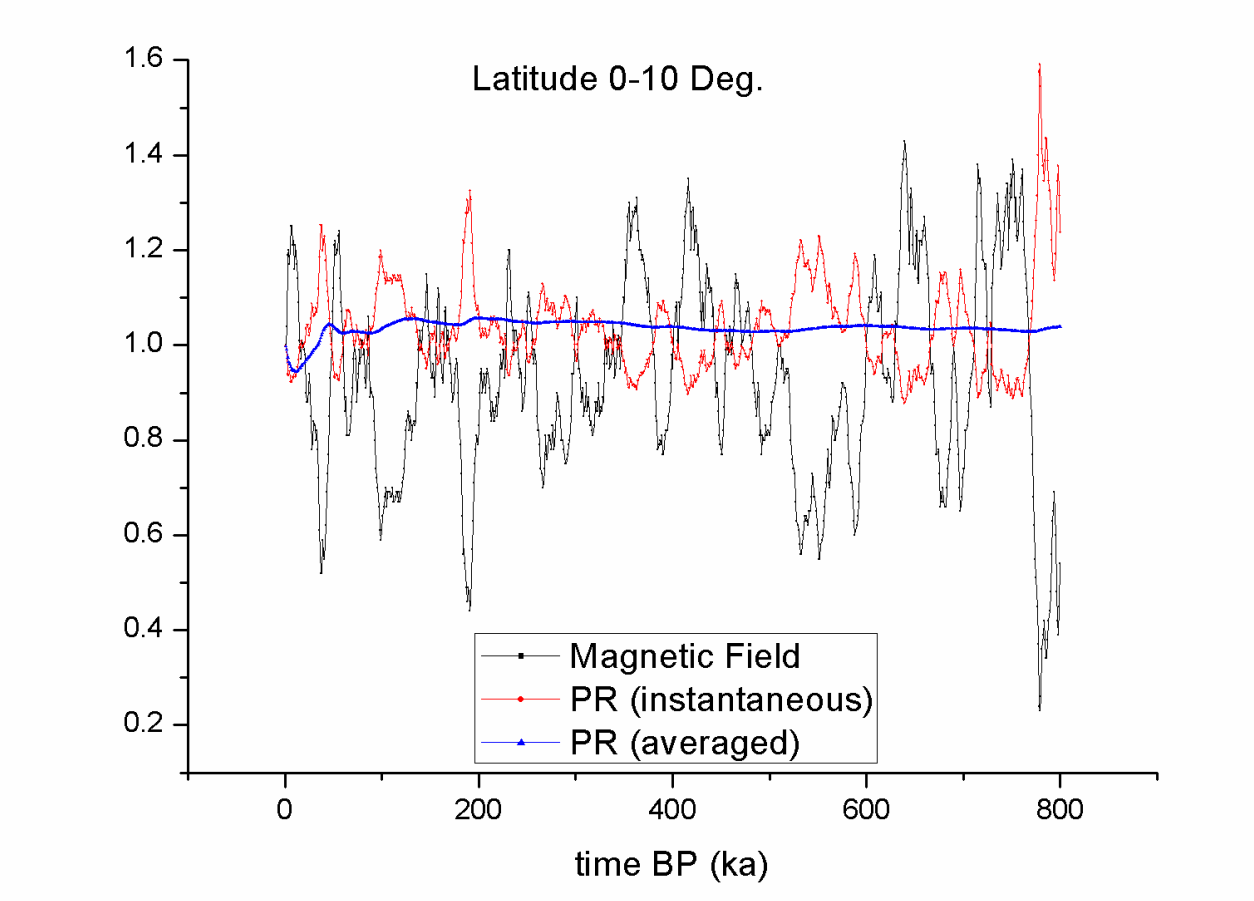

Figure 2.5.2- 1: The production rates of ^{81}Kr over time. The black line shows the relative magnetic field intensity in the past 800 kyr adopted in this work. For the past 10 kyr we use the field reconstruction based on the dendrochronologically derived ^{14}C record [74]; for the period 10-800 kyr, we rely on the reconstruction by [73]. The red line shows the calculated production rate of ^{81}Kr, normalized to the present-day global average production rate. The blue line is the resulting mean or integrated relative production up to the present.

Results of our calculations are presented in Figure 2.5.1-1. The black line shows the relative magnetic field intensities adopted in this work. The red line represents the corresponding variation of the instantaneous global average production rate of ^{81}Kr in the Earth's atmosphere. We note that the instantaneous production rate varies less than the magnetic field. The blue line shows the average production rate integrated from present-day to the respective time, a quantity directly relevant to the interpretation of the measured ^{81}Kr/Kr ratio. Note that integrated production rate is robust to short-term changes in field intensity, a characteristic that contributes significantly to the advantages of ^{81}Kr dating.

The statistical uncertainties introduced by the calculations are ~ 5%. The systematic uncertainties in the cross sections contribute approximately 10-15 %. The standard deviations on the order of 15-20% for their stacked paleomagnetic field records, but short-term variations of such amplitudes around the adopted smoothed field intensity curves have a negligible influence on the integrated production rates of ^{81}Kr. Therefore, possible systematic errors in the paleomagnetic records are likely the dominant source of uncertainty for the production rate reported here [73,75]. The systematic uncertainties in our calculated fluxes are difficult to determine, but are probably on the order of 10%. Differences in the calculated and measured neutron fluxes lead to the difference in production rates of investigated nuclides on the level 5-13%. Taking into account all sources of uncertainties mentioned above, production rate of ^{81}Kr corresponding to present geomagnetic field intensity and long term average solar activity is (1.34 ± 0.10) x 10-6 atoms cm^{-2} s^{-1}. After correcting this value for geomagnetic field variations during the last 800 ky, the averaged production rate is (1.39 ± 0.15) x 10-6 atoms cm^{-2} s^{-1}. As during last 10 thousand years average geomagnetic field was higher than present, the global average production rate is decreased in comparison of present to value (1.27±0.1) x 10-6 atoms cm^{-2} s^{-1}. The production rate of ^{81}Kr derived from multiple independent measurements was determined to be (1.2 ± 0.1) x 10^6 [83], which is in good agreement with our results.

3. Conclusion

This work was dedicated to the Monte-Carlo modelling of cosmic ray interactions with extra-terrestrial and terrestrial matter. We discuss results achieved using calculation models oriented on production of cosmogenic radionuclides commonly used in applied nuclear physics.

3.1 Effect of pre-atmospheric shape

The LCS/HMCP code has been used for an investigation of effect of preatmospheric shape on production rates of cosmogenic radionuclides. The bodies investigated in this work had different shapes yet equal volumes. The particle fluxes were calculated in the small area in the vicinity of major axes for the particular geometry. The cosmogenic radionuclides calculated in this work are ^{10}Be (as a product of high-energy spallation reactions) and ^{60}Co (as a product of low-energy neutron capture). Results of our simulation show that for the meter-sized meteoroids production rates for ^{10}Be are insensitive to shape of the preatmospheric body as the simulated depth profile for all axes of all geometries are almost identical and small differences in calculated depth profiles are rather issue related to statistic. The production rates of ^{60}Co in non-spherical objects vary significantly for the same depth and the value in the centre of meteoroid is lowered in comparison with maximal value reached in spherical geometry, except the cylindrical geometry with length to radius ratio 2:1, which means that bulk of this object is similar to sphere with rather deformed surface (the length of the main object's axes are the same). Calculated depth profiles (one meter-sized meteorite) of ^{10}Be and ^{60}Co lead to the conclusion that the shape of the preatmospheric body rather influences particle of lower energy than those of higher energy.

Considering ~2 meter-sized geometries the production rate of ^{60}Co show similar results as in case of a 1 meter sized meteoroid but differences among production rates for various axes are lowered. Also maximal value for nonspherical geometry is close to the value obtained for sphere due to the additional space for cascade development added by enlarging the size of meteoroid resulting into slight compensation of differences in depth profiles. The depth profiles of ^{10}Be show not only remarkable differences in production rate for the same depth but also inverted

effect, where production rate is reduced on shortest axis (and sphere) and increased on longer axes at the same depth.

The explanation for observed results lies in distance which is required for particle cascade development and number of particles escaping from meteoroid's body. In general flattening of a particular geometry in comparison to sphere renders interior of the meteorite more accessible by particles of higher energy while reduce effective distance for particle cascade development which leads to the leakage of particles of lower energies. The importance of described effects might have different demonstration in geometries with various masses (volumes) in which additional effects related to the size of investigated bodies apply.

We have also investigated production rates of cosmogenic radionuclides in The Peekskill meteorite which as modelled as H chondrite with specific composition and with the proposed flattened cylindrical geometry. The results of simulations show sufficient accuracy of calculation for all calculated radionuclides (^{10}Be, ^{26}Al and ^{60}Co). The precise determination of the pre-atmospheric shape of a meteorite is not really possible due to very deformed shapes of real meteoroids, although approximation used in our work suggest possible explanation of measured data.

3.2 Calculation model for short-lived nuclides

We have designed a simple calculation model of short-lived radionuclides which allowed us to reconstruct production rates and activities of cosmogenic radionuclides for known meteorite falls. Production rate of cosmogenic radionuclide is immediate response to changes in GCR as it is directly dependent on the source of irradiation, while activity rather integrates those changes over time (depending on half-life). The comparison of relative changes in activity in the solar minimum and maximum shows increasing tendency (in variation) with decreasing half-life from about 14 % for ^{60}Co (5.27 y) to ~70 % for ^{58}Co (70.86 d). Those effects are due to aggregation and decay of radionuclides through the longer period of time. Radionuclides with longer half-lives are less sensitive on changes in GCR flux and their response to change is weaker and slightly delayed. Radionuclides with half-life much longer than 11y solar cycle period average

out changes in solar activity and they are rather influenced by averaged GCR spectrum. The variation in activity of a radionuclide is also naturally higher near surface, where many lower energetic particles contribute to production and decreases with depth.

Precisely calculated activities of short-lived radionuclides are useful tool for estimation of depth of a particular sample in meteorite body and can provide very helpful information about characteristics of investigated meteorite.

3.3 The Chelyabinsk meteorite and The Košice meteorite

Using available experimental data we were able to model meteoroid bodies for The Chelyabinsk meteorite and The Košice meteorite. These results of calculations were compared with experimental data. According to calculated depth profiles we were able to estimate approximate positions for all measured samples inside of the Chelyabinsk meteorite and The Košice meteorite. Every sample was assigned to depth in order to be in the best agreement with all simulated depth profiles.

For the case of the Košice meteorite we have also modelled multiple spherical meteoroids with radii (40, 45, 55, 62.5 cm). The most probable preatmospheric size of the meteorite is between 40 - 45 cm. Meteorites with smaller sizes would not allow full particle cascade development, which leads to lower activity of ^{60}Co in the centre of the meteorite than are observed. Thus sizes with radii < 40cm can be excluded from estimation. Meteoroids with radii > 45 cm can't be excluded from size estimation but according to measured data in comparison with simulation no fragment form centre would have been found, which is highly unlikely. This kind of estimation is not applicable for large meteorites as is the case of the Chelyabinsk meteorite.

3.4 Atmospheric 81Kr as an integrator of cosmic-ray flux over the past 800 kyr

Using known records of magnetic field intensity in the past 800 kyr, and designed model of Earth's atmosphere including latitudal variation of magnetic field we were able to calculate the instantaneous global average production rate of ^{81}Kr in the Earth's atmosphere up to present day $(1.39 \pm 0.15) \times 10^{-6}$ atoms.cm^{-2}s^{-1}. Calculated value is in the good agreement with experimental results reached by experimental measurement $(1.2 \pm 0.1) \times 10^{-6}$ atoms.cm^{-2}s^{-1}. The measured and calculated $^{81}Kr/Kr$ ratio, due to its simplicity, can help verifying models simulating cosmic-ray fluxes and calculating production rates of cosmogenic nuclides

4. Zhrnutie

Táto práca je zameraná na Monte Carlo modelovanie interakcií kozmického žiarenia s atmosférou zeme a hmotou slnečnej sústavy. Práca diskutuje výsledky dosiahnuté modelovaním produkcie kozmogénnych rádionuklidov, ktoré sú bežne používané v aplikovanej jadrovej fyzike.

4.1 Vplyv tvaru meteoroid na produkciu kozmogénnych rádionuklidov

LCS a HMCP kódy boli použité na skúmanie vplyvu tvaru meteoroid na produkciu kozmogénnych rádionuklidov. ^{10}Be ako produkt vysokoenergetických trieštivých reakcií a ^{60}Co ako produkt nízkoenergetických záchytových reakcií neutrónov. Modelované telesá boli: Guľa, elipsoidy a valce s rôznymi pomermi dĺžok osí (poloosí). Toky častíc a produkcie nuklidov boli počítané v malom okolí hlavných osí telies. Výsledky simulácií ukazujú, že pre meteoroid s veľkosťou jedného metra, nie sú pozorované žiadne štatisticky významné rozdiely v produkcií ^{10}Be na osiach meteoroidu. Naopak produkcia ^{60}Co vykazuje veľké rozdiely na jednotlivých osiach deformovaného meteoroidu pre rovnakú hĺbku a to aj v porovnaní s guľovou geometriou. Taktiež bol pozorovaný pokles maximálnej produkcie dosiahnutej v centrálnej časti meteoroid v porovnaní s guľovou geometriou. Jediným prípadom, ktorý vykazuje podobné výsledky ako guľová geometria a to pre všetky hlavné osi je valec s pomerom priemeru podstavy a dĺžky 1:1. Teda teleso ktoré nemá deformáciu hlavných osí ale má skôr deformovaný povrch (v porovnaní s guľovou geometriou). Výsledky simulácií produkcie ^{10}Be a ^{60}Co pre meteoroid s približnou veľkosťou 1 m ukazujú, že tvar meteoroid ovplyvňuje viac toky častíc s nízkou energiou ako tie vysokou energiou.

Produkčná rýchlosť ^{60}Co počítaná pre meteoroid s veľkosťou približne 2 m ukazuje podobný trend ako v predchádzajúcom prípade s tým rozdielom, že rozdiely v produkcií na osiach sú nižšie a aj maximálna dosiahnutá hodnota v centrálnej časti meteoroidu je menej vychýlená v porovnaní s guľovou geometriou. Tento efekt je zapríčinený zvýšením objemu meteoritu oproti predchádzajúcemu prípadu, čo vedie k nárastu priestoru pre vývoj kaskády

častíc. Porovnanie produkčných rýchlostí ^{10}Be ukazuje mierne rozdiely medzi osami, kde najväčšia produkcia pre danú hĺbku je na najdlhšej osi a naopak na najkratšej osi a guľovej geometrii je najnižšia produkcia.

Vysvetlenie pozorovaných efektov spočíva vo vzdialenosti, ktorá je nevyhnutná pre vývoj kaskád sekundárnych častíc a v počte častíc unikajúcich z telesa meteoroidu. Vo všeobecnosti osová deformácia geometrie (v porovnaní s guľovou) robí vnútorné časti meteoroidu viac prístupné pre častice s vysokou energiou zatiaľ čo redukuje efektívnu vzdialenosť nevyhnutú pre vývoj kaskád sekundárnych častíc, čo podporuje únik častíc s nízkou energiou z telesa meteoroidu. Popísané efekty môžu mať mierne odlišné prejavy v závislosti od zvolenej veľkosti telesa.

Ako aplikáciu sme sa rozhodli modelovať produkciu kozmogénnych rádionuklidov pre prípad The Peekskill meteorite. Ten bol modelovaný ako H chondrit s vlastným (meraným) zložením a s sploštenou geometriou, ktorá bola navrhovaná vzhľadom na dynamické optické pozorovania a aj merania aktivity rádionuklidov. Výsledky simulácií rádionuklidov (^{10}Be, ^{26}Al a ^{60}Co) ukazujú dobrú zhodu s meraním. Vzhľadom na komplikovanosť tvarov, ktoré môžu reálne meteority nadobúdať, nie je možné určovať presný tvar meteoroidov týmto spôsobom, ale i napriek tomu výsledky priniesli možné vysvetlenie pre namerané experimentálne dáta.

4.2 Výpočtový model pre krátkožijúce rádionuklidy

Navrhli sme jednoduchý výpočtový model pre výpočet aktivity krátkožijúcich rádionuklidov. Tento model umožnil urobiť rekonštrukciu produkčných rýchlostí a aktivít pre známe meteority. Produkčná rýchlosť predstavuje okamžitú odozvu na zmeny v kozmickom žiarení, kvôli jej priamej závislosti na zdroji ožarovania, zatiaľ čo aktivita skôr tieto zmeny integruje. Porovnanie relatívnych zmien v aktivite v solárnom maxime a minime ukazuje pokles variácie s rastúcim polčasom rozpadu od ~14 % pre ^{60}Co (5,27 r) až k ~70 % pre ^{58}Co (70,86 d). Efekty viažuce sa na polčas rozpadu súvisia s nahromadením a priebežným rozpadom rádionuklidu v čase, kde rádionuklidy s dlhším polčasom rozpadu sú menej citlivé na zmeny v toku kozmického žiarenia a

ich odozva na tieto zmeny je mierne oneskorená. Rádionuklidy s polčasom oveľa dlhším ako 11 rokov sú skôr ovplyvňované priemerným spektrom kozmického žiarenia. Variácia aktivity rádionuklidu je tiež prirodzene vyššia blízkosti povrchu, kde k produkcii prispievajú aj nízkoenergetické častice (silne ovplyvňované slnečným cyklom, ale nie schopné preniknúť do väčších hĺbok) a táto tendencia klesá s hĺbkou.

4.3 Meteorit Čeljabinsk a meteorit Košice

S použitím dostupných experimentálnych dát sme namodelovali telesá, ktoré svojim zložením, hustotou a ďalšími parametrami zodpovedajú nájdeným úlomkom meteoritov Košice a Čeljabinsk. Vypočítané aktivity boli porovnané s meranými experimentálnymi hodnotami. Vzhľadom na to sme určili približné pozície pre všetky merané fragmenty meteoritov. Odhad hĺbok bol určený na základe simulovaných hĺbkových profilov, kde sa brala do úvahy pozícia vzorky na základe najlepšej zhody so simuláciami.

Pre meteorit Košice bolo modelovaných niekoľko variant veľkostí (sférických) meteoroidov: 40, 45, 55, 62,5 cm (polomer). Porovnanie výsledkov simulácií s experimentmi ukazujú ako najpravdepodobnejší odhad medzi 40-45 cm. Menší meteoroid by nemal dostatočný priestor nevyhnutný pre vývoj kaskády častíc, čo vedie k zníženiu výslednej aktivity ^{60}Co. To umožňuje vylúčiť geometrie s polomerom menším ako 40 cm. Meteoroid s veľkosťou nad 45 cm sa priamo vylúčiť nedá, ale vzhľadom na meranie aktivít ^{60}Co vo vzorkách by nebol nájdený žiaden fragment s centrálnej časti meteoroidu, čo je pri 18 nájdených fragmentoch nepravdepodobné. Odhad založený na produkcií kozmogénnych rádionuklidoch nie je aplikovateľný pre veľké meteoroidy ako napríklad Čeljabinsk.

4.4 Produkcia ^{81}Kr v atmosfére Zeme za posledných 800 000 rokov

Meranie efektov vyvolaných magnetickým poľom v sedimentoch za posledných 800 000 rokov a model atmosféry zahrňujúci variáciu magnetického poľa so zemepisnou šírkou, umožnilo vypočítať okamžitú priemernú globálnu produkciu ^{81}Kr v zemskej atmosfére až dodnes. Vypočítaná súčasná hodnota $(1.39 \pm 0.15) \times 10^{-6}$ atómov.cm^{-2}s^{-1} je v dobrej zhode s meraním $(1.2 \pm 0.1) \times 10^{-6}$ atómov.cm^{-2}s^{-1}.Pomer atmosférického ^{81}Kr/Kr môže napomôcť overiť modely simulujúce tok kozmických častíc a produkčných rýchlostí kozmogénnych nuklidov.

References

[1] B. Heber, J. Kóta, R. Von Steiger, Cosmic Rays in the Heliosphere, Reprinted from Space Science Reviews Volume 176, 1-4, (2013)

[2] J. Beer, K. McCracken, R. Von Steiger, Cosmogeinc Radionuclides, Springer-Verlag, Berlin (2012)

[3] D.Lal, B. Peters, Cosmic Ray Produced Radioactivity on the Earth, in Handbuch

der Physik XLVI/2, Springer-Verlag, pages 551–612, (1967).

[4] T. E. Greadel, P. J. Crutzen, Atmospheric change, an earth system approach, W.H. Freeman and Company, New York, p 446, (1993)

[5] R. Michel, G. Brinkmann and R. Stuck, Solar cosmic-ray-produced radionuclides in meteorites, Earth and Planetary Science Letters, 59 (1982).

[6] G. Castagnoli and D. Lal, Solar modulation effects in terrestrial production of carbon-

14, Radiocarbon 22, 133–158 (1980).

[7] R. Michel, P. Dragovitch, P. Cloth, G. Dagge, D. Filges, On the production of cosmogenic nuclides in meteoroids by galactic protons, Meteoritics 26, 221-242 (1991)

[8] R. C. Reedy, J. R. Arnold, and D. Lal, Cosmic-ray record in solar system matter,

Science 219, 127–135 (1983).

[9] J. A. Simpson, Elemental and isotopic composition of the galactic cosmic rays, Ann.

Rev. Nucl. Part. Sci. 33, 323–381 (1983)

[10] Gaisser, Thomas K. Cosmic rays and particles physics, Cambridge University Press (1990)

[11] R.G. Allsmiller, R.T. Santoro, J. Barish and H.C. Claiborne, Shielding of manned space vehicle against protons and α-particles, ORNL-RISC-35 (1972)

[12] A.M. Davis, H.D. Holland and K.K. Turekian, Meteorites, Comets, and Planets: Treatise on Geochemistry, Second Edition, Volume 1 (2006)

[13] R. E. Lingenfelter, Int. Cosmic Ray Conf. 14, 135 (1979)

[14] Cut-off rigidity models (2004) - http://www.geomagsphere.org/geomag/

[15] R. E. Prael and H. Lichtenstein, User guide to LCS: The LAHET Code System, Los Alamos National Laboratory report, LA-UR-89-3014, 1989.

[16] MCNP manual vol I Overview and Theory, X-5 Monte Carlo Team (2003)

[17] MCNP manual vol II User's Guide, X-5 Monte Carlo Team (2003)

[19] Beech, Martin. "The Peekskill Meteorite and Fireball". University of Regina, Canada. Retrieved 2012-06-20.

[20] Andrew M. Davis, University of Chicago Meteorites, Comets and Planets, Vol.1., 84-120 (2009)

[21] J. T. Wasson, Meteorites: Classification and Properties. Springer-Verlag, (1974).

[22] J.Masarik, J.Beer, Simulation of particle fluxes and cosmogenic nuclide production in Earth's atmosphere, Journal of Geophysical Research, D104 (10) 12,099-12,012, (1999)

[23] Experimental Nuclear Reaction Data (EXFOR) http://www.nndc.bnl.gov/exfor/exfor.htm

[24] Evaluated Nuclear Data File (ENDF) http://www.nndc.bnl.gov/exfor/endf.htm

[25] Japanese Evaluated Nuclear Data Library (JENDL) http://wwwndc.jaea.go.jp/jendl/jendl.html

[26] D.T.L. Jones, Monoenergetic neutron sources below 100 MeV, Radiation Physics and Chemistry, Volume 61, Issues 3–6, Pages 469–472, (June 2001)

[27] F.P. Brady, J.L. Romero, Summary of monoenergetic neutron beam sources for energies >14 MeV, Nucl. Sci. Eng., 106, pp. 318–331, (1990)

[28] R. C. Reedy, A model for GCR-particle fluxes in stony meteorites and production rates of cosmogenic nuclides, J. Geophys. Res. 90, 722 (1985).

[29] J. Masarik and R. C. Reedy, Terrestrial cosmogenic-nuclide production systematics calculated from numerical simulations, Earth Planet. Sci. Lett. 136, 381–395 (1995)

[30] TALYS software for the simulation of nuclear reactions. http://www.talys.eu/home/

[31] P. Cloth, D. Filges, R. D. Neef, G. Sterzenbach, C. Reul, T. W. Armstrong, B. L. Colborn, B. Anders, and H. Brueckmann, HERMES – High Energy Radiation Monte Carlo Elaborate System, Juel-2203, (1988).

[32] R. C. Reedy (2011) Cosmogenic-Nuclide Production Rates: Reaction Cross Section Update. Book of Abstracts for the Twelfth International Conference on Accelerator Mass Spectrometry, Wellington, New Zealand, (National Isotope Centre, GNS Sciences, Lower Hutt, New Zealand), p. 159, (20-25 March 2011).

[33] Andrew S. Rivkin, Asteroids, comets and dwarf planets, Greenwood Guides to the Universe, p 52-55, (2009)

[34] J. Masarik, R.C.Reedy, Effects of bulk composition on nuclide production processes in meteorites, Geochemica et Cosmochemica Acta, Vol. 58, No. 23, pp5307-5317 (1994)

[35] J. Masarik, K. Nishiizumi, R. C. Reedy, Production rates of cosmogenic helium-3, neon-21, and neon-22 in ordinary chondrites and the lunar surface, Meteoritics & Planetary Science 36, 643-650 (2001)

[36] I. G. Usoskin, G. A. Bazilevskaya, G. A. Kovaltsov, Solar modulation parameter for cosmic rays since 1936 reconstructed from ground-based neutron monitors and ionization chambers, Journal of geophysic research, vol. 116 A02104, (2011)

[37] http://sidc.oma.be/ - Solar Influences Data Analysis Center

[38] http://cosmicrays.oulu.fi/#solar –Source of modulation parameter data

[39] E. M. Galimov, V. P. Kolotov, M. A. Nazarov, Yu. A. Kostitsyn, I. V. Kubrakova, N. N. Kononkova, I. A. Roshchina, V. A. Alexeev, L. L. Kashkarov, D. D. Badyukov, and V. S. Sevast'yanov, Analytical Results for the Material of the Chelyabinsk Meteorite, ISSN 0016_7029, Geochemistry International, 2013, Vol. 51, No. 7, pp. 522–539. © Pleiades Publishing, Ltd., (2013)

[41] Lal,D., J.R. Arnold, M. Honda, Phys. Rev. 118,1626 (1960)

[42] Pidwirny, M. Atmospheric composition (2013) http://www.eoearth.org/view/article/150296

[43] Brown et al., Astronomical and physical aspects of the Chelyabinsk Event, Solar System Research, Vol. 47, No. 4, pp 240-254 (2013)

[44] Borovicka, J., Spurny, P., and Shrbeny, L., trajectory and orbit of the chelyabinsk superbolide, Electronic Telegram Central Bureau for Astronomical Telegrams, IAU (2013), No. 3423.

[45] An Overwiev if Cosmic-Ray Elemental Composition, http://www.srl.caltech.edu/ACE/ACENews/ACENews83.html

[46] O. Popova et al., Chelyabinsk Airburst, Damage Assessment, Meteorite Recovery, and Characterization, Science 29 November 2013: Vol. 342 no. 6162 pp. 1069-1073

[47] Farinella et al., Probable asteroidal origin of the Tunguska Cosmic Body, Astronomy and Astrophysics, v.377, p.1081-1097 (2001)

[48] Pidwirny, M. "The Layered Atmosphere". Fundamentals of Physical Geography, 2nd Edition. (2006). http://www.physicalgeography.net/fundamentals/7b.html

[49] Leya I. and Masarik J. 2009. Cosmogenic nuclides in stony meteorites revisited. Meteoritics & Planetary Science 44:1061–1086

[50] E. M. Galimov et al., Analytical Results for the Material of the Chelyabinsk Meteorite, Geokhimiya, 2013, Vol. 51, No. 7, pp. 580–598 (2013)

[51] S. Merchel et al., A multi-radionuclide approach for in situ produced terrestrial cosmogenic nuclides: 10Be, 26Al, 36Cl and 41Ca from carbonate rocks, Nuclear Instruments and Methods in Physics Research B 268 1179–1184, (2010)

[52] Eberhardt P., Geiss J., and Lutz H. 1963. Neutrons in meteorites. In Earth science and meteoritics, edited by Geiss J. and Goldberg E. P. Amsterdam: North-Holland Publishing Co. pp. 143–169

[53] Bonino, G., Cini Castagnoli, G., Cane, D., Taricco, C., & Bhandari, N., Solar modulation of the galactic cosmic ray spectra since the maunder minimum, Proceedings of the 27th International Cosmic Ray Conference. 07-15 August, 2001. Hamburg, Germany. Under the auspices of the International Union of Pure and Applied Physics (IUPAP)., pp.3769

[54] Garcia-Munoz The anomalous 4He component in the cosmic ray spectrum at < 50 MeV per nucleon during 1972-1974, Astrphys. J., 202,265

[55] W. R. Weber and P. R. Higbie, Production of cosmogenic Be nuclei in the Earth's atmosphere by cosmic rays: Its dependence on solar modulation and interstellar cosmic ray spectrum, J. Geophys. Res., 108(A9), 1355, doi: 10.1029/2003JA009863

[56] T. Kohout et al., Density, porosity and magnetic susceptibility of the Košice meteorite shower and homogeneity of its parent meteoroid, Planetary and Space Science (2014), In Press

[57] Ozdín, D., Uher, P., Porubčan, V., Tóth, J., Svoreň, J., Konečný, P., Povinec, P., Veis, P., Sitek, J., Mineralogy, petrography, geochemistry and classification of the Košice meteorite,Meteoritics & Planetary Science, (2014), under review.

[58] J. Borovička, J. Tóth, A. Igaz, P. Spurný, P. Kalenda., J. Haloda, J. Svoreň, L. Kornoš, E. Silber, P. Brown, M. Husárik, 2013. The Košice meteorite fall: Atmospheric trajectory,fragmentation, and orbit. Meteoritics and Planetary Science 48, 1757-1779 (2013)

[59] J. Masarik private communication (2013).

[60] D. Kováčik, I. Sýkora, P. P. Povinec, V. Porubčan, Non-destructive gamma-spectrometry analysis of cosmogenic radionuclides in fragments of the Košice meteorite, Journal of Radioanalytical & Nuclear Chemistry;Jul2012, Vol. 293 Issue 1, p339

[61] Th. Graf et al. Exposure history of the Peekskill (H6) meteorite, Meteoritics & Planetary Science 32, 25-30 (1997)

[62] Z. Ceplecha et al., The Fall of the Peekskill Meteorite: Video Observaüons, Atmospheric Path, Fragmentation Record and Orbit, Earth, Moon, and Planets 68: 189-197, (1995)

[63] Beer, J., McCracken, K.G., Abreu, J., Heikkila, U., Steinhilber, F. Cosmogenic radionuclides as an extension of the neutron monitor era into the past: potential and limitations. Space Sci. Rev. 176, 89-100, (2013)

[64] Finkel, R.C., Nishiizumi, K., 1997. Beryllium 10 concentrations in the Greenland Ice Sheet Project 2 ice core from 3-40 ka. J. Geophys. Res. – Oceans 102, 26699-26706. DOI:10.1029/97JC01282

[65] Masarik, J. and Beer, J., 1999. Simulation of Particle Fluxes and Cosmogenic Nuclides Production in the Earth's Atmosphere. J. Geophys. Res. 104 (D10) 12099-12111. DOI: 10.1029/1998JD200091

[66] Champion, K.S.W., Cole, A.E., Kantor, A.J., 1985. Standard and reference atmosphere, in A. S. Jursa, (Ed.), Handbook of Geophysics and the Space Environment, Air Force Geophys. Lab., U.S. Air Force, pp. 14-1 - 14-43
.
[67] Masarik, J., Reedy, R.C., 1995. Terrestrial cosmogenic-nuclide production systematic calculated from numerical simulations, Earth Planet. Sci. Lett. 136, 381-395.

[68] Masarik, J., Reedy, R.C., 1994. Effects of bulk chemical composition on nuclide production processes in meteorites, Geochim. Cosmochim. Acta 58, 5307-5317.

[69] Reedy, R.C., 1987. Nuclide production by primary-ray protons, Proceedings of the 17th Lunar Planetary Science Conference, J. Geophys. Res. 92, 697-702.

[70] Masarik, J. and Beer, J., 1999. Simulation of Particle Fluxes and Cosmogenic Nuclides Production in the Earth's Atmosphere. J. Geophys. Res. 104 (D10) 12099-12111.

[71] Brendel, K.J., Kuipers, J., Barkema, G.T., Hoyng, P., 2007. An analysis of the fluctuations of the geomagnetic dipole, Phys. Earth Planet. Interiors 162, 249-255.

[72] Wagner, G., et al., 2000. Reconstruction of the geomagnetic field between 20 and 60 kyr BP from cosmogenic radionuclides in the GRIP ice core, Nucl. Instr. Meth. Phys. Res. B, 172, 597-604.

[73] Guyodo, Y., Valet, J.-P., 1996. Relative variations in geomagnetic intensity from sedimentary records: the past 200,000 years, Earth Planet. Sci. Lett. 143, 23-36.

[74] Stuiver, M., et al., 1998. INTCAL98 radiocarbon age calibration, 24,000–0 cal BP, Radiocarbon 40, 1041–1083.

[75] Frank, M., et al., 1997. A 200 kyr record of cosmogenic radionuclide production rate and geomagnetic field intensity from 10Be in globally stacked deep-sea sediments. Earth Planet. Sci. Lett. 149, 121-129.

[76] Pavel P. Povinec, et al., Cosmogenic radionuclides and mineralogical properties of the Chelyabinsk (LL5) meteorite: What do we learn on the meteoroid?, Meteoritics & Planetary Science, submitted (2014)

[77] Bischoff, A.; Geiger, T. (1995). "Meteorites for the Sahara: Find locations, shock classification, degree of weathering and pairing". Meteoritics 30 (1): 113–122.

[78] Meteoretical Bulletin Database, http://www.lpi.usra.edu/meteor/

[79] The Catalogue of Meteorites, http://www.nhm.ac.uk/nature-online/space/meteorites-dust/science-meteoritecatalogue/

[80] Bhandari N. et al. Geochim. Cosmochim. Acta 57 2361-2375, (1993)

[81] Masarik J. and Reedy R.C. 1994 Geochim. Cosmochim. Acta 58, 5307-5317

[82] Pavel P. Povinec, Jozef Masarik, Ivan Sýkora, Andrej Kováčik, Juraj Beňo, Matthias Laubstein, Vladimir Porubčan, Cosmogenic radionuclides in the Košice meteorite: Experimental investigations and Monte Carlo simulations, Meteoritics & Planetary Science, to be published, (2014)

[83] Philippe Collon, Walter Kutschera, and Zheng-Tian Lu, TRACING NOBLE GAS RADIONUCLIDES IN THE ENVIRONMENT, Annual Review of Nuclear and Particle Science, Vol. 54: 39-67 (2004)

APPENDICES

A Examples of inputs for LCS HMCNP calculations:

Input file for the LAHET, isotropic irradiation of a spherical LL chondrite with radius of 9 m:

```
LL-R9m

 10856371
5500,20,01,23,2e6,1e9,0,,,,,,0.0/
,-1,,1,12/
,,/
20001.,,,,,,,,,,8.0,,8.0/
0.00e-00,26,26/
 8,  16,  4.52E-02,7
11,  23,  6.39E-04,8
12,  24,  1.09E-02,8
12,  26,  1.49E-03,8
13,  27,  8.45E-04,8
14,  28,  1.22E-02,9
14,  30,  4.08E-04,9
15,  31,  6.24E-05,9
16,  32,  1.37E-03,10
16,  34,  6.11E-05,10
19,  39,  4.94E-05,10
20,  40,  6.37E-04,11
20,  44,  1.37E-05,11
22,  48,  2.18E-05,11
24,  52,  1.49E-04,12
25,  55,  9.50E-05,13
26,  54,  4.08E-04,13
26,  56,  6.46E-03,13
26,  57,  1.55E-04,13
27,  59,  1.61E-05,13
28,  58,  2.34E-04,14
28,  60,  9.01E-05,14
28,  62,  1.23E-05,14
62, 149,  2.83E-09,19
64, 155,  1.79E-09,19
64, 157,  2.02E-09,19
1    1  -3.21   -2  3
2    1  -3.21   -3  4
3    1  -3.21   -4  5
4    1  -3.21   -5  6
5    1  -3.21   -6  7
6    1  -3.21   -7  8
7    1  -3.21   -8  9
8    1  -3.21   -9 10
9    1  -3.21   -10 11
10   1  -3.21   -11 12
11   1  -3.21   -12 13
12   1  -3.21   -13 14
13   1  -3.21   -14 15
14   1  -3.21   -15 16
15   1  -3.21   -16 17
16   1  -3.21   -17 18
17   1  -3.21   -18 19
18   1  -3.21   -19 20
19   1  -3.21   -20 21
20   1  -3.21   -21
21   0         -1 2
22   0          1

1     so 900.1
2     so 900.0
3     so 890.0
4     so 880.0
5     so 870.0
6     so 860.0
7     so 850.0
8     so 840.0
9     so 820.0
10    so 800.0
11    so 780.0
12    so 760.0
13    so 740.0
14    so 720.0
15    so 700.0
16    so 670.0
17    so 640.0
18    so 610.0
19    so 550.0
20    so 500.0
21    so 455.0

in    1 20r  0
print

15,,0.0,,900.01/
10.,20.,30.,40.,50.,60.,70.,80.,90.,100.,150.,200.,250.,
300.,350.,400.,450.,500.,550.,600.,650.,700.,750.,800.,
850.,900.,950.,1000.,1500.,2000.,2500.,3000.,3500.,4000.,4
500.,
5000.,5500.,6000.,6500.,7000.,7500.,8000.,8500.,9000.,950
0.,
10000.,11000.,12000.,13000.,14000.,15000.,16000.,17000.,
18000.,19000.,20000./
0.0,0.0004549,0.0007361,0.0009965,0.001243,0.001472,0.
001688,
0.001889,0.002076,0.002250,0.01354,0.01660,0.01854,0.0
1993,
0.02083,0.02149,0.02160,0.02163,0.02149,0.02122,0.0208
7,
0.02045,0.02010,0.01948,0.01896,0.01785,0.01785,0.0173
3,
```

0.1355,0.0955,0.076,0.0566,0.04306,0.03365,0.02667,0.02149,
0.01757,0.01455,0.01219,0.01028,0.008785,0.007569,0.006563,
0.005764,0.005035,0.004444,0.007465,0.006007,0.004896,0.004063,
0.003406,0.002885,0.002469,0.001132,0.001854,0.001625/

Input for the HMCNP, isotropic irradiation of a spherical LL chondrite with radius of 9 m :

```
LL-Chely-9m
1    1  -3.21   -2  3
2    1  -3.21   -3  4
3    1  -3.21   -4  5
4    1  -3.21   -5  6
5    1  -3.21   -6  7
6    1  -3.21   -7  8
7    1  -3.21   -8  9
8    1  -3.21   -9 10
9    1  -3.21   -10 11
10   1  -3.21   -11 12
11   1  -3.21   -12 13
12   1  -3.21   -13 14
13   1  -3.21   -14 15
14   1  -3.21   -15 16
15   1  -3.21   -16 17
16   1  -3.21   -17 18
17   1  -3.21   -18 19
18   1  -3.21   -19 20
19   1  -3.21   -20 21
20   1  -3.21   -21
21   0         -1 2
22   0          1

1     so 900.1
2     so 900.0
3     so 890.0
4     so 880.0
     16032.50c  -0.0238e+00
     19000.50c  -0.0010e+00
     20000.50c  -0.0135e+00
     22000.50c  -0.0054e-01
     24000.50c  -0.0265e-01
     25055.50c  -0.0040e+00
     26000.55c  -0.2030e+00
     28000.50c  -0.0102e+00
     62149.50c  -0.2200e-06
     64155.50c  -0.3100e-06
m2    27059.50c  -1.0
fm2   (5.0070e-06 2 102)
f2:n  1 2 3 4 5 6 7 8 9 10 11 12 13 14 15 16 17 18 19 20 21
e2   2.0e-09 4.0e-09 6.0e-09 8.0e-09 1.0e-08 2.0e-08 4.0e-08
    6.0e-08 8.0e-08 1.0e-07 2.0e-07
    4.14e-07 5.32e-07 6.83e-07 8.76e-07 1.13e-06 1.44e-06 1.86e-06
    2.38e-06 3.06e-06 3.93e-06 5.04e-06 6.48e-06 8.32e-06 1.07e-05
    1.37e-05 2.26e-05 2.90e-05 3.73e-05 4.79e-05 6.14e-05 7.89e-05
    1.01e-04 1.30e-04 1.67e-04 2.14e-04 2.75e-04 3.54e-04 4.54e-04
    5.83e-04 7.49e-04 9.61e-04 1.23e-03 1.58e-03 2.03e-03 2.61e-03
    3.35e-03 4.31e-03 5.53e-03 7.10e-03 9.12e-03 1.17e-02 1.50e-02
5     so 870.0
6     so 860.0
7     so 850.0
8     so 840.0
9     so 820.0
10    so 800.0
11    so 780.0
12    so 760.0
13    so 740.0
14    so 720.0
15    so 700.0
16    so 670.0
17    so 640.0
18    so 610.0
19    so 550.0
20    so 500.0
21    so 455.0

imp:n  1 20r  0
files  77  neutp s u 0  70 11mh. s u 0
c     material 1 is entered as weight fractions
m1
      8016.50c  -0.3740e+00
     11023.50c  -0.0076e+00
     12000.50c  -0.1550e+00
     13027.50c  -0.0118e+00
     14000.50c  -0.1830e+00
     15031.50c  -0.0010e+00
    1.93e-02 2.48e-02 3.18e-02 4.09e-02 5.25e-02 6.74e-02 8.65e-02
    1.11e-01 1.23e-01 1.36e-01 1.50e-01 1.66e-01 1.83e-01 2.02e-01
    2.24e-01 2.47e-01 2.73e-01 3.02e-01 3.34e-01 4.08e-01 4.50e-01
    4.98e-01 5.50e-01 6.08e-01 6.72e-01 7.43e-01 8.21e-01 9.07e-01
    1.0
f12:n  1 2 3 4 5 6 7 8 9 10 11 12 13 14 15 16 17 18 19 20 21
e12   2.0e-09 4.0e-09 6.0e-09 8.0e-09 1.0e-08 2.0e-08 4.0e-08
    6.0e-08 8.0e-08 1.0e-07 2.0e-07
    4.14e-07 5.32e-07 6.83e-07 8.76e-07 1.13e-06 1.44e-06 1.86e-06
    2.38e-06 3.06e-06 3.93e-06 5.04e-06 6.48e-06 8.32e-06 1.07e-05
    1.37e-05 2.26e-05 2.90e-05 3.73e-05 4.79e-05 6.14e-05 7.89e-05
    1.01e-04 1.30e-04 1.67e-04 2.14e-04 2.75e-04 3.54e-04 4.54e-04
    5.83e-04 7.49e-04 9.61e-04 1.23e-03 1.58e-03 2.03e-03 2.61e-03
    3.35e-03 4.31e-03 5.53e-03 7.10e-03 9.12e-03 1.17e-02 1.50e-02
    1.93e-02 2.48e-02 3.18e-02 4.09e-02 5.25e-02 6.74e-02 8.65e-02
```

```
   1.11e-01 1.23e-01 1.36e-01 1.50e-01 1.66e-01 1.83e-01
2.02e-01
   2.24e-01 2.47e-01 2.73e-01 3.02e-01 3.34e-01 4.08e-01
4.50e-01
   4.98e-01 5.50e-01 6.08e-01 6.72e-01 7.43e-01 8.21e-01
9.07e-01
```

```
   1.0 2.0 3.0 4.0 5.0 6.0 7.0 8.0 9.0 10.0 11.0 12.0 13.0
14.0 15.0 16.0 17.0 18.0 19.0 20.0
wwg:n  2 1 0 0. 0. 0.
Print
```

Input for the HTAPE, isotropic irradiation of a spherical LL chondrite with radius of 9 m with output fluxes of neutrons and protons:

```
Lchon,  E1i/
sept 7, 2013/
2,-58,0,2,0,21/
1.0,2.0,3.0,4.0,5.0,6.0,7.0,8.0,9.0,10.0,11.0,12.0,13.0,
14.0,15.0,16.0,17.0,18.0,19.0,20.,30.,40.,50.,60.,70.,80.,90.,100.,
120.,140.,160.,180.,200.,250.,300.,350.,400.,450.,500.,550.,600.,
700.,800.,900.,1000.,1500.,2000.,2500.,3000.,3500.,4000.,4500.,5000.,
6000.,7000.,8000.,9000.,10000./
0,1/
/
```

Example of the input files for ellipsoidal geometry:

Input file for the LAHET, isotropic irradiation of an ellipsoidal L chondrite with smilaxes a = 74.29 cm, b = 49.53 cm, c = 24.76 cm:

```
Lchon- Elipsoid

221235837
27000,20,01,23,2e6,1e9,0,,,,,,0.0/
,-1,,1,12/
,,/
20001.,,,,,,,,,,,8.0,,8.0/
8.4841e-04,16,16/
  6,  12,  6.050e-04, 5
  8,  16,  5.033e-02, 7
 11,  23,  7.346e-04, 8
 12,  24,  1.331e-02, 8
 13,  27,  1.061e-03, 8
 14,  28,  1.448e-02, 9
 15,  31,  9.663e-05,10
 16,  32,  1.540e-03,10
 19,  39,  6.015e-05,10
 20,  40,  5.974e-04,11
 22,  48,  2.680e-05,11
 24,  52,  1.850e-04,12
 25,  55,  8.950e-05,13
 26,  56,  7.714e-03,13
 27,  59,  1.814e-05,13
 28,  58,  3.788e-04,14
1    1  -3.55   -2  3
2    1  -3.55   -3  4
3    1  -3.55   -4  5
4    1  -3.55   -5  6
5    1  -3.55   -6  7
6    1  -3.55   -7  8
7    1  -3.55   -8  9
8    1  -3.55   -9 10
9    1  -3.55   -10 11
10   1  -3.55   -11 12
11   1  -3.55   -12 13
12   1  -3.55   -13 14
13   1  -3.55   -14 15
14   1  -3.55   -15 16
15   1  -3.55   -16 17
16   1  -3.55   -17 18
17   1  -3.55   -18 19
18   1  -3.55   -19 20
19   1  -3.55   -20 21
20   1  -3.55   -21
21   0         -1 2
22   0          1

1    so 74.31
2    sq 0.00018118 0.00040760 0.00163060 0 0 0 -1 0 0 0
3    sq 0.00020798 0.00046800 0.00187180 0 0 0 -1 0 0 0
4    sq 0.00022930 0.00051590 0.00206370 0 0 0 -1 0 0 0
5    sq 0.00026089 0.00058700 0.00234800 0 0 0 -1 0 0 0
6    sq 0.00029949 0.00067390 0.00269550 0 0 0 -1 0 0 0
7    sq 0.00034734 0.00078150 0.00312610 0 0 0 -1 0 0 0
```

```
8     sq 0.00040765 0.00091720 0.00366880 0 0 0 -1 0 0 0
9     sq 0.00048513 0.00109150 0.00436620 0 0 0 -1 0 0 0
10    sq 0.00058701 0.00132080 0.00528310 0 0 0 -1 0 0 0
11    sq 0.00072470 0.00163060 0.00652230 0 0 0 -1 0 0 0
12    sq 0.00091720 0.00206370 0.00825480 0 0 0 -1 0 0 0
13    sq 0.00119798 0.00269550 0.01078180 0 0 0 -1 0 0 0
14    sq 0.00163058 0.00366880 0.01467520 0 0 0 -1 0 0 0
15    sq 0.00217089 0.00488450 0.01953800 0 0 0 -1 0 0 0
16    sq 0.00303207 0.00682220 0.02728870 0 0 0 -1 0 0 0
17    sq 0.00452939 0.01019110 0.04076450 0 0 0 -1 0 0 0
18    sq 0.00748736 0.01684660 0.05738630 0 0 0 -1 0 0 0
19    sq 0.01467523 0.03301930 0.13207710 0 0 0 -1 0 0 0
20    sq 0.02293005 0.05159260 0.20637050 0 0 0 -1 0 0 0
21    sq 0.04076453 0.09172020 0.36688080 0 0 0 -1 0 0 0

in   1 20r  0
print

15,,0.0,,74.294/
10.,20.,30.,40.,50.,60.,70.,80.,90.,100.,150.,200.,250.,
300.,350.,400.,450.,500.,550.,600.,650.,700.,750.,800.,
850.,900.,950.,1000.,1500.,2000.,2500.,3000.,3500.,4000.,4
500.,
5000.,5500.,6000.,6500.,7000.,7500.,8000.,8500.,9000.,950
0.,
10000.,11000.,12000.,13000.,14000.,15000.,16000.,17000.,
18000.,19000.,20000./
0.0,0.0004549,0.0007361,0.0009965,0.001243,0.001472,0.
001688,
0.001889,0.002076,0.002250,0.01354,0.01660,0.01854,0.0
1993,
0.02083,0.02149,0.02160,0.02163,0.02149,0.02122,0.0208
7,
0.02045,0.02010,0.01948,0.01896,0.01785,0.01785,0.0173
3,
0.1355,0.0955,0.076,0.0566,0.04306,0.03365,0.02667,0.02
149,
0.01757,0.01455,0.01219,0.01028,0.008785,0.007569,0.00
6563,
0.005764,0.005035,0.004444,0.007465,0.006007,0.004896,
0.004063,
0.003406,0.002885,0.002469,0.001132,0.001854,0.001625/
```

Input file for the HMCNP, isotropic irradiation of an ellipsoidal L chondrite with smilaxes a = 74.29 cm, b = 49.53 cm, c = 24.76 cm:

```
Le321-co
1    1  -3.55   -2  3
2    1  -3.55   -3  4
3    1  -3.55   -4  5
4    1  -3.55   -5  6
5    1  -3.55   -6  7
6    1  -3.55   -7  8
7    1  -3.55   -8  9
8    1  -3.55   -9 10
9    1  -3.55   -10 11
10   1  -3.55   -11 12
11   1  -3.55   -12 13
12   1  -3.55   -13 14
13   1  -3.55   -14 15
14   1  -3.55   -15 16
15   1  -3.55   -16 17
16   1  -3.55   -17 18
17   1  -3.55   -18 19
18   1  -3.55   -19 20
19   1  -3.55   -20 21
20   1  -3.55   -21
21   0         -1 2
22   0          1

1     so 74.31
2     sq 0.00018118 0.00040760 0.00163060 0 0 0 -1 0 0 0
3     sq 0.00020798 0.00046800 0.00187180 0 0 0 -1 0 0 0
4     sq 0.00022930 0.00051590 0.00206370 0 0 0 -1 0 0 0
5     sq 0.00026089 0.00058700 0.00234800 0 0 0 -1 0 0 0
6     sq 0.00029949 0.00067390 0.00269550 0 0 0 -1 0 0 0
7     sq 0.00034734 0.00078150 0.00312610 0 0 0 -1 0 0 0
8     sq 0.00040765 0.00091720 0.00366880 0 0 0 -1 0 0 0
9     sq 0.00048513 0.00109150 0.00436620 0 0 0 -1 0 0 0
10    sq 0.00058701 0.00132080 0.00528310 0 0 0 -1 0 0 0
11    sq 0.00072470 0.00163060 0.00652230 0 0 0 -1 0 0 0
12    sq 0.00091720 0.00206370 0.00852480 0 0 0 -1 0 0 0
13    sq 0.00119798 0.00269550 0.01078180 0 0 0 -1 0 0 0
14    sq 0.00163058 0.00366880 0.01467520 0 0 0 -1 0 0 0
15    sq 0.00217089 0.00488450 0.01953800 0 0 0 -1 0 0 0
16    sq 0.00303207 0.00682220 0.02728870 0 0 0 -1 0 0 0
17    sq 0.00452939 0.01019110 0.04076450 0 0 0 -1 0 0 0
18    sq 0.00748736 0.01684660 0.06738630 0 0 0 -1 0 0 0
19    sq 0.01467523 0.03301930 0.13207710 0 0 0 -1 0 0 0
20    sq 0.02293005 0.05159260 0.20637050 0 0 0 -1 0 0 0
21    sq 0.04076453 0.09172020 0.36688080 0 0 0 -1 0 0 0
22    cx 2.5

imp:n  1 20r  0
files  77  neutp s u 0  70 11mh. s u 0
c     material 1 is entered as weight fractions
m1
      6012.50c  -0.0034e+00
      8016.50c  -0.3767e+00
     11023.50c  -0.7900e-02
     12000.50c  -0.1514e+00
     13027.50c  -0.0134e+00
     14000.50c  -0.1902e+00
     15031.50c  -0.0014e+00
     16032.50c  -0.0231e+00
     19000.50c  -0.0011e+00
     20000.50c  -0.0112e+00
     22000.50c  -0.0006e+00
     24000.50c  -0.0045e+00
     25055.50c  -0.0023e+00
```

```
     26000.55c  -0.2015e+00
     27059.50c  -0.0005e+00
     28000.50c  -0.0104e+00
m2    27059.50c  -1.0
fm2   (5.11e-06 2 102)
f2:n  1 2 3 4 5 6 7 8 9 10 11 12 13 14 15 16 17 18 19 20 21
fs2  -22
sd2  39.2699  41r
e2   2.0e-09 4.0e-09 6.0e-09 8.0e-09 1.0e-08 2.0e-08 4.0e-
08
    6.0e-08 8.0e-08 1.0e-07 2.0e-07
    4.14e-07 5.32e-07 6.83e-07 8.76e-07 1.13e-06 1.44e-06
1.86e-06
    2.38e-06 3.06e-06 3.93e-06 5.04e-06 6.48e-06 8.32e-06
1.07e-05
    1.37e-05 2.26e-05 2.90e-05 3.73e-05 4.79e-05 6.14e-05
7.89e-05
    1.01e-04 1.30e-04 1.67e-04 2.14e-04 2.75e-04 3.54e-04
4.54e-04
    5.83e-04 7.49e-04 9.61e-04 1.23e-03 1.58e-03 2.03e-03
2.61e-03
    3.35e-03 4.31e-03 5.53e-03 7.10e-03 9.12e-03 1.17e-02
1.50e-02
    1.93e-02 2.48e-02 3.18e-02 4.09e-02 5.25e-02 6.74e-02
8.65e-02
    1.11e-01 1.23e-01 1.36e-01 1.50e-01 1.66e-01 1.83e-01
2.02e-01
    2.24e-01 2.47e-01 2.73e-01 3.02e-01 3.34e-01 4.08e-01
4.50e-01
    4.98e-01 5.50e-01 6.08e-01 6.72e-01 7.43e-01 8.21e-01
9.07e-01
    1.0
wwg:n  2 1 0 0. 0. 0.
vol  1 21r
area 1 20r
print
```

Input file for the HTAPE, isotropic irradiation of an ellipsoidal L chondrite with smilaxes: a = 74.29 cm, b = 49.53 cm, c = 24.76 cm with collimating window on x axis with R = 2.5 cm:

```
Lchon,  /

sept  2012/
10,-58,0,2,1,21/
1.0,2.0,3.0,4.0,5.0,6.0,7.0,8.0,9.0,10.0,11.0,12.0,13.0,
14.0,15.0,16.0,17.0,18.0,19.0,20.,30.,40.,50.,60.,70.,80.,90.,100.,
120.,140.,160.,180.,200.,250.,300.,350.,400.,450.,500.,550.,600.,
700.,800.,900.,1000.,1500.,2000.,2500.,3000.,3500.,4000.,4500.,5000.,
6000.,7000.,8000.,9000.,10000./
0,1/
/
1,0,0,2.5/
```

B Major cross sections used for calculation: